**Title**
Interfacing Inorganic Materials and Biological Systems for Practical Applications in CO2 and N2 Fixation



**Author**
Rodrigues, Roselyn

**Publication Date**
2021

Peer reviewed|Thesis/dissertation

UNIVERSITY OF CALIFORNIA

Los Angeles

# Interfacing Inorganic Materials and Biological Systems for Practical Applications in $CO_2$ and $N_2$ Fixation

A dissertation submitted in partial satisfaction of the requirements for the degree Doctor of Philosophy in Chemistry and Biochemistry

by

Roselyn Rodrigues

2021

ABSTRACT OF THE DISSERTATION

Interfacing Inorganic Materials and Biological Systems

for Practical Applications in $CO_2$ and $N_2$ Fixation

by

Roselyn Rodrigues

Doctor of Philosophy in Chemistry and Biochemistry

University of California, Los Angeles, 2021

Professor Chong Liu, Chair

With the surge of intermittent, renewable electricity, the storage of excessive electricity and reduction of $CO_2$ or $N_2$ into value-added chemicals is of great significance for a sustainable society. One viable route that fulfills such a target is to construct a hybrid inorganic-biological system that converts electricity into chemical energy and reduces $CO_2$/$N_2$ into commodity chemicals. In this general approach, water is split into $H_2$ and $O_2$ by renewable electricity and the yielded $H_2$ is consumed by microbes as a reducing equivalent for $CO_2$/$N_2$ reduction. The throughput of this system is limited by the poor gas solubility in the aqueous environment. The control and design of the gas environment in these hybrid systems is crucial to achieving high throughput and sustainable reactions. To this end, my thesis has focused on combining perfluorocarbon (PFC) nanoemulsions with the hybrid system to enhance $H_2$ or $O_2$ gas solubility and optimize reaction performance.

My first research project focused on combining PFC nanoemulsions with a hybrid biological inorganic $CO_2$ fixation system to enhance the faradaic efficiency of acetic acid production (**Chapter 2**). PFC nanoemulsions are biologically inert and have reported high $H_2$ gas solubilities. We determined that the nanoemulsions are compatible with the acetogenic microbe strain *Sporomusa ovata* and the electrochemical water-splitting catalysts used in the hybrid $CO_2$ fixation system. When 2.5 % (v/v) PFC nanoemulsion was combined with the hybrid system we observed approximately 90 % or greater faradaic efficiency at all tested current densities. After 4 days, we were able to achieve an average acetic acid titer of 6.4 ± 1.1 $g \cdot L^{-1}$ (107 mM), which equates to one of the highest reported productivities of 1.1 $mM \cdot h^{-1}$. With this observed enhancement, we decided to explore the change in the gas environment made by the addition of PFC nanoemulsions.

We performed experiments to understand the mechanism of the observed enhancement when PFC nanoemulsions were added to the hybrid $CO_2$ fixation system (**Chapter 3**). Experiments of flow cytometry were performed using fluorescently tagged PFC nanoemulsions to probe the association of the *S. ovata* with the nanoemulsions. We found a non-specific binding interaction between the nanoemulsion and the bacteria that could result in an increase in the local $H_2$ concentration or an increase in the rate of $H_2$ transfer to the microbes. Rotating disk electrode (RDE) experiments were performed as an electrochemical surrogate to understand the $H_2$ transfer kinetics. Our experiments revealed that there was 3.5 times increase in the kinetic current density with the addition of the nanoemulsion. Additionally, we found that the local $H_2$ concentration was 1.2 times the calculated bulk $H_2$ concentration. This suggests that the addition of the PFC nanoemulsions resulted in a local increase in $H_2$ concentration and an increase in the rate of transfer of the reducing equivalent to the microbe. We theorized that the addition of PFC nanoemulsions

to other hybrid systems could result in similar enhancement and an ability to control the gas environment.

With the success of the PFC nanoemulsion in the hybrid $CO_2$ fixation system, my research shifted to focus on using the nanoemulsions with a hybrid $N_2$ fixation system to enhance ammonia production and self-sufficiency (**Chapter 4**). The hybrid $N_2$ fixation reaction utilizes *Xanthobacter autotrophicus*, a microaerobic bacterial strain that reduces $N_2$ to $NH_3$ through its nitrogenase enzyme. This has previously been accomplished through a precise supplied gas mixture, since the electrochemically generated $O_2$ is poorly soluble in the aqueous solution. We added the PFC nanoemulsions to this system to utilize the electrochemically generated $O_2$ and enhance the throughput of the $N_2$ fixation system. Our experiments demonstrated that the use of PFC nanoemulsions drastically reduced the loss of cell viability in a supplied anaerobic atmosphere and led to a 3-fold increase in Faradaic efficiency of the system during 5-days of running.

We performed mechanistic studies to understand the $O_2$ gas-PFC nanoemulsion environment within the hybrid system (**Chapter 5**). Confocal microscopy images of the PFC nanoemulsions interacting with the microbes revealed binding and complete coverage of the microbe surface by the PFC nanoemulsions. Experiments of RDE were performed to ascertain the $O_2$ transfer kinetics between the PFC nanoemulsions and the microbes. We found that there was a 20-fold increase in the kinetic $O_2$ reduction rate when the PFC nanoemulsions were added. Assuming a Langmuir adsorption model of the PFC nanoemulsion binding to the microbe, we were able to use flow cytometry to determine the maximum number of nanoemulsions that could adsorb to the microbe surface and the equilibrium constant for the adsorption. Our results showed that the number of nanoemulsions that could bind to a given microbe or particle is dependent on

the size of the particle, but the equilibrium constant is more influenced by the surface charge, with the -COOH functionalized microspheres having the largest binding affinity.

In conclusion, my thesis research was able to integrate PFC nanoemulsions with hybrid biological inorganic systems to enhance throughput and alter the gas environment in the systems. The ability to understand and alter the gas environment using these PFC nanoemulsions can allow for other aqueous systems with poor gas transfer rates or gas restrictions to function with enhanced benefits. This dissertation also serves as groundwork for continued research in customizing the PFC nanoemulsion to achieve the optimal binding and gas environment.

The dissertation of Roselyn Rodrigues is approved.

Ellen M. Sletten

Richard B. Kaner

Jeffrey I. Zink

Chong Liu, Committee Chair

University of California, Los Angeles

2021

## DEDICATION

I dedicate this thesis to my parents, Mark Rodrigues and Brigid Crabtree. Thank you for encouraging me to never give up on my dreams, even when they were to be a brain surgeon or Dunkin Donuts. I love you.

## TABLE OF CONTENTS

## LIST OF FIGURES

### CHAPTER 2. PERFLUOROCARBON NANOEMULSION ENHANCED HYBRID BIOLOGICAL INORGANIC CARBON DIOXIDE FIXATION



### CHAPTER 3. HYDROGEN GAS ENVIRONMENT IN HYBRID CARBON DIOXIDE FIXATION SYSTEM

## LIST OF TABLES

### CHAPTER 2. PERFLUOROCARBON NANOEMULSION ENHANCED HYBRID BIOLOGICAL INORGANIC CARBON DIOXIDE FIXATION

## LIST OF ABBREVIATIONS

| | |
|---|---|
| °C | Degrees Celsius |
| C | Coulomb |
| cm | Centimeter |
| $CH_4$ | Methane |
| $CO_2$ | Carbon dioxide |
| Co−P | Cobalt Phosphorus |
| $CoP_i$ | Cobalt Phosphate |
| d | Days |
| DLS | Dynamic Light Scattering |
| *F. E.* | Faradaic Efficiency |
| g | Gram |
| h | Hours |
| $H^+$ | Proton |
| $H_2$ | Hydrogen |
| $N_2$ | Nitrogen |
| l | Liter |
| mA | Milliamp |
| ml | Milliliter |
| mM | Millimolar |
| min | Minutes |
| µl | Microliter |
| nm | Nanometer |

| | |
|---|---|
| NMR | Nuclear Magnetic Resonance |
| PFC | Perfluorocarbon |
| PFD | Perfluorodecalin |
| PFH | Perfluorohexane |
| RDE | Rotating Disk Electrode |
| RHE | Reversible Hydrogen Electrode |
| SHE | Standard Hydrogen Electrode |
| TMSP-$d_4$ | 2,2,3,3-D4 sodium-3-trimethylsilylpropionate |
| V | Voltage |

## ACKNOWLEDGEMENTS

I would like to acknowledge my advisor, Dr. Chong Liu, for taking a chance on me as his first graduate student in his lab. When I joined Dr. Liu's laboratory, I had never performed any electrochemical experiments nor knew how to culture microbes, but Dr. Liu took the time to teach me everything he knows. I want to thank him for his dedication to my graduate career and his constant support.

My dissertation would not be possible without the help from my laboratory group members. Dr. Liu's group members have always been eager to help and listen when projects are difficult. A special thanks to Dr. Shengtao Lu who mentored me on all my culturing experiments. When I struggled with cultures not continuing to grow, Dr. Lu was there to help me try everything he or I could think of to get the microbes growing again. As a co-first author on my second paper Dr. Lu was my partner in writing and experimentation, and the second half of this research is as much mine as it is his. I would also like to thank Xun Guan, Ben Natinsky, Jesus Iñiguez, and Shuyuan Huang from Dr. Liu's lab for all their contributions to my research over the years.

I would also like to give a tremendous thanks to our collaborators at UCLA in the lab of Dr. Ellen Sletten. Dr. Sletten's research sparked the idea for our collaboration, and she has always been a source of inspiration to me. I would also like to recognize the members of Dr. Sletten's lab, Dr. Daniel Estabrook and John Chapman, who were a constant source of support and nanoemulsions. Dr. Estabrook was always there to offer input on the best course of synthesizing nanoemulsions and he taught me how to synthesize and characterize the nanoemulsions myself.

In addition to Dr. Sletten's contribution as a collaborator, I would like to thank her and the other members of my committee Dr. Zink and Dr. Kaner for their advice and support throughout

this process. As Dr. Liu's first graduate student I am grateful for my committee's guidance over the course of my Ph.D.

Lastly, I would like to thank my friends in Dr. Liu's lab and within the department. Benjamin Natinksy, Benjamin Hoar, Dr. Mary Grumbles, and Zachary Hern have all been there for me when my research was at a standstill, or when I had a particularly challenging week of research. I would like to thank them for being a constant source of laughs and encouragement when I was not sure I could continue.

# VITA

## EDUCATION

*University of California, Los Angeles,* Los Angeles, CA
Doctor of Philosophy in Chemistry – Inorganic Concentration — Expected: June 2021
Master of Science in Chemistry – Inorganic Concentration — June 2018

*State University of New York, University at Albany,* Albany, NY
Bachelor of Science in Honors Chemistry – Chemistry Concentration — May 2016

## WORK EXPERIENCE

**Graduate Student Teaching Assistant** — September 2016 − June 2020
Department of Chemistry & Biochemistry, University of California, Los Angeles, Los Angeles, CA
Advisors: Dr. Lavelle, Dr. Liu, Dr. Pang, Dr. Henary, and Dr. Baugh

- Taught General Chemistry for Life Scientists I (Chem 14A) and II (Chem 14B), Chemical Structure (Chem 20A), General and Organic Chemistry Laboratory II (Chem 14CL), and Intermediate Inorganic Chemistry (Chem 171) for a total of 12 quarters with an average overall teaching assistant rating of 8.18 out of a possible 9, with 9 being the best.

**Graduate Student Researcher** — June 2017 – Present
Department of Chemistry & Biochemistry**,** University of California, Los Angeles, Los Angeles, CA
Advisor: Dr. Chong Liu

- Designing hybrid bio-inorganic systems that utilize microbes, electrochemistry, and perfluorocarbon nanoemulsions to efficiently generate value added products from $CO_2$ or $N_2$.
- Utilizing both anaerobic and aerobic microbial growth techniques, electrode synthesis and characterization, electrochemical measurements, and both anaerobic and aerobic electrochemical cell set-up and operation to generate samples.
- Using analytical techniques such as $^1$H NMR, dynamic light scattering (including zeta-potential), flow cytometry, ICP-MS, and UV-Vis spectroscopy to analyze samples.

**Naval Research Enterprise Internship Program (NREIP) Intern**
Naval Research Laboratory, Washington, DC — July 2019 — Sept 2019
Advisor: Dr. Courtney Roberts

- Assisted in testing novel hydrogen-bond (HB) acidic sorbent materials for their adsorption properties when exposed to HB basic compounds of interest.
- Used quartz crystal microbalance (QCM) to measure kinetics of HB basic compound uptake and used attenuated total reflectance infrared (ATR-IR) spectroscopy to measure the shift in the -OH stretching frequency of the sorbent material when exposed to different HB bases.

**Undergraduate Research Assistant**
State University of New York, University at Albany, Albany, NY — July 2014 — May 2016
Advisor: Dr. Jan Halamek

- Designed two different assays to measure creatine kinase or alkaline phosphatase levels in a simulated blood sample to determine characteristics of the donor, such as ethnicity or age, respectively.

## AWARDS AND FELLOWSHIPS

| | |
|---|---|
| **UCLA Inorganic Chemistry Dissertation Award** ($500) | June 2021 |
| **UCLA Graduate Division Dissertation Year Fellowship** ($20,000) | Fall 2020 – June 2021 |
| **UCLA Chemistry & Biochemistry Excellence in Research Fellowship** ($3250) | Spring 2020 |
| **Dafni Amirsakis Memorial excellence in Research Award** ($500) | Spring 2020 |
| **UCLA Excellence in Second Year Academics and Research Award** ($500) | 2019 |
| **UCLA Hanson-Dow Excellence in Teaching Award** ($500) | 2018 |
| **University at Albany Chemistry Faculty Award** | 2016 |
| **CRC Press Freshman Book Award for Outstanding Achievement in Chemistry** | 2013 |

## PUBLICATIONS

1. S. Lu, R. M. Rodrigues, S. Huang, D. A. Estabrook, J. O. Chapman, X. Guan, E. M. Sletten and C. Liu. "Perfluorocarbon Nanoemulsions Create a Beneficial $O_2$ Microenvironment in $N_2$-fixing Biological | Inorganic Hybrid", *Chem Catalysis,* (In press).
2. T. G. Grissom, C. A. Roberts, R. Rodrigues, M. R. Papantonakis, V. Nguyen, and R. A. McGill, "Sorbent interactions with hazardous chemicals and spectral detection strategies," Proc. SPIE 11416, Chemical, Biological, Radiological, Nuclear, and Explosives (CBRNE) Sensing XXI, 114160J, doi: 10.1117/12.2558949, (27 April 2020).
3. R. M. Rodrigues, X. Guan, J. Iñiguez, D. A. Estabrook, J.O. Chapman, S. Huang, E. M. Sletten, and C. Liu. "Perfluorocarbon Nanoemulsion Promotes the Delivery of Reducing Equivalents for Electricity-driven Microbial $CO_2$ Reduction", *Nat. Cat.,* doi:10.1038/s41929-019-0264-0, (2019).
4. J. Agudelo, L. Halámková, E. Brunelle, R. Rodrigues, C. Huynh, and J. Halámek. "Ages at a Crime Scene: Simultaneous Estimation of the Time since Deposition and Age of Its Originator", *Analytical Chemistry,* 88, 6479-6484, (2016).

## RESEARCH POSTERS/ORAL PRESENTATIONS

1. "Perfluorocarbon nanoemulsions alleviate kinetic bottlenecks in electricity-driven microbial $CO_2$ reduction," **Materials Research Society Fall 2018 Meeting, Symposium on Materials Science Facing Global Warming—Practical Solutions for Our Future (Nov. 2018),** *ORAL PRESENTATION*.
2. "Perfluorocarbon nanoemulsions enhance kinetics in hybrid biological inorganic $CO_2$-reducing system for increased output." **2018 Glenn T. Seaborg Symposium and Medal Award Dinner, University of California Los Angeles (Nov. 2018),** *POSTER PRESENTATION.*
3. "Enzymatic determination of the time since deposition and age of a blood sample originator at crime scenes," **Honors Undergraduate Thesis Presentation, University at Albany (May 2016)**, *ORAL PRESENTATION.*
4. "Bloodstains: Enzyme-based analysis for discerning the age of the orginator," **UAlbany Undergraduate Research Symposium, University at Albany (April 2016),** *ORAL PRESENTATION.*
5. "Enzymatic determination of the age of a blood sample originator." **State University of New York (SUNY) Undergraduate Research Conference, SUNY Cobleskill, Cobleskill, NY (April 2016),** *ORAL PRESENTATION.*
6. "Spectrophotometric enzyme analysis to determine age of a blood spot originator," **Eastern New York ACS Undergraduate Research Symposium, Sienna College, Loudonville, NY (April 2016),** *ORAL PRESENTATION.*
7. "Forensic estimation of originator's age from blood samples," **UAlbany Undergraduate Symposium for Chemistry Research, University at Albany (October 2015),** *ORAL PRESENTATION.*

# CHAPTER 1. INTRODUCTION

## Importance of $CO_2$ Fixation

With global levels of carbon dioxide ($CO_2$) rising steadily since the industrial revolution, the world has begun investing in alternative energy sources. The main renewable energy sources, wind and solar, only produce energy on an intermittent basis. The unreliable nature of renewable energy has led to a search for strategies to store the electrical energy generated.[1] One promising approach is to store the electrical energy in covalent chemical bonds by producing commodity chemicals. Of particular interest is the conversion of $CO_2$ into useful chemicals. This approach achieves removal of atmospheric $CO_2$ while simultaneously storing intermittent electrical energy. Techniques to convert $CO_2$ into commodity chemicals include electrochemical, photocatalytic, thermocatalytic, and biocatalytic $CO_2$ reduction.[2-6] While these approaches have had varying levels of success, the combination of an electrochemical system with biocatalytic $CO_2$ reduction has been performed to achieve maximum chemical output with minimum energy input.

## Electrochemical $CO_2$ Fixation

Electrochemical $CO_2$ fixation has been demonstrated using metal electrodes in aqueous and organic solution to produce a variety of commodity chemicals. The most common products of electrochemical $CO_2$ production, in either organic or aqueous solution, are formic acid, oxalic acid, and carbon monoxide.[7,8] One challenge to aqueous electrochemical $CO_2$ reduction is the generation of hydrogen from the competing electrochemical hydrogen evolution reaction (HER).[7,8] This competition results in large overpotentials to avoid HER and attempt to selectively make the desired products. Selectivity is also a concern, as controlling the reduction to only generate one product is difficult. This results in low faradaic efficiency, which is the efficiency of the

electrochemical system using the supplied electrons to generate a select product. Efforts to enhance faradaic efficiency and avoid competing HER have focused on optimizing the electrode materials. While selectivity and efficiency are a challenge for electrochemical $CO_2$ fixation, biological $CO_2$ fixation using microorganisms allows for more specific products to be generated and requires far less energy input.

**Hybrid $CO_2$ Fixation**

In a hybrid biological and electrochemical system, microbes are coupled with an electrochemical system as the source of electrons for the microbial $CO_2$ reduction. The most widely used microbes for hybrid $CO_2$ fixation are the acetogenic anaerobic strain *Sporomusa ovata.* This strain is so common due to its ability to accept reducing equivalents from the electrochemical system and reduce $CO_2$ via the Wood-Ljungdhal pathway.[9-12] *S. ovata* can accept $H_2$ gas as the electron donor, however, it is not considered widely practical due to requiring expensive catalysts and substantial energy inputs.[10] Liu *et. al.* have developed a catalytic water-splitting electrode system that is biologically compatible, contributes minimal reactive oxygen species, and allows for $H_2$ as the electron donor with minimal energy input.[13] In this system water is split into protons and $O_2$ gas at the anode while the cathode performs hydrogen evolution reaction (HER).[13] While this system has been coupled with other microbes to produce methane with high faradaic efficiency, the throughput of the system has a bottleneck due to poor solubility of the $H_2$ reducing equivalent in the system.[13] The solubility of the hydrogen creates a maximum threshold, where no matter the volume of gas that is produced by the cathode, the output of commodity chemicals will not increase. To apply this system to real world applications, the solubility of the gas must be increased to allow for maximum device throughput. Increasing the accessibility of the reducing equivalent

in the system would alleviate this bottleneck, allow for enhanced throughput, and increase the chemical output.

**$N_2$ Fixation**

The conversion of $N_2$ into $NH_3$ is an essential process for the production of fertilizers for global agriculture, however, the industrial method of $NH_3$ production is energy intensive and produces large quantities of $CO_2$.[14-16] Hybrid biological | inorganic $N_2$ fixation systems have been designed to produce $NH_3$ and biofertilizers under ambient conditions, while simultaneously fixing $CO_2$.[17-19] In this approach, an electrochemical water-splitting system is coupled with $N_2$ fixing microbes *Xanthobacter autrophicus* to convert $H_2$ and $CO_2$ into biomass and $N_2$ into $NH_3$. The biomass production requires $O_2$ as a terminal electron acceptor, however, the nitrogenase enzyme required to produce $NH_3$ is sensitive to $O_2$ levels greater than 5%. As a result, the system is microaerobic and requires a precise control of the $O_2$ concentration in solution. The water-splitting reaction electrochemically generates $O_2$, but its weak solubility in solution necessitates an additional external supply of $O_2$ to keep the $O_2$ levels ideal. Previously reported systems have used a precise mixture of gases to maintain the optimal $O_2$ concentration for microbe growth and $N_2$ fixation. While effective, this mixture is expensive and energy intensive to produce. The ability to increase the $O_2$ solubility and transport within the hybrid system would allow for the system to be more self-sufficient and operate under anaerobic gas conditions.

**Perfluorocarbon Nanoemulsions**

Perfluorocarbon (PFC) chemicals are a class of fluorinated hydrocarbons that are proven to be chemically stable, biologically inert, and have the capability to physically dissolve large quantities

of gas.[20-23] The carbon-fluorine bond makes the chemicals hydrophobic and highly stable under a variety of reaction conditions. The stability, biological inertness, and high gas solubility of PFCs has made them a widely studied chemical for use as potential blood substitutes.[20-23] However, the hydrophobic nature of the PFCs necessitates their emulsification if they are to be used in aqueous environments. A variety of surfactants have been used to emulsify the PFCs and create emulsions with a wide range of applications.[22,24-26] By varying the surfactant, the PFC, and the ratio of the components the properties of the emulsion can be adjusted. In recent years, these molecules have been used to enhance microbe growth in biomass production due to their exceptional ability to increase the solubility of gases that are important to their growth, such as $O_2$, $CO_2$, and $H_2$ gas.[27]

**SUMMARY**

Both hybrid biologic inorganic $CO_2$ and $N_2$ fixation reactors couple electrochemical water-splitting systems with microbes to achieve high efficiency reduction with minimal energy input. This approach takes advantage of an inorganic catalyst's capability to efficiently transduce electricity into a chemical driving force, as well as a biocatalyst's high reaction selectivity and versatility. However, both systems are limited by the supply of gas, $H_2$ or $O_2$, to the microbes. This prompted my research into using PFC nanoemulsions to increase the gas solubility of $H_2$ gas for the $CO_2$ fixation system (**Chapter 2**). We observed enhanced throughput and were able to perform mechanistic studies into the microbe and PFC nanoemulsion interaction in the $CO_2$ fixation system (**Chapter 3**). This led us to apply the PFC nanoemulsions to the hybrid $N_2$ fixation system (**Chapter 4**) and further characterize the $O_2$ gas environment created with the PFC nanoemulsions (**Chapter 5**).

**References**


1. Lewis, N. S. & Nocera, D. G. Powering the planet: Chemical challenges in solar energy utilization. *Proc. Natl. Acad. Sci.* **103**, 15729, doi:10.1073/pnas.0603395103 (2006).
2. Atsonios, K., Panopoulos, K. D. & Kakaras, E. Thermocatalytic CO 2 hydrogenation for methanol and ethanol production: Process improvements. *Int. J. Hydrog. Energy* **41**, 792-806, doi:10.1016/j.ijhydene.2015.12.001 (2016).
3. Kumar, A. *et al.* Enhanced CO(2) fixation and biofuel production via microalgae: recent developments and future directions. *Trends. Biotechnol.* **28**, 371-380, doi:10.1016/j.tibtech.2010.04.004 (2010).
4. Jones, J.-P., Prakash, G. K. S. & Olah, G. A. Electrochemical CO2 Reduction: Recent Advances and Current Trends. *Isr. J. Chem.* **54**, 1451-1466, doi:10.1002/ijch.201400081 (2014).
5. Hori, H., Johnson, F. P. A., Koike, K., Ishitani, O. & Ibusuki, T. Efficient photocatalytic CO2 reduction using [Re(bpy) (CO)3{P(OEt)3}]+. *Journal of Photochemistry and Photobiology A: Chemistry* **96**, 171-174, doi:https://doi.org/10.1016/1010-6030(95)04298-9 (1996).
6. Windle, C. D. & Perutz, R. N. Advances in molecular photocatalytic and electrocatalytic CO2 reduction. *Coord. Chem. Rev.* **256**, 2562-2570, doi:10.1016/j.ccr.2012.03.010 (2012).
7. Mikkelsen, M., Jørgensen, M. & Krebs, F. C. The teraton challenge. A review of fixation and transformation of carbon dioxide. *Energy Environ. Sci.* **3**, 43-81, doi:10.1039/b912904a (2010).
8. Jhong, H.-R. M., Ma, S. & Kenis, P. J. A. Electrochemical conversion of CO2 to useful chemicals: current status, remaining challenges, and future opportunities. *Curr. Opin. Chem. Eng.* **2**, 191-199, doi:10.1016/j.coche.2013.03.005 (2013).

9. Drake, H. L., Gossner, A. S. & Daniel, S. L. Old acetogens, new light. *Ann. N. Y. Acad. Sci.* **1125**, 100-128, doi:10.1196/annals.1419.016 (2008).
10. Nevin, K. P., Woodard, T. L., Franks, A. E., Summers, Z. M. & Lovley, D. R. Microbial electrosynthesis: feeding microbes electricity to convert carbon dioxide and water to multicarbon extracellular organic compounds. *MBio* **1**, doi:10.1128/mBio.00103-10 (2010).
11. Nevin, K. P. *et al.* Electrosynthesis of organic compounds from carbon dioxide is catalyzed by a diversity of acetogenic microorganisms. *Appl. Environ. Microbiol.* **77**, 2882-2886, doi:10.1128/AEM.02642-10 (2011).
12. Aryal, N., Tremblay, P. L., Lizak, D. M. & Zhang, T. Performance of different Sporomusa species for the microbial electrosynthesis of acetate from carbon dioxide. *Bioresour. Technol.* **233**, 184-190, doi:10.1016/j.biortech.2017.02.128 (2017).
13. Liu, C., Colón, B. C., Ziesack, M., Silver, P. A. & Nocera, D. G. Water splitting–biosynthetic system with $CO_2$ reduction efficiencies exceeding photosynthesis. *Science* **352**, 1210 (2016).
14. Tilman, D., Cassman, K. G., Matson, P. A., Naylor, R. & Polasky, S. Agricultural sustainability and intensive production practices. *Nature* **418**, 671-677, doi:10.1038/nature01014 (2002).
15. Jensen, E. S. & Hauggaard-Nielsen, H. How can increased use of biological N2 fixation in agriculture benefit the environment? *Plant and Soil* **252**, 177-186, doi:10.1023/A:1024189029226 (2003).
16. Tilman, D., Balzer, C., Hill, J. & Befort, B. L. Global food demand and the sustainable intensification of agriculture. *Proc. Natl. Acad. Sci. U.S.A.* **108**, 20260-20264, doi:10.1073/pnas.1116437108 (2011).

17. Liu, C., Sakimoto, K. K., Colón, B. C., Silver, P. A. & Nocera, D. G. Ambient nitrogen reduction cycle using a hybrid inorganic–biological system. *Proc. Natl. Acad. Sci.* **114**, 6450-6455 (2017).
18. Zhang, L. *et al.* Efficient Electrochemical N2 Reduction to NH3 on MoN Nanosheets Array under Ambient Conditions. *ACS Sustain. Chem. & Eng.* **6**, 9550-9554, doi:10.1021/acssuschemeng.8b01438 (2018).
19. Liu, H. *et al.* Homogeneous, Heterogeneous, and Biological Catalysts for Electrochemical N2 Reduction toward NH3 under Ambient Conditions. *ACS Catal.* **9**, 5245-5267, doi:10.1021/acscatal.9b00994 (2019).
20. Spahn, D. Blood substitutes Artificial oxygen carriers: perfluorocarbon emulsions. *Critical Care* **3**, R93, doi:10.1186/cc364 (1999).
21. Squires, J. E. Artificial blood. *Science* **295**, 1002-1005 (2002).
22. Riess, J. G. Understanding the Fundamentals of Perfluorocarbons and Perfluorocarbon Emulsions Relevant to In Vivo Oxygen Delivery. *Artif. Cells, Blood Substit., and Biotechnol.* **33**, 47-63, doi:10.1081/BIO-200046659 (2005).
23. Castro, C. I. & Briceno, J. C. Perfluorocarbon-based oxygen carriers: review of products and trials. *Artif. Organs* **34**, 622-634, doi:10.1111/j.1525-1594.2009.00944.x (2010).
24. Sletten, E. M. & Swager, T. M. Fluorofluorophores: fluorescent fluorous chemical tools spanning the visible spectrum. *J. Am. Chem. Soc.* **136**, 13574-13577, doi:10.1021/ja507848f (2014).
25. Day, R. A., Estabrook, D. A., Logan, J. K. & Sletten, E. M. Fluorous photosensitizers enhance photodynamic therapy with perfluorocarbon nanoemulsions. *Chem. Commun. (Camb)* **53**, 13043-13046, doi:10.1039/c7cc07038a (2017).

26. Estabrook, D. A., Ennis, A. F., Day, R. A. & Sletten, E. M. Controlling nanoemulsion surface chemistry with poly(2-oxazoline) amphiphiles. *Chem. Sci.* **10**, 3994-4003, doi:10.1039/c8sc05735d (2019).

27. Lowe, K. C., Davey, M. R. & Power, J. B. Perfluorochemicals: their applications and benefits to cell culture. *Trends Biotechnol.* **16**, 272-277, doi:https://doi.org/10.1016/S0167-7799(98)01205-0 (1998).

# CHAPTER 2: PERFLUOROCARBON NANOEMULSION ENHANCED HYBRID BIOLOGICAL INORGANIC CARBON DIOXIDE FIXATION

This chapter is a version of Rodrigues, R. M.; Guan, X.; Iñiguez, J. A.; Estabrook, D. A.; Chapman, J. O.; Huang, S.; Sletten, E. M.; and Liu, C. "Perfluorocarbon nanoemulsion promotes the delivery of reducing equivalents for electricity-driven microbial $CO_2$ reduction." *Nature Catalysis.* **2019**, 2, 407-414.

## Abstract

Hybrid biological inorganic hybrid systems for $CO_2$ fixation have been used to electrochemically split water while converting $CO_2$ into value added chemicals. While these systems have demonstrated high efficiencies, their throughput can be limited by the poor solubility of the reducing equivalents in solution. Here, we utilized PFC nanoemulsions to enhance the productivity of the hybrid system. A mixture of PFH and PFD in a percentage of 2.5 % (v/v) was combined with the bacteria *Sporomusa ovata* to enhance the conversion of $CO_2$ into acetic acid. Our improved system demonstrated up to 190 % enhancement in acetic acid production and nearly 100 % *F.E.* for all tested current densities with PFC nanoemulsions. We proved that the addition of the PFC nanoemulsions led to an enhanced system throughput.

## Introduction

The reduction of carbon dioxide ($CO_2$) into commodity chemicals and fuels is a promising way to transform and store renewable energies while removing greenhouse gases.[1,2] A variety of approaches have been explored with the use of electricity, light, or heat as the thermodynamic driving forces.[3-7] Current research focus is shifting towards developing strategies to improve the

overall energy efficiency, productivity, and selectivity towards multi-carbon organic molecules.[2,8,9] We are interested in integrating inorganic electrochemical catalysts with $CO_2$-fixing microorganisms, an approach that has demonstrated versatile selectivity towards complex molecules.[10-12] Such a hybrid approach has achieved great strides in recent years, thanks to the synergy of favorable properties between materials and biology.[10,13-18] In order to achieve an energetically efficient and kinetically fast transfer of energy and electrons, interfacing materials and biology is essential.[19-21] To date, there have been extensive studies for the catalytic materials and the biocatalysts separately but successful combination of the two has not been fully achieved.

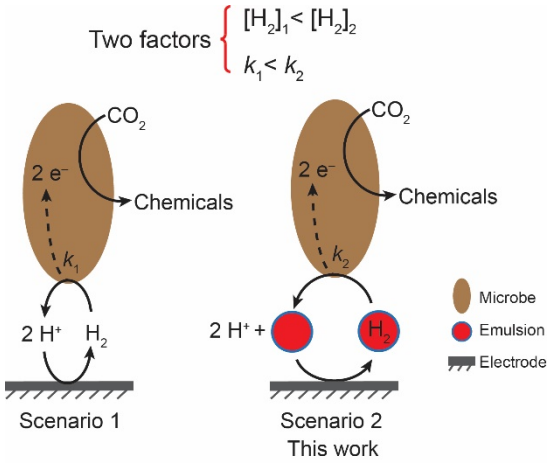


**Figure 2.1. Schematic of the hybrid system that integrates water-splitting catalysts with $CO_2$-fixing microorganisms.** Scenario 1: Traditional electrochemical catalysts yield $H_2$, a gaseous product with limited solubility in water ($[H_2]_1$). The generated $H_2$ is transferred as a reducing equivalent to microbes for $CO_2$ reduction with a kinetic rate $k_1$. Scenario 2: In this work, we applied perfluorocarbon (PFC) nanoemulsions as a $H_2$ carrier to accelerate the transfer of reducing equivalents. PFC nanoemulsions not only increase the $H_2$ concentration in the solution ($[H_2]_2$) but also accelerate the transfer kinetics ($k_2$), which increases the rate of $CO_2$ fixation by 190%. In both

Scenario 1 and Scenario 2 the conversion of protons to $H_2$ occurs at the electrode surface, but the microbes are in the bulk solution.

We recently developed a biocompatible biological-inorganic hybrid that displayed high efficiencies for electricity-driven $CO_2$ and $N_2$ fixations.[10,22] In these systems, water is split to oxygen by a cobalt phosphate ($CoP_i$) catalyst and hydrogen ($H_2$) is produced by a cobalt-phosphorous (Co-P) alloy catalyst with small thermodynamic driving forces. The generated $H_2$ is selectively consumed by the hydrogenases of autotrophic microorganisms[23] in the solution and powers the biochemical reduction of $CO_2$ and $N_2$ into commodity chemicals (Scenario 1 in Fig. 1). High energy efficiency is achievable with the developed biocompatible catalytic system that yields minimal toxic metals or reactive oxygen species (ROS).[10] However, the interface between inorganic catalysts and microorganisms is not ideal for high reaction throughput. We found that the kinetics of $H_2$ oxidation in hydrogenases is rate-determining due to the limited $H_2$ delivery from the electrode.[10,24] As $H_2$ has a limited solubility of 0.79 mM in water at ambient conditions,[25] a high flux of water-splitting reactions on the electrodes is not readily translatable to a high productivity of $CO_2$ fixation and may lead to a decrease of *F. E.*[24] Replacing $H_2$ with other more soluble redox mediators has been reported, but the less selective delivery of reducing equivalents can create stress in microbes and lead to lower efficiency.[11,20,26] Here, we demonstrate that the productivity bottleneck may be overcome by introducing a carrier of high $H_2$ solubility and fast delivery kinetics, at the same time retaining the desirable selectivity and biocompatibility of $H_2$ as the redox mediator.[23]

PFC nanoemulsions are a suitable $H_2$ carrier for high productivity of $CO_2$ fixation (Scenario 2 in Fig. 2.1). PFC molecules are biologically inert and have an impressive ability to dissolve a

substantial volume of gas due to the molecules' rigidity and weak intermolecular interactions.[27] Taking these advantages, PFC emulsions have been used as blood substitute[27] and in microbial reactors for enhanced biofuel production.[28,29] As a potential $H_2$ carrier, the solubility of $H_2$ in PFCs is up to one order of magnitude higher than in water.[30] Moreover, PFC nanoemulsions are an attractive platform for multifunctional nanomaterials with simple preparation methods.[31,32] We postulate that the small size of nanoemulsions, at the range of hundreds of nanometers, can accelerate the kinetics of $H_2$ delivery and thereby alleviate the throughput constraints. Here we report our finding that the introduction of PFC nanoemulsions significantly increases the rate of electricity-driven $CO_2$ fixation to acetic acid in bacterium *Sporomusa ovata*,[33] a model microbial catalyst that can receive reducing equivalents from electrodes, or from the oxidation of hydrogen as we report here, to reduce $CO_2$ via the Wood-Ljungdahl pathway.[34-37]

## Results

### Compatibility of PFC nanoemulsion with the hybrid system.

The addition of PFC nanoemulsions does not inhibit the $CO_2$-fixing metabolism in bacterium *S. ovata*. The *S. ovata* was chosen as a model microbial catalyst due to its previous success in similar systems[34-37] and the ease of product quantification. Aqueous PFC nanoemulsions composed of perfluorohexane and perfluorodecalin were prepared by point-sonication with the addition of biocompatible surfactant Pluronic F68 (see Methods for details).[31] These specific PFCs were chosen due to their relatively high $H_2$ solubilities, 7.57 and 5.37 mM respectively, stability under our necessary conditions (Supplementary Fig. 1), and relative low cost. Dynamic light scattering (DLS) experiments show that the nanoemulsions have an average size of 236 ± 19 nm immediately after preparation (Supplementary Fig. 1). Continuous monitoring with DLS measurements shows

that the average size of the nanoemulsion increased initially but stabilized at 500 ~ 600 nm in the media solution within 4 days (Supplementary Fig. 1). The viability of *S. ovata* in the presence of nanoemulsion was tested by incubating the microbial culture in a $H_2/CO_2$ (80/20) gas mixture. The accumulation of acetic acid, the major product of the Wood-Ljungdahl pathway from $H_2$ oxidation,[14] is used as the indicator of microbial growth. The concentration of acetic acid was monitored with $^1H$ Nuclear Magnetic Resonance (NMR) (Supplementary Fig. 2), and the difference of acetate concentration before and after the three-day incubation was recorded (see Methods for details). We found that the rate of $CO_2$ reduction indeed increased with the presence of PFC nanoemulsion (Supplementary Fig. 3). Such an observed increase is not from the surfactant, as control experiment with only surfactant added did not show any prominent enhancement (Supplementary Fig. 3). Our experiments also indicate that Pluronic F68 did not participate in the metabolism of *S. ovata* and all the detected acetic acid was the result of $CO_2$ fixation. The accumulation rate of acetic acid can be increased by 137% with the addition of 5% PFC (v/v, same below), implying the favorable properties of PFC nanoemulsion as a $H_2$ carrier.

The PFC nanoemulsions as a proposed $H_2$ carrier did not significantly perturb the activities of inorganic water-splitting catalysts. An inorganic Co-P alloy catalyst loaded on stainless steel electrode was prepared by electrochemical deposition based on a previously reported recipe (see Methods for details).[10] Co-P alloy catalyst is capable of electrochemically reducing proton into $H_2$,[38,39] and exhibits little toxicity to biocatalysts as it generates minimal ROS.[10,22] We studied the possible activity change of $H_2$ generation for Co-P alloy in 2.5% PFC nanoemulsions (see Methods for details). The *j*-V correlations determined by multi-step chronoamperometry is plotted in Fig. 2.2A. The introduction of nanoemulsion did not significantly modify the catalytic behavior within experimental uncertainties. Similar behaviors were also observed by cyclic voltammetry at other

PFC percentages up to 5% (Supplementary Fig. 4). Additionally, electrochemical impedance spectroscopy revealed that the electric resistivity of the media solution did not increase when the nanoemulsions were added (Supplementary Fig. 5), thanks to the small volume percentage of the PFC nanoemulsion $H_2$ carriers. These results indicate that there won't be much additional voltage and energy cost from solution resistivity when PFC nanoemulsions are added. These electrochemical characterizations and the biological viability test show that PFC nanoemulsions are compatible with the hybrid system.

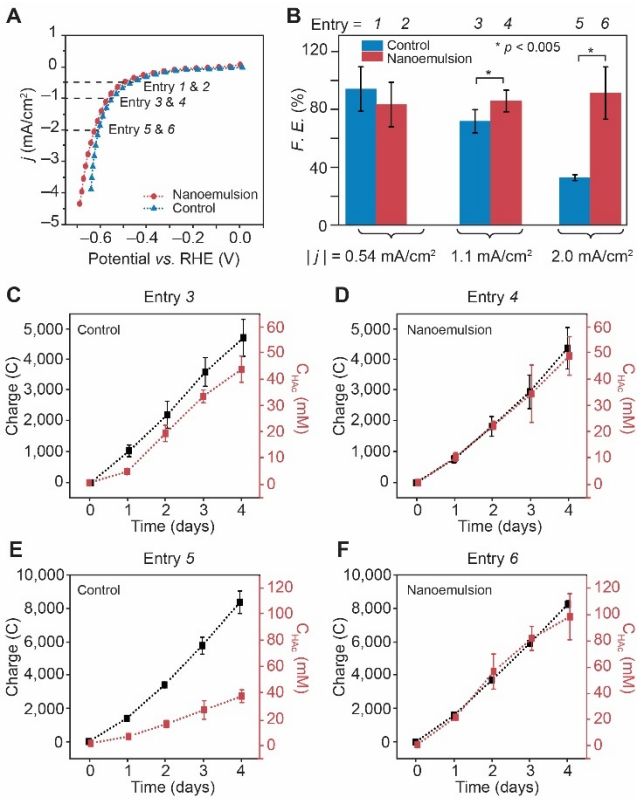


**Figure 2.2. The introduction of PFC nanoemulsions increases the productivity of $CO_2$ reduction. A,** *j*-V curves of Co-P alloy for hydrogen generation with (red) and without (blue) the addition of PFC nanoemulsion (2.5% v/v). RHE, reversible hydrogen electrode. **B**, Faradaic efficiencies (*F. E.*) of electricity-driven $CO_2$ reduction into acetate at current densities of 0.54 (Entry *1* and *2*), 1.1 (Entry *3* and *4*), and 2.0 mA/cm$_2$ (Entry *5* and *6*). Comparisons were made

between solutions with (red) and without (blue) PFC nanoemulsion (2.5%). **C to F,** Acetic acid (HAc) was selectively produced from $CO_2$ with electricity input without (C and E) and in the presence of nanoemulsion (d and f) at different current densities. The electric charge (black) and acetate concentrations (red) are plotted versus the duration of the experiments. The error bar denotes SEM, $n \geq 3$ in b to f, and * represents a $p$-value < 0.005.

**Observation of enhanced productivity from PFC nanoemulsions**.

The introduction of PFC nanoemulsions increased the productivity of electricity-driven $CO_2$ reduction to acetic acid by 190%. $CO_2$ fixation proceeded in a two-chamber three-electrode reactor that was half-filled with *S. ovata* culture under a $CO_2/N_2$ (20/80) gas mixture (Supplementary Fig. 6). A constant potential versus the reference electrode was applied to the Co-P alloy catalyst for proton reduction (Supplementary Fig. 7). At a current density ($j$) of 0.54 mA/cm$^2$, *F. E.* = 94 ± 15 % and 90 ± 16 % for reactors without and with the addition of 2.5% nanoemulsions, respectively (entry *1* and *2* in Fig. 2B, $n \geq 3$). In 4 days, both conditions yielded about 20 mM of acetic acid (Supplementary Fig. 8), which corresponds to a productivity ($r_{CO2}$) of about 0.39 g·L$^{-1}$·day$^{-1}$ (Supplementary Table 1). This shows that the introduction of PFC nanoemulsions does not disrupt the transfer of reducing equivalents. When $j$ = 1.0 mA/cm$^2$, the *F. E.* without nanoemulsion decreased to 71 ± 8 % (entry *3,* $n$ = 4), while *F. E.* remained close to unity (92 ± 8%) when PFC nanoemulsions were added (entry *4,* $n$ = 3). A linear concentration increase of acetic acid was observed within 4 days along with the passage of electric charge (Fig. 2C and 2D), implying that the generation of acetic acid is powered by electricity. It also shows that with the absence of nanoemulsion the hybrid system may have reached its throughput bottleneck and about 29% of the generated $H_2$ was not used by the microbes, probably due to the limited solubility of $H_2$ in water.

In contrast, the addition of nanoemulsion seemed to lift this bottleneck and almost all of the generated $H_2$ was utilized. Such a contrast should be more prominent at even higher current density. However, as $H_2$ production on Co-P catalyst will deplete proton and generate pH gradient near the electrodes, high current density of water-splitting is not readily compatible with bacterial culture. We observed that in the standard medium solution with 18.5 mM of phosphate buffer, there is significant inhibition of microbial growth when $j > 1.0$ mA/cm$^2$, even in the absence of PFC nanoemulsions (Supplementary Table 1). We believe this inhibition is the result of a detrimental increase in pH that occurs when the applied current density surpasses the maximum buffered current density. This led us to develop a model of predicting the conditions needed to afford a high current density without significant pH gradient (see Methods for details) and test the viability of *S. ovata* at higher salt concentrations (Supplementary Fig. 9). We found that when the concentration of phosphate buffer is 55.5 mM, the metabolism of *S. ovata* is not hindered as the detrimental pH gradient is minimized. We were able to achieve a continuous $CO_2$ reduction to acetic acid with $j = 2.0$ mA/cm$^2$ (Fig. 2E and 2F, respectively). At $j = 2.0$ mA/cm$^2$, *F. E.* = 33 ± 2 % in the absence of nanoemulsions (entry *5, n* = 3), while *F. E.* = 99 ± 19 % when PFC nanoemulsions were added (entry *6, n* = 4). The introduction of PFC nanoemulsions lead to a final titer $C_{HAc} = 6.4 \pm 1.1$ g·L$^{-1}$ (107 mM) for acetic acid within 4 days (Supplementary Table 1), which is 2.9 times of the titer when nanoemulsions were not used ($2.2 \pm 0.3$ g·L$^{-1}$). This final titer reaches the maximum predicted acetic acid that could be produced under our electrochemical conditions. According to calculations, with a total electrode area of 12 cm$^2$ and an applied $j = 2$ mA/cm$^2$, the total current is 24 mA. When applied for 4 days there is a total transfer of 86 mmol of electrons, which corresponds to a maximum acetic acid generation of 0.644 g in a 100-mL volume or 6.44 g/L. The highest productivity $r_{CO2} = 1.6$ g·L$^{-1}$·day$^{-1}$ with the PFC nanoemulsion $H_2$ carrier is

greater than other existing bioelectrochemical systems for the generation of acetic acid from $CO_2$ (Supplementary Table 2 and 3). Furthermore, this productivity is on par with gas fermentation powered by an electrolyzer (Supplementary Table 4).[40] Lastly, the linear correlation between electric charge and $C_{HAc}$ (Fig. 2F) implies that the beneficial effect of the PFC nanoemulsions is stable over the duration of experiments and could be applied for long-term operation.

## Discussion

The process of transferring $H_2$ as a reducing equivalent to microbes is significantly accelerated and the local environment is enriched with $H_2$ at the nanoemulsion's surface. Such an accelerated $H_2$ transfer lead to the observed 190% increase of productivity. As PFC is biologically inert and compatible with inorganic catalysts, the benefits of PFC nanoemulsions are generally applicable to other biohybrid systems. We posit that further improvements to this system could be made through combining our approach with other $CO_2$ reducing micro-organisms, an external electrolyzer, or an optimized electrochemical set-up. Our reported approach allows us to alleviate the throughput bottlenecks in electricity-driven microbial $CO_2$ reduction, thus providing a platform with high productivity for distributed chemical production with renewable electricity.

## Methods

### Materials and chemicals.

All chemicals were purchased from Sigma−Aldrich, Thermo Fisher Chemical, or VWR International, unless otherwise stated. Perfluorocarbons (PFCs) were purchased from SynQuest Laboratories. $^1$H-Nuclear Magnetic Resonance (NMR) standard TMSP-$d_4$ (2,2,3,3-D4 sodium-3-trimethylsilylpropionate, 98%) and NMR solvent deuterium oxide ($D_2O$) were purchased from

Cambridge Isotope Laboratories, Inc. All deionized (DI) water was obtained from a Millipore Millipak® Express 40 system. Stainless steel (SS) mesh was purchased from Alfa Aesar and carbon cloth (CC) was purchased from Fuel Cell Earth.

**Synthetic procedures of materials**

*PFC Nanoemulsions.* Nanoemulsions were prepared via previously reported procedure.[31] 2.8 wt% of surfactant, Pluronic F68, was added to the relevant buffer and sonicated in a bath sonicator, Branson 3800 ultrasonic cleaner, to thoroughly dissolve the polymer. 450 μL of perfluorodecalin, PFD, and 450 μL of perfluorohexane, PFH, were combined in a 15-mL centrifuge tube. The total volume was diluted up to 10 mL with relevant surfactant-containing buffer. Baseline medium, detailed in section "Medium Recipes of Microbial Cultures", was used as the buffer for all experiments, except rotating disk electrode experiments where a phosphate buffer was used instead. The liquid was then sonicated at 35% amplitude for 5 minutes (3 watts, Qsonica). Size distributions of resulting nanoemulsions were analyzed following procedure outlined below in section "Dynamic Light Scattering".

*Electrode preparations.* The Co-P alloy and $CoP_i$ electrodes were both prepared via electrochemical deposition using a Gamry Interface 1000 potentiostat, following previously reported procedures.[10] The electrochemical deposition was run using a three-electrode system consisting of a working electrode of the substrate to be electrodeposited, a Pt counter electrode, and a Ag/AgCl reference electrode (1M KCl) purchased from CH Instruments. The Co-P alloy catalyst was prepared via cathodic electrochemical deposition onto SS mesh. The deposition solution consists of 0.15 M $H_3BO_3$, 0.1 M NaCl, 0.33 $Na_2H_2PO_2$, and 0.2 M $CoCl_2$. The SS mesh was sequentially cleaned with acetone, isopropanol, and then soaked in DI water before

electrodeposition. To deposit the Co-P alloy catalyst, the SS mesh as the substrate underwent chronocoulometry for 15 min at an applied voltage of −1.5 V *vs.* reference. The $CoP_i$ electrode was prepared using a deposition solution containing 10 mM $Co(NO_3)_2$ and 0.1 M methylphosphonate ($MeP_i$) buffer of pH 8. $CoP_i$ catalyst loaded on CC substrate was deposited via chronocoulometry at 0.85 V *vs.* reference until 500 $mC/cm^2$ of charge was passed.

**Dynamic Light Scattering**

Dynamic light scattering (DLS) experiments were conducted with a Malvern Zetasizer Nano ZSP instrument. 20 μL PFC nanomulsions were diluted in 2 mL DI water in a plastic cuvette. Data in Supplementary Fig. 1 is representative of three repeated measurements ($n = 3$). Error bars represent the averaged half-width at half-maximum of the measurements. The stability of the PFC nanoemulsion over the course of the experiment was tested with a small-scale mimic of the reactors applied in electricity-driven $CO_2$ fixation. A 20-mL screw-top vial with 10 mL of solution containing 2.5% PFC nanoemulsion and 97.5% baseline medium was stirred at 150 rpm in the water bath. 83.3 μL of liquid was sampled daily from the vial and diluted to a final volume 2 mL with DI water. This 2 mL of sample was then analyzed using DLS following the same protocol as outlined above.

**Protocols of culturing microorganisms**

*Protocol of culturing anaerobic microorganisms.* The anaerobic bacterium *Sporomosa ovata* (ATCC 35899, DSM 2662) was purchased from American Type Culture Collection (ATCC).[33] Detailed recipes of the culture media mentioned in this section are provided in section "Medium Recipes of Microbial Cultures". An ampule of the bacterium was removed from the −80°C freezer.

The ampule was broken open under $N_2$ gas and rehydrated with 0.5 mL of DSMZ 311 medium following previous methods for opening an ampule under anaerobic conditions.[41] The microbes were then added to a sealed anaerobic culture tube containing 20 mL of DSMZ 311 medium. The bacterial culture was then incubated at 34°C for three days until the culture reached the stationary phase of growth. At stationary phase, the microbes were transferred to two anaerobic bottles each containing 250 mL of DSMZ 311 medium. A large quantity of *S. ovata* cultures was obtained after a three-day incubation at 34°C. The microbes were transferred to anaerobic culture tubes containing 20% (v/v) dimethyl sulfoxide (DMSO) and 80% (v/v) DSMZ 311 medium. These vials were sealed under anaerobic conditions and stored in a −80°C freezer until experimental use.

When needed a frozen sample of *S. ovata* was removed from the −80°C freezer and thawed. Vials containing 10 mL of the baseline medium were sealed under $H_2/CO_2$ (80/20) gas mixture. Before adding microbes to the container, the sulfide-containing reducing agent was added in a ratio of 0.25 mL per 10 mL of solution to ensure an air-free environment. Microbial culture was subsequently added in a ratio of 0.5 mL per 10 mL of solution. The inoculated tube was then incubated for 3 days at 34°C.

*Protocol of testing viability of S. ovata in PFC nanoemulsions.* Living cultures of *S. ovata* after a three-day incubation were prepared as outlined above for the viability test. In a 10-mL vial for anaerobic cultures, 4-mL solution combining baseline medium, reducing agent, and PFC nanoemulsion were combined anaerobically under a gas environment of $H_2/CO_2$ (80/20) gas mixture. Five different conditions with varying percentages of PFC chemicals were tested: 0%, 0.5%, 2.5%, 5%, and 10% (v/v). Control samples in which only surfactant was added were prepared following a similar procedure. 0.4 mL of bacterial culture was added to each vial under strict anaerobic condition. An additional 10 mL of $H_2/CO_2$ (80/20) gas mixture was injected to

each vial so that the microbial metabolism will not be limited by the substrates. A baseline sample with 0% PFC was injected with 10 mL of air right after inoculation in order to determine the initial concentration of acetic acid. The concentrations of accumulated acetic acid after a three-day incubation at 34 °C was quantified based on the procedure listed in section "Product Quantification". We calculated the ratio of accumulations of acetic acid between samples with and without PFC nanoemulsion (termed as "relative enhancement" in figures), which was used to evaluate the metabolic activities of *S.* ovata with the presence of different amounts of PFC nanoemulsion. The results of such a viability test is displayed Supplementary Fig. 3. A total of four trials were run per experiment ($n = 4$).

*Protocol of testing the viability of S. ovata in higher salt concentrations.* The compatibility of *S. ovata* at higher salt concentrations was tested and evaluated using the same procedure described above. Four different conditions of varying phosphate buffer concentrations were tested: 18.5 mM (1x, baseline medium), 27 mM (2x), 55.5 mM (3x, high salinity medium), and 92.5 mM (5x). These results are plotted in Supplementary Fig. 9 ($n \geq 3$).

**Electrochemical characterizations**

The electrochemical potentials reported in this manuscript were all referenced to the Reversible Hydrogen Electrode (RHE). We converted experimental data with a Ag/AgCl reference electrode (0.209 V *vs.* SHE, Standard Hydrogen Electrode) with the following formula: Voltage *vs*. RHE = Voltage *vs.* SHE + pH × 0.059 V. Here pH denotes the pH of the solution tested in experiments. All potentials reported here are after *i*R correction.

*Experiments of characterizing the j-V correlations.* Experiments were run on a Gamry Interface 1000E potentiostat using a three-electrode set up consisting of a SS mesh loaded with Co-P alloy

catalysts as the working electrode, a Pt counter electrode, and a Ag/AgCl reference electrode (1M KCl). Experiments of cyclic voltammetry were conducted both in baseline media and in 1 M potassium phosphate buffer ($KP_i$). Steady-state *j*-V correlations were established with multi-step chronoamperometry. At each voltage step, a constant potential on the working electrode was maintained for 2 min ranging from −0.6 to −1.6 V *vs*. reference at an interval of 0.05 V in the setup that the bulk electrolysis was performed. The steady-state current density at each potential step was subsequently determined.

*Bulk electrolysis*. Living cultures of *S. ovata* after a three-day incubation were prepared as outlined above for the experiments of bulk electrolysis. Four electrochemical experiments were run in parallel using a Gamry Interface 1000E potentiostat interfaced with a Gamry ECMB multiplexer. Experiments of bulk electrolysis were conducted in custom-made two-chamber glass electrochemical cells (Adams and Chittenden Scientific Glass). Two 150-mL chamber were separated by a Nafion®117 membrane. A picture of the set-up is displayed in Supplementary Fig. 6. In order to prevent possible contamination, a leak-free Ag/AgCl reference electrode (Innovative Instruments, Inc) was used as the reference. The working electrode was a SS mesh loaded with Co-P alloy catalyst, and a CC electrode loaded with $CoP_i$ catalyst was the counter electrode. The total volume of liquid in each chamber is about 100 mL. The experiments were conducted in a 34 °C water bath with constant stirring at 150 rpm. Before inoculation, the cathode chamber was maintained under anaerobic conditions under a $N_2/CO_2$ (80/20) gas mixture with the addition of reducing agent. 4 mL of bacterial culture was subsequently added to each reactor. Multiplexed chronoamperometry was performed on the reactors under the selected voltages that would yield the target current densities. 1 mL of sample was removed under anaerobic conditions from the cathodic chamber every day for product quantification. 1 mL of solution was also sampled before

the experiment of bulk electrolysis in order to determine the starting concentration of acetic acid. In addition to the results presented here, no acetic acid was observed in the anodic chamber. The uncertainties of the reported performance are mostly attributed to the variation of the biological samples. While all the bacterial samples are inoculated from the same batch, there are variations of the phenotypes in experiments. In addition, the evaporation of solution during the multi-day experiments may also contribute to the observed uncertainties.

*Electrochemical impedance spectroscopy.* Measurements of Electrochemical Impedance Spectroscopy (EIS) were performed in the same setup described above, with a DC voltage of 0 V *vs*. open circuit potential and an AC amplitude of 50 mV. Frequencies between 100 kHz and 10 Hz were tested with 10 data points per decade. Nyquist plots were used to extract the approximated series resistances ($R_s$) of reactors at day 0 of experiments under different conditions. The results for setups without and with the introduction of PFC nanoemulsions are displayed in Supplementary Fig. 5.

**Product Quantification**

$^1$H NMR was applied to quantify the accumulation of acetic acid from $CO_2$ reduction using TMSP-$d_4$ as the internal standard. All $^1$H-NMR were performed on a Bruker AV400 Sample Changer at the Molecule Instrumentation Center in UCLA. The liquid samples for NMR experiments had a total volume of 0.5 mL, containing 0.1 mL of $D_2O$ with 1 mM TMSP-$d_4$ as well as 0.4 mL of sample solution. Chemical shifts are reported on a parts-per-million (ppm) scale. The peak of acetate, the predominant species of acetic acid at neutral pH, exhibits a singlet at 1.77 ppm, while the singlet from TMSP-$d_4$ peak resides at −0.15 ppm (Supplementary Fig. 2). A calibration curve was constructed by determining the ratio of the integrated area between the NMR peaks of acetate

and TMSP-$d_4$ ($I_{HAc}/I_{TMSP}$), which is shown Supplementary Fig. 2. For samples that contained PFC nanoemulsions, the concentration of acetate was corrected and reported based on the volume of aqueous phase.

**Efforts to Attain 2.0 mA/cm$^2$ in Bulk Electrolysis**

We found in the experiments of bulk electrolysis that in baseline medium with 18.5 mM phosphate buffer the microbes exhibited minimal growth at a current density of 2.0 mA/cm$^2$ (See Supplementary Table 1). We considered that the concentration of phosphate buffer in the solution was too low, resulting in both an inability to reach higher current densities at lower overpotentials and a possible increase of local pH near the electrode, which will decrease the microbial viability. We hypothesized that a concentration increase of phosphate buffer in the medium will alleviate such adverse effects. As the conjugated acid ($H_2PO_4^-$) of phosphate buffer serves as the proton carrier at neutral pH, the minimal concentration of phosphate buffer ($C_{min}$) to achieve a current density of 2.0 mA/cm$^2$ without significant overpotential increase can be calculated as,[42]

$$C_{min} = \frac{jL}{FD_{Pi}} \quad (1)$$

Where $j$ = 2.0 mA/cm$^2$, $F$ is the Faraday's constant, $D_{Pi}$ = 9.7×10$^{-6}$ cm$^2$/s the diffusion coefficient of $H_2PO_4^-$,[43] and $L$ = 190 μm, the thickness of diffusion layer which was measured in the previous session. Our calculation yields $C_{min}$ = 40.6 mM. At the same time, the viability *of S. ovata* in higher salt concentrations was tested and we found that the microbes are compatible with a phosphate buffer concentration up to 92.5 mM (5x), as displayed in Supplementary Fig. 9. This led us to develop recipe of high-salinity medium (3x, 55.5 mM) described in section "Medium Recipes of Microbial Cultures".

**Calculation of Faradaic efficiency**

The Faradaic efficiency (*F. E.*) of each experiment was determined using the following formula:[35]

$$F.E. = \frac{\Delta C_{HAc}(mol/L) \times V_{solution}(L) \times 8 \times F(C \cdot mol^{-1})}{Overall\ charge\ (C)} \times 100\% \quad (2)$$

Here $\Delta C_{HAc}$ (mol/L) is the change in the concentration of acetic acid during the 4-day experiment, $V_{solution}$ the total volume of solution in the cathodic chamber, $F$ the Faraday's constant, and "Overall charge" is the total electric charges passed through the cathodic chamber. The number 8 is the number of electrons required to generate one molecule of acetic acid from $CO_2$ as determined by the chemical equation,

$$2\ CO_2 + 8\ e^- + 8\ H^+ \rightarrow CH_3COOH + 2\ H_2O \quad (3)$$

**Data availability**

All data reported or included in this analyzed during this study are included in this published article (and its supplementary information).

**References**


1. Chu, S., Majumdar, A. Opportunities and challenges for a sustainable energy future. *Nature* **488**, 294−303 (2012).
2. Nocera, D. G. Solar Fuels and Solar Chemicals Industry. *Acc. Chem. Res.* **50**, 616−619 (2017).
3. Jia, J. *et al.* Heterogeneous catalytic hydrogenation of $CO_2$ by metal oxides: defect engineering – perfecting imperfection. *Chem. Soc. Rev.* **46**, 4631−4644 (2017).
4. Dinh, C.-T. *et al.* $CO_2$ electroreduction to ethylene via hydroxide-mediated copper catalysis at an abrupt interface. *Science* **360**, 783−787 (2018).

5. White, J. L. *et al.* Light-Driven Heterogeneous Reduction of Carbon Dioxide: Photocatalysts and Photoelectrodes. *Chem. Rev.* **115**, 12888−12935 (2015).
6. Jouny, M., Luc, W., Jiao, F. High-rate electroreduction of carbon monoxide to multi-carbon products. *Nat. Catal.* **1**, 748−755 (2018).
7. Li, J. *et al.* Efficient electrocatalytic $CO_2$ reduction on a three-phase interface. *Nat. Catal.* **1**, 592−600 (2018).
8. Bushuyev, O. S. *et al.* What Should We Make with $_{CO2}$ and How Can We Make It? *Joule* **2**, 825−832 (2018).
9. Appel, A. M. *et al.* Frontiers, Opportunities, and Challenges in Biochemical and Chemical Catalysis of $CO_2$ Fixation. *Chem. Rev.* **113**, 6621−6658 (2013).
10. Liu, C., Colón, B. C., Ziesack, M., Silver, P. A., Nocera, D. G. Water Splitting-Biosynthetic System with $CO_2$ reduction Efficiencies Exceeding Photosynthesis. *Science* **352**, 1210−1213 (2016).
11. Kornienko, N., Zhang, J. Z., Sakimoto, K. K., Yang, P., Reisner, E. Interfacing nature's catalytic machinery with synthetic materials for semi-artificial photosynthesis. *Nat. Natotech.* **13**, 890−899 (2018).
12. Li, H. *et al.* Integrated Electromicrobial Conversion of $CO_2$ to Higher Alcohols. *Science* **335**, 1596−1596 (2012).
13. Sakimoto, K. K., Wong, A. B., Yang, P. Self-photosensitization of nonphotosynthetic bacteria for solar-to-chemical production. *Science* **351**, 74−77 (2015).
14. Claassens, N. J., Sousa, D. Z., dos Santos, V. A. P. M., de Vos, W. M., van der Oost, J. Harnessing the power of microbial autotrophy. *Nat. Rev. Micro.* **14**, 692−706 (2016).

15. Brown, K. A. *et al.* Light-driven dinitrogen reduction catalyzed by a CdS:nitrogenase MoFe protein biohybrid. *Science* **352**, 448−450 (2016).

16. Liao, J. C., Mi, L., Pontrelli, S., Luo, S. Fuelling the future: microbial engineering for the production of sustainable biofuels. *Nat. Rev. Microbiol.* **14**, 288−304 (2016).

17. Cornejo, J. A., Sheng, H., Edri, E., M. Ajo-Franklin, C. & Frei, H. Nanoscale membranes that chemically isolate and electronically wire up the abiotic/biotic interface. *Nat. Commun.* **9**, 2263 (2018).

18. Rabaey, K. & Rozendal, R. A. Microbial electrosynthesis — revisiting the electrical route for microbial production. *Nat. Rev. Microbiol.* **8**, 706−716 (2010).

19. Sakimoto, K. K. *et al.* Physical Biology of the Materials–Microorganism Interface. *J. Am. Chem. Soc.* **140**, 1978−1985 (2018).

20. Milton, R. D., Wang, T., Knoche, K. L., Minteer, S. D. Tailoring Biointerfaces for Electrocatalysis. *Langmuir* **32**, 2291−2301 (2016).

21. Zhang, T. More efficient together. *Science* **350**, 738−739 (2015).

22. Liu, C., Sakimoto, K. K., Colón, B. C., Silver, P. A., Nocera, D. G. Ambient nitrogen reduction cycle using a hybrid inorganic–biological system. *Proc. Natl. Acad. Sci. U. S. A.* **114**, 6450−6455 (2017).

23. Lubitz, W., Ogata, H., Rüdiger, O., Reijerse, E. Hydrogenases. *Chem. Rev.*, **114**, 4081−4148 (2014).

24. Liu, C., Nangle, S. N., Colón, B. C., Silver, P. A., Nocera, D. G. $^{13}$C-Labeling the carbon-fixation pathway of a highly efficient artificial photosynthetic system. *Faraday Discuss.* **198**, 529−537 (2017).

25. Gevantman, L. H. in *CRC Handbook of Chemistry and Physics* (ed W. M. Haynes) Ch. 5, 147 (CRC Press, 2015).

26. Watanabe, K., Manefield, M., Lee, M., Kouzuma, A. Electron shuttles in biotechnology. *Curr. Opin. Biotechnol.* **20**, 633−641 (2009).

27. Squires, J. E. Artificial Blood. *Science* **295**, 1002−1005 (2002).

28. Ju, L. K., Lee, J. F. & Armiger, W. B. Enhancing oxygen transfer in bioreactors by perfluorocarbon emulsions. *Biotechnol. Prog.* **7**, 323−329 (1991).

29. Yamamoto, S., Honda, H., Shiragami, N. & Unno, H. Enhancement of autotrophic growth rate of Alcaligenes eutrophus in a medium containing perfluorocarbon under low oxygen partial pressure. *Biotechnol. Lett.* **14**, 733−736 (1992).

30. *Dissolving gases in FLUTEC™ Liquids*, Technical article by F2 Chemicals Ltd., http://f2chemicals.com/pdf/technical/Gas%20solubility.pdf (2005).

31. Sletten, E. M., Swager, T. M. Readily accessible multifunctional fluorous emulsions. *Chem. Sci.* **7**, 5091−5097 (2016).

32. Sletten, E. M., Swager, T. M. Fluorofluorophores: fluorescent fluorous chemical tools spanning the visible spectrum. *J. Am. Chem. Soc.* **136**, 13574−13577 (2014).

33. Möller, B., Oßmer, R., Howard, B. H., Gottschalk, G., Hippe, H. Sporomusa, a new genus of gram-negative anaerobic bacteria including Sporomusa sphaeroides spec. nov. and Sporomusa ovata spec. nov. *Arch. Microbiol.* **139**, 388−396 (1984).

34. Nevin, K. P., Woodard, T. L., Franks, A. E., Summers, Z. M., Lovley, D. R. Microbial Electrosynthesis: Feeding Microbes Electricity To Convert Carbon Dioxide and Water to Multicarbon Extracellular Organic Compounds. *mBio* **1**, e00103-00110 (2010).

35. Liu, C. *et al.* Nanowire–Bacteria Hybrids for Unassisted Solar Carbon Dioxide Fixation to Value-Added Chemicals. *Nano. Lett.* **15**, 3634−3639 (2015).

36. Aryal, N., Tremblay, P. L., Lizak, D. M. & Zhang, T. Performance of different Sporomusa species for the microbial electrosynthesis of acetate from carbon dioxide. *Bioresour. Technol.* **233**, 184−190 (2017).

37. LaBelle, E. V., May, H. D. Energy Efficiency and Productivity Enhancement of Microbial Electrosynthesis of Acetate. *Front. Microbiol.* **8**, 756 (2017).

38. Paseka, I., Velicka, J. Hydrogen evolution and hydrogen sorption on amorphous smooth Me−P(x) (Me = Ni, Co and Fe−Ni) electrodes. *Electrochim. Acta.* **42**, 237−242 (1997).

39. Jiang, N., You, B., Sheng, M., Sun, Y. Electrodeposited Cobalt-Phosphorous-Derived Films as Competent Bifunctional Catalysts for Overall Water Splitting. *Angew. Chem., Int. Ed.* **54**, 6251−6254 (2015).

40. Haas, T., Krause, R., Weber, R., Demler, M., Schmid, G. Technical photosynthesis involving CO2 electrolysis and fermentation. *Nat. Catal.* **1**, 32−39 (2018).

41. Nichols, E. M. *et al.* Hybrid bioinorganic approach to solar-to-chemical conversion. *Proc Natl Acad Sci U S A* **112**, 11461-11466, doi:10.1073/pnas.1508075112 (2015).

42. Bard, A. J. & Faulkner, L. R. *Electrochemical Methods: Fundamentals and Applications*. 2 edn, (John Wiley & Sons, inc., 2001).

43. Jeremiasse, A. W., Hamelers, H. V. M., Kleijn, J. M. & Buisman, C. J. N. Use of Biocompatible Buffers to Reduce the Concentration Overpotential for Hydrogen Evolution. *Environmental Science & Technology* **43**, 6882-6887, doi:10.1021/es9008823 (2009).

**Supplementary Information**

**Medium Recipes of Microbial Cultures**

*DSMZ 311 Medium*

| | |
|---|---|
| $NH_4Cl$ | 0.50 g |
| $MgSO_4$ • 7 H2O | 0.50 g |
| $CaCl_2$ • 2 $H_2O$ | 0.25 g |
| NaCl | 2.25 g |
| $FeSO_4$ • 7 $H_2O$ | 0.002g |
| Trace element solution SL-10 (see below) | 1.00 ml |
| Selenite-tungstate solution (see below) | 1.00 ml |
| Yeast extract | 2.00 g |
| Casitone | 2.00 g |
| Betaine • $H_2O$ | 6.70 g |
| Na-resazurin solution (0.1% w/v) | 0.50 ml |
| $K_2HPO_4$ | 0.35 g |
| $KH_2PO_4$ | 0.23 g |
| $NaHCO_3$ | 4.00 g |
| Vitamin solution (see below) | 10.00 ml |
| Distilled water | 1000.00 ml |

All ingredients (except phosphates, bicarbonate, vitamins, cysteine and sulfide) were dissolved first. And the medium was sparged with $N_2/CO_2$ (80/20) gas mixture while boiling to make the solution anoxic. Once cool, and while still sparging with the same gas, phosphates, vitamins (sterilized by filtration) and carbonate were added. The medium was dispensed under the same gas

into anaerobic culture tubes and then autoclaved. The pH of the complete medium was adjusted to pH 7.0, if necessary.

*Trace element solution (SL-10)*

| | |
|---|---|
| Nitrilotriacetic acid | 1.50 g |
| $MgSO_4 \cdot 7\ H_2O$ | 3.00 g |
| $MnSO_4 \cdot H_2O$ | 0.50 g |
| NaCl | 1.00 g |
| $FeSO_4 \cdot 7\ H_2O$ | 0.10 g |
| $CoSO_4 \cdot 7\ H_2O$ | 0.18 g |
| $CaCl_2 \cdot 2\ H_2O$ | 0.10 g |
| $ZnSO_4 \cdot 7\ H_2O$ | 0.18 g |
| $CuSO_4 \cdot 5\ H_2O$ | 0.01 g |
| $KAl(SO_4)_2 \cdot 12\ H_2O$ | 0.02 g |
| $H_3BO_3$ | 0.01 g |
| $Na_2MoO_4 \cdot 2\ H_2O$ | 0.01 g |
| $NiCl_2 \cdot 6\ H_2O$ | 0.03 g |
| $Na_2SeO_3 \cdot 5\ H_2O$ | 0.30 mg |
| Na2WO4 • 2 $H_2O$ | 0.40 mg |
| Distilled water | 1000.00 ml |

The nitrilotriacetic acid was first dissolved and the pH adjusted to 6.5 with KOH, then the minerals were added. The final pH was adjusted to pH 7.0 with KOH.

*Vitamin solution*

| | |
|---|---|
| Biotin | 2.00 mg |
| Folic acid | 2.00 mg |
| Pyridoxine-HCl | 10.00 mg |
| Thiamine-HCl • 2 H2O | 5.00 mg |
| Riboflavin | 5.00 mg |
| Nicotinic acid | 5.00 mg |
| D-Ca-pantothenate | 5.00 mg |
| Vitamin B12 | 0.10 mg |
| p-Aminobenzoic acid | 5.00 mg |
| Lipoic acid | 5.00 mg |
| Distilled water | 1000.00 ml |

*Selenite-tungstate solution*

| | |
|---|---|
| NaOH | 0.5 g |
| $Na_2SeO_3$ • 5 $H_2O$ | 3.0 mg |
| $Na_2WO_4$ • 2 $H_2O$ | 4.0 mg |
| Distilled water | 1000.0 ml |

*Reducing agent solution*

All the water used in this procedure was boiled and gassed under $N_2$ prior to the experiments. 12.5 g cysteine-HCl was dissolved in 500 mL water in a 2-L Erlenmeyer flask. The pH of the solution was adjusted to 9.5 with NaOH. 12.5 g of washed crystals of $Na_2S{\cdot}9H_2O$ was weighted in a plastic

tray and then transferred into the flask containing cysteine-HCl. The volume of the solution was brought up to 1000 mL. The whole solution was brought to boil and cool again under gassing with $N_2$. 20 mL of the prepared solution was dispensed into one 25-mL vial which was pre-flushed with $N_2$. The vials were sealed and then autoclaved for 15 min at 121 °C.

*Baseline Medium*

| | |
|---|---|
| $K_2HPO_4$ | 0.348 g |
| $KH_2PO_4$ | 0.227 g |
| $Na_2HPO_4 \cdot 7H_2O$ | 2.145 g |
| $NaH_2PO_4 \cdot H_2O$ | 0.938 g |
| $NH_4Cl$ | 0.500 g |
| $MgSO_4 \cdot 7H_2O$ | 0.500 g |
| $CaCl_2 \cdot 2H_2O$ | 0.250 g |
| NaCl | 0.918 g |
| $FeSO_4 \cdot 7H_2O$ | 0.002 g |
| $NaHSeO_3$ | 10-7 mol/L |
| $NaHCO_3$ | 4.000 g |
| SL-10 solution | 1 mL |
| Vitamin solution | 10 mL |
| Yeast extract | 2.000 g |

Compared to the DSMZ-recommended growth medium, the concentration of phosphate buffer was increased by 5 times from 3.7 mM to 18.5 mM without changing the overall $K^+$ and $Na^+$ concentration. All ingredients (except phosphates, bicarbonate, vitamins, cysteine and sulfide)

were dissolved first. And the medium was sparged with $N_2/CO_2$ (80/20) gas mixture while boiling to make the solution anoxic. Once cool, and while still sparging with the same gas, phosphates, vitamins (sterilized by filtration) and carbonate were added. The medium was dispensed under the same gas into anaerobic culture tubes and then autoclaved. The pH of the complete medium was adjusted to pH 7.0, if necessary. High-salinity medium was prepared based on the recipe above, while the concentration of the phosphate buffer was increased three-fold from 18.5 mM to 55.5 mM. Minimal medium, which was used in the experiments of flow cytometry, was prepared following the same procedure as the baseline media, however it only included $NH_4Cl$, NaCl, $K_2HPO_4$, $KH_2PO_4$, and $NaHCO_3$.

**Supplementary Table 2.1.** List of experiments reported in this work [a]

| Entry | PFC nanoemulsion (v/v, %) | E° [b] (mV vs. SHE) | *j* (mA/cm$^2$) | Titer (g·L$^{-1}$) | $r_{CO2}$ (g·L$^{-1}$·d$^{-1}$) | $r_{CO2}$' (g·m$^{-2}$·d$^{-1}$) | *F. E.* (%) |
|---|---|---|---|---|---|---|---|
| *1* | 0 | −871 | −0.50 ± 0.09 | 1.59 ± 0.49 | 0.39 ± 0.10 | 32.2 ± 8.0 | 94 ± 15 |
| *2* | 2.5 | −911 | −0.58 ± 0.07 | 1.59 ± 0.26 | 0.38 ± 0.12 | 31.9 ± 10.0 | 90 ± 16 |
| *3* | 0 | −961 | −1.14 ± 0.14 | 2.63 ± 0.30 | 0.65 ± 0.25 | 54.0 ± 20.5 | 71 ± 8 |
| *4* | 2.5 | −971 | −1.05 ± 0.16 | 3.17 ± 0.47 | 0.78 ± 0.11 | 64.7 ± 8.9 | 92 ± 8 |
| *5* | 0 [c] | −1001 | −2.01 ± 0.16 | 2.23 ± 0.29 | 0.54 ± 0.13 | 44.8 ± 11.2 | 33 ± 2 |
| *6* | 2.5 [c] | −1021 | −1.99 ± 0.05 | 6.39 ± 1.14 | 1.58 ± 0.44 | 132.0 ± 36.7 | 99 ± 19 |
| | 0 [d] | −981 | −1.45 ± 0.0001 | 0.96 ± 0.40 | 0.23 ± 0.15 | 19.1± 12.6 | 20 ± 8 |
| | 2.5 [d] | −1001 | −1.67 ± 0.0001 | 0.59 ± 0.17 | 0.13 ± 0.07 | 10.6 ± 5.9 | 9 ± 4 |

[a] General conditions: *S. ovata* (DSM 2662) is used as the biocatalyst; Co-P alloy loaded on SS mesh (both sides, 2 cm × 3 cm). The reported data here are the results during four-day experiments. Baseline medium was used unless mentioned specifically. $n \geq 3$. All reported error corresponds to the standard error of the mean (SEM). [b] The reported voltage was the averaged values from all replicates. [c] High-salinity medium which contains 55.5 mM phosphate buffer. [d] Slow microbial growth was observed.

**Supplementary Table 2.2.** List of previous reports for pure cultures of *Sporomusa ovata* in electricity-driven microbial $CO_2$ fixation.

| Strain of *S. ovata* | Cathode | E° (mV *vs.* SHE) | *j* (mA/cm²) | *t* (d) | Titer (g·L⁻¹) | $r_{CO2}$ (g·L⁻¹·d⁻¹) | $r_{CO2}$' (g·m⁻²·d⁻¹) | *F. E.* (%) | Ref |
|---|---|---|---|---|---|---|---|---|---|
| *DSM 2662* [a] | Graphite stick | −400 | −0.0695 [d]<br>−0.0207 [e] | 6 | 0.0625 | 0.01 [EV]<br>0.045 [STY] | 4.64[d]<br>1.38[e] | 85 | 1 |
| *DSM 2662* [b] | Chitosan-coated CC | −400 | −0.0475 [d] | 9 | 0.59 | 0.065 ± 0.16 | 2.75 ± 0.67[d] | 82 ± 12 | 2 |
| *DSM 2662* [b] | Ni-coated nanowire | −400 | −0.218 [d]<br>−0. 65 [e] | 8 | 0.54 | 0.068 | 11.35[d]<br>3.38[e] | 82 ± 14 | 3 |
| *DSM 2662* [c] | Si-$TiO_2$ nanowire | −595 to −571 | −0.35 [d]<br>−0.012 [e] | 5 | 1.2 | 0.24 | N. D. [f] | 86 ± 9 | 4 |
| *DSM 2662* [b] | Reduced Graphene Oxide paper | −690 | −0.258 ± 0.054 [d] | 12 | N. D. [f] | N. D. [f] | 10.11 ± 1.34 [d] | 91 ± 9 | 5 |
| *DSM 2662* [b] | Carbon paper | −690 | −0.037 ± 0.010 [d] | 12 | N. D. [f] | N. D. [f] | 1.20 ± 0.30 [d] | 84 ± 4 | 5 |
| *DSM 2662* [b] | Carbon felt | −690 | −0.040 ± 0.010 [d] | 12 | N. D. [f] | 0.019 ± 0.006 | 1.02 ± 0.33 [d] | 77 ± 2 | 6 |
| *DSM 2662* [b] | 3D-Graphene on Carbon felt | −690 | −0.245 ± 0.016 [d] | 12 | N. D. [f] | 0.125 ± 0.004 | 6.95 ± 0.22 [d] | 87 ± 3 | 6 |
| *DSM 2662* [b] | Carbon Cloth | −690 | −0.03 ± 0.01 [d] | 14 | 0.2 | N. D. [f] | 1.64 ± 0.27 [d] | 87 ± 7 | 7 |
| *DSM 2662* [b] | PEDOT: PSS on Carbon cloth | −690 | −0.32 ± 0.08 [d] | 14 | 1.6 | N. D. [f] | 15.15 ± 1.06 [d] | 79 ± 6 | 7 |
| *DSM 2662* [b] | Graphite stick | −690 | −0.045 ± 0.015 [d] | 14 | 0.51 | 0.029 ± 0.006 [d] | 2.06 ± 0.42 [d] | 92 ± 5 | 8 |
| *DSM 2663* [b] | Graphite stick | −690 | −0.078 ± 0.019 [d] | 14 | 0.99 | 0.053 ± 0.016 [d] | 3.67 ± 1.09 [d] | 61 ± 12 | 8 |
| *DSM 3300* [b] | Graphite stick | −690 | −0.019 ± 0.0005 [d] | 14 | 0.20 | 0.011 ± 0.005 [d] | 0.77 ± 0.34 [d] | 85 ± 4 | 8 |
| N. A. [b,g] | Graphite disk | −660 | −0.017 ± 0.004 [d] | 28 | 0.54 | 0.020 ± 0.003 [d] | 1.68 ± 0.24 [d] | 105 ± 5 | 9 |

[a] Estimates based on continuous feed linear production and flow rates reported (EV is rate calculated per exit volume, STY is the space-time yield). [b] Estimates based on batch operation (volume in cathode chamber). [c] Light as energy source. [d] Based on projected surface area. e Based on total surface area. [f] N. D.: not determined. [g] N. A.: The specific strain information was not available in the report. All reported error corresponds to SEM.

**Supplementary Table 2.3.** List of previous reports for other acetogen strains in electricity-driven microbial $CO_2$ fixation.

| Microorganism/ strain | Cathode | E° (mV *vs.* SHE) | *j* (mA/cm$^2$) | *t* (days) | Titer (g·L$^{-1}$) | $r_{CO2}$ (g·L$^{-1}$·d$^{-1}$) | $r_{CO2}$' (g·m$^{-2}$·d$^{-1}$) | *F.E.* (%) | Ref |
|---|---|---|---|---|---|---|---|---|---|
| *Sporomusa malonica DSM 5090* [a] | Graphite stick | −690 | −0.070 ± 0.017 [d] | 14 | 0.63 | 0.039 ± 0.004 [d] | 2.73 ± 0.29 [d] | 91 ± 14 | [8] |
| *Sporomusa acidovorans DSM 3132* [a] | Graphite stick | −690 | −0.057 ± 0.021 [d] | 14 | 0.72 | 0.038 ± 0.012 [d] | 2.65 ± 0.85 [d] | 70 ± 1 | [8] |
| *Sporomusa aerivorans DSM 13326* [a] | Graphite stick | −690 | −0.0026 ± 0.0002 [d] | 14 | N. D. [c] | N. D. [c] | N. D. [c] | N. D. [c] | [8] |
| *Sporomusa sphaeroides DSM 2875* [b] | Graphite stick | −400 | −0.057 [d] −0.017 [e] | 8 | 0.0028 | 0.00035 [EV] 0.0027 [STY] | 0.208 [d] 0.062 [e] | 39 | [1] |
| *Sporomusa silvacetica DSM 10669* [b] | Graphite stick | −400 | −0.02 [d] −0.006 [e] | 10 | 0.002 | 0.0002 [EV] 0.0025 [STY] | 0.15 [d] 0.045 [e] | 84 | [1] |
| *Clostridium aceticum DSM 1496* [b] | Graphite stick | −400 | −0.08 [d] −0.024 [e] | 13 | 0.0027 | 0.0002 [EV] 0.0042 [STY] | 0.02 [d] 0.006 [e] | 27 | [1] |
| *Clostridium ljungdahlii DSM 13528* [b] | Graphite stick | −400 | −0.104 [d] −0.031 [e] | 7 | 0.0065 | 0.0009 [EV] 0.0054 [STY] | 0.47 [d] 0.14 [e] | 72.2 ± 0.2 | [1] |
| *Clostridium ljungdahlii DSM 13528* [a] | Graphite felt + stainless steel | −695 | −1.0 [d] | 11 | 0.56 | 0.056 to 0.144 | 7.51 to 19.2 | 39-89 | [10] |
| *Moorella thermoacetica DSM 21394* [b] | Graphite stick | −400 | −0.03 [d] −0.009 [e] | 9 | 0.0047 | 0.0006 [EV] 0.0045 [STY] | 0.35 [d] 0.104 [e] | 85 ± 7 | [1] |
| *Acetobacterium woodii DSM 1030* [b] | Graphite stick | −400 | N. D. [c] | -- | N. D. [c] | N. D. [c] | N. D. [c] | N. D. [c] | [1] |
| *Acetobacterium woodii DSM 1030* [a] | Stainless steel felt | −690 | −1.5 [d] | 1 | 0.127 | 0.046 | 12.8 [d] | 81 | [11] |

[a] Estimates based on batch operation (volume in cathode chamber). [b] Estimates based on continuous feed linear production and flow rates reported (EV is rate calculated per exit volume, STY is the space-time yield). [c] N. D.: not determined or not reported. [d] Based on projected surface area. [e] Based on total surface area. All reported error denotes SEM.

**Supplementary Table 2.4.** List of previous reports of the production of acetic acid combining electrolyzes with gas fermentation.

| Microorganism/ strain | *t* (days) | Titer ($g \cdot L^{-1}$) | $r_{CO2}$ ($g \cdot L^{-1} \cdot d^{-1}$) | $r_{CO2}$' ($g \cdot m^{-2} \cdot d^{-1}$) | *F. E.* (%) | Ref |
|---|---|---|---|---|---|---|
| *Clostridium autoethanogenum DSM 10061* [a,b] | 2 | 2.33 | 1.17 | N. D. [f] | 100 [g] | [12] |
| *Moorella thermoacetica DSM 6867* [a,b,c] | 7 | 30 | 26.4 | N. D. [f] | 3.7 | [13] |
| *Acetobacterium woodii DSM 1030* [b,d] | 3.2 | 21.7 | 18.24 | N. D. [f] | 10 | [14] |
| *Acetobacterium woodii DSM 1030* [b,d,e] | 3.2 | 17.6 | 147.84 | N. D. [f] | 56 | [14] |

[a] Estimates based on batch operation [b] Equipped with a pH auxostat system. [c] Bubble column reactor setup. [d] Continuous stirred-tank reactors (CSTR). [e] Hollow fiber membrane in the system. [f] N. D.: not determined or not reported. [g] reported as "almost 100%" without the exact values provided.

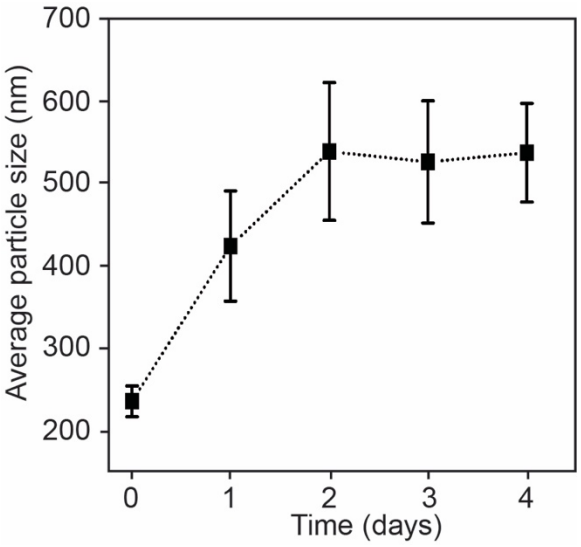


**Figure S2.1.** The change of average size of 2.5% PFC nanoemulsion over 4 days at 34°C in baseline medium. Detailed experimental conditions are listed in section "Dynamic Light Scattering". Error bars denote SEM. ($n \geq 3$)

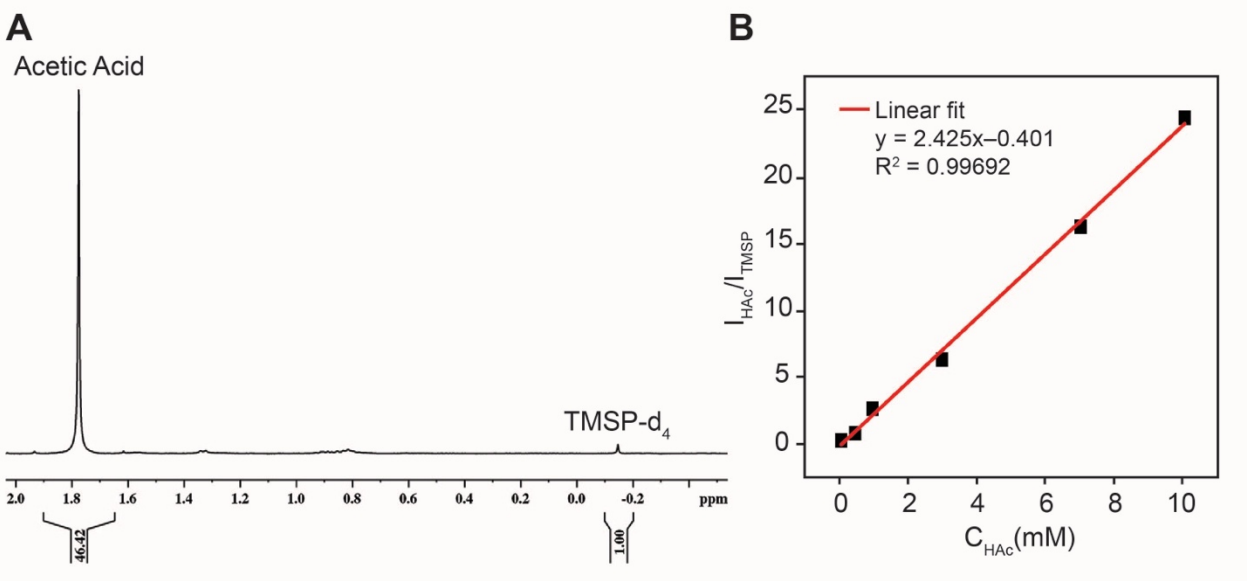


**Figure S2.2. a**, Representative $^{1}$H NMR spectrum of a sample with the addition of internal standard, TMSP-$d_4$, in $D_2O$. **b**, Calibration curve that plots the ratio of integration area between acetate (1.77 ppm) and TMSP-$d_4$ (−0.15 ppm) *vs.* the concentrations of acetate in standard solutions.

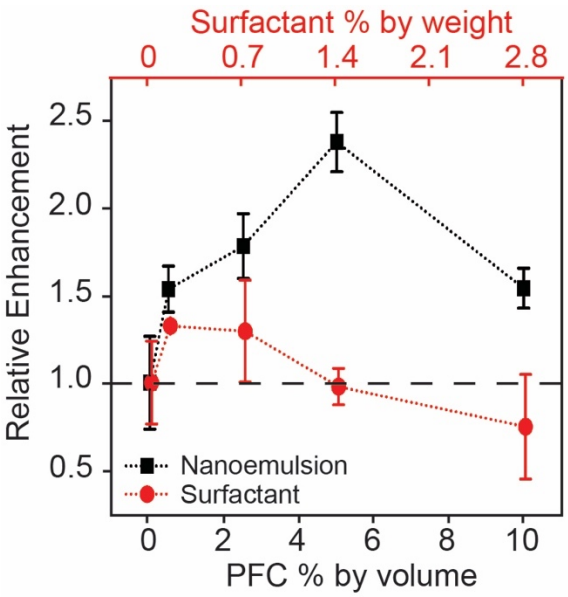


**Figure S2.3.** Viability test of *S. ovata* in PFC nanoemulsions. The relative enhancements of the accumulation of acetic acid by microbial $CO_2$ fixation are plotted against the volumetric percentage of PFC in the nanoemulsion (black). As the PFC nanoemulsion also contains surfactants that might interfere with experiments, results of the corresponding control experiments with only surfactant added (red) are also displayed. The error bars denote SEM, $n = 4$.

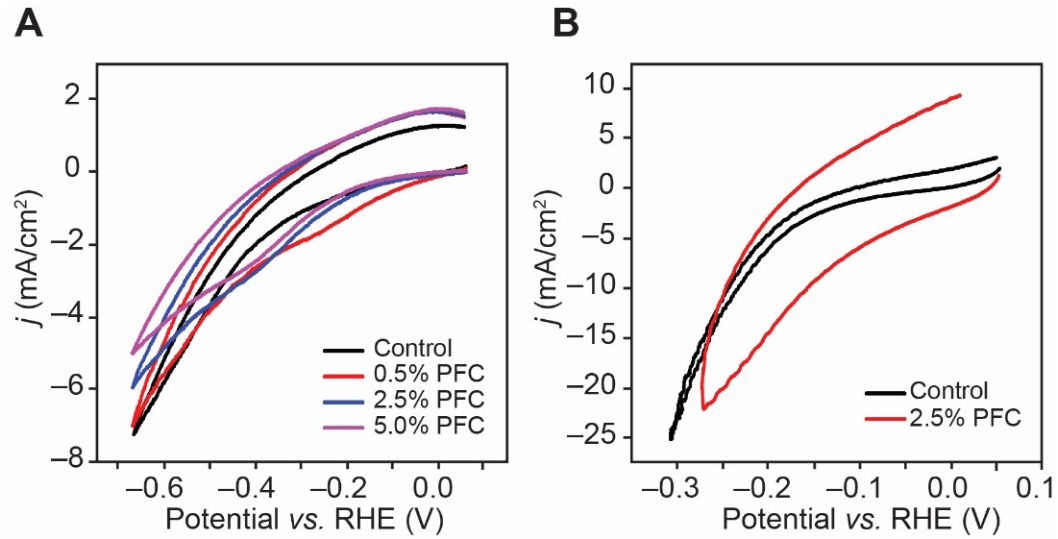


**Figure S2.4.** Cyclic voltammograms of Co-P alloy catalyst loaded on SS mesh substrate for varying percentages of PFC nanoemulsion in the baseline media (**a**) and 1 mol/L potassium phosphate buffer (**b**) at pH 7. The scan rate is at 10 $mV \cdot s^{-1}$.

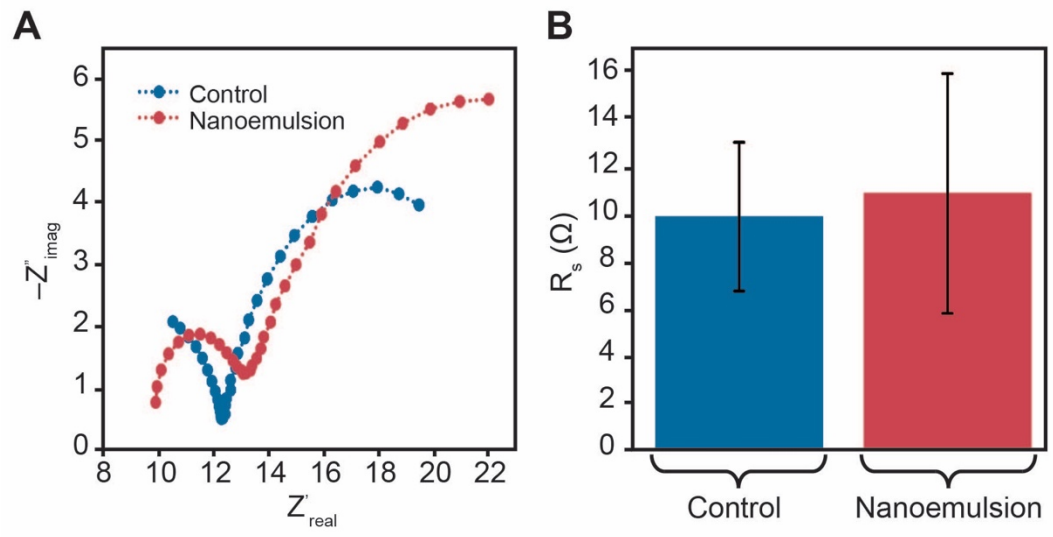


**Figure S2.5. a**, Representative Nyquist plots of Co-P alloy catalyst loaded on SS mesh substrate in solutions without (blue) and with (red) the introduction of PFC nanoemulsions. **b**, Statistical average of series resistance ($R_s$) in solutions without (blue) and with (red) the introduction of PFC nanoemulsions. Error bars denote SEM, $n \geq 16$.

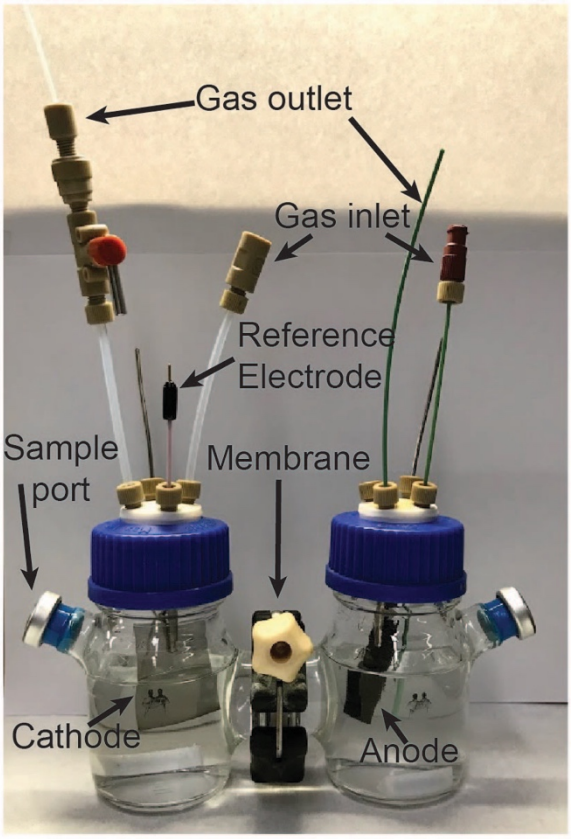


**Figure S2.6.** Experimental setup of bulk electrolysis depicting the electrodes, membrane separator, gas inlets/outlets, and sampling ports.

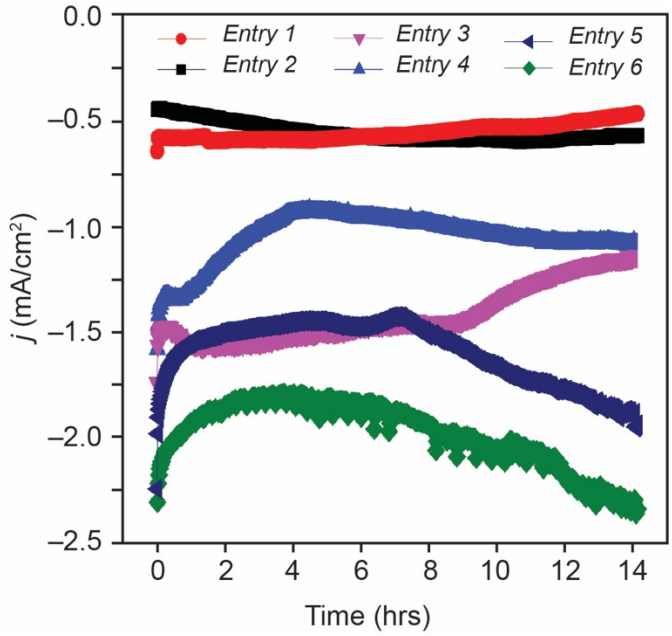


**Figure S2.7**. Representative chronoamperometry plots at varying current densities over the course of the first day during the bulk electrolysis experiments. The detailed experimental conditions of the denoted entries is shown in Supplementary Table 1.

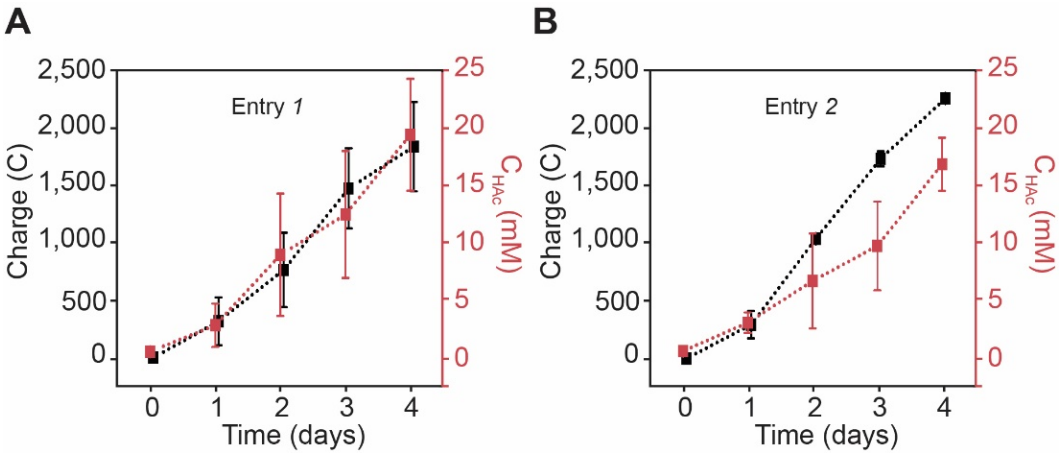


**Figure S2.8.** Acetic acid (HAc) was selectively produced from $CO_2$ with electricity input without (**a**, entry *1* in Supplementary Table 2.1) and in the presence of nanoemulsion (**b**, entry *2* in Supplementary Table 2.1) at a current density of 0.54 mA/cm$^2$. The electric charge (black) and acetate concentrations (red) are plotted versus the duration of experiments. Error bars denote SEM, $n \geq 3$.

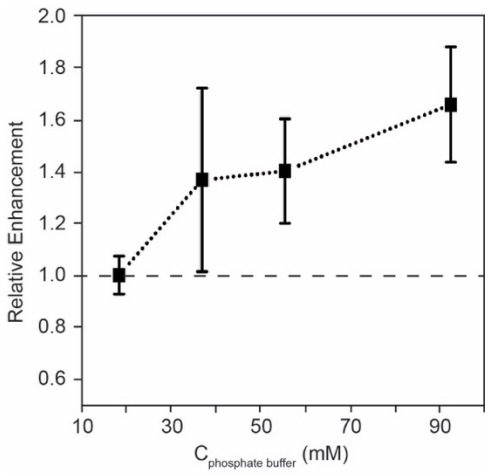


**Figure S2.9.** Viability test of *S. ovata* in media of different concentrations of phosphate buffer. The relative enhancements of the accumulation of acetic acid by microbial $CO_2$ fixation are plotted against the concentrations of phosphate buffer. Error bars denote SEM, $n \geq 3$.

**Supplementary References**

1. Nevin, K. P. *et al.* Electrosynthesis of organic compounds from carbon dioxide is catalyzed by a diversity of acetogenic microorganisms. *Appl. Environ. Microbiol.* **77**, 2882-2886, doi:10.1128/AEM.02642-10 (2011).
2. Zhang, T. *et al.* Improved cathode materials for microbial electrosynthesis. *Energy Environ. Sci.* **6**, 217-224, doi:10.1039/c2ee23350a (2013).
3. Nie, H. *et al.* Improved cathode for high efficient microbial-catalyzed reduction in microbial electrosynthesis cells. *Phys. Chem. Chem. Phys.* **15**, 14290-14294, doi:10.1039/c3cp52697f (2013).
4. Liu, C. *et al.* Nanowire-bacteria hybrids for unassisted solar carbon dioxide fixation to value-added chemicals. *Nano. Lett.* **15**, 3634-3639, doi:10.1021/acs.nanolett.5b01254 (2015).

5. Aryal, N., Zhang, T. & Tremblay, P.-L. *Microbial electrosynthesis for acetate production from carbon dioxide: innovative biocatalysts leading to enhanced performance*, Technical University of Denmark, (2017).
6. Aryal, N., Halder, A., Tremblay, P.-L., Chi, Q. & Zhang, T. Enhanced microbial electrosynthesis with three-dimensional graphene functionalized cathodes fabricated via solvothermal synthesis. *Electrochimica. Acta.* **217**, 117-122, doi:10.1016/j.electacta.2016.09.063 (2016).
7. Aryal, N., Tremblay, P.-L., Xu, M., Daugaard, A. E. & Zhang, T. Highly Conductive Poly(3,4-ethylenedioxythiophene) Polystyrene Sulfonate Polymer Coated Cathode for the Microbial Electrosynthesis of Acetate From Carbon Dioxide. *Frontiers in Energy Research* **6**, doi:10.3389/fenrg.2018.00072 (2018).
8. Aryal, N., Tremblay, P. L., Lizak, D. M. & Zhang, T. Performance of different Sporomusa species for the microbial electrosynthesis of acetate from carbon dioxide. *Bioresour. Technol.* **233**, 184-190, doi:10.1016/j.biortech.2017.02.128 (2017).
9. Giddings, C. G., Nevin, K. P., Woodward, T., Lovley, D. R. & Butler, C. S. Simplifying microbial electrosynthesis reactor design. *Front. Microbiol.* **6**, 468, doi:10.3389/fmicb.2015.00468 (2015).
10. Bajracharya, S. *et al.* Carbon dioxide reduction by mixed and pure cultures in microbial electrosynthesis using an assembly of graphite felt and stainless steel as a cathode. *Bioresour. Technol.* **195**, 14-24, doi:10.1016/j.biortech.2015.05.081 (2015).
11. Arends, J. B. A. *Optimizing the plant microbial fuel cell: diversifying applications and product outputs* Ph.D. thesis, Ghent University, Belgium, (2013).

12. Haas, T., Krause, R., Weber, R., Demler, M. & Schmid, G. Technical photosynthesis involving CO2 electrolysis and fermentation. *Nat. Catal.* **1**, 32-39, doi:10.1038/s41929-017-0005-1 (2018).

13. Hu, P. *et al.* Integrated bioprocess for conversion of gaseous substrates to liquids. *Proc. Natl. Acad. Sci. U.S.A.* **113**, 3773-3778, doi:10.1073/pnas.1516867113 (2016).

14. Kantzow, C., Mayer, A. & Weuster-Botz, D. Continuous gas fermentation by Acetobacterium woodii in a submerged membrane reactor with full cell retention. *J. Biotechnol.* **212**, 11-18, doi:10.1016/j.jbiotec.2015.07.020 (2015).

# CHAPTER 3. HYDROGEN GAS ENVIRONMENT IN HYBRID CARBON DIOXIDE FIXATION SYSTEM.

This chapter is a version of Rodrigues, R. M.; Guan, X.; Iñiguez, J. A.; Estabrook, D. A.; Chapman, J. O.; Huang, S.; Sletten, E. M.; and Liu, C. "Perfluorocarbon nanoemulsion promotes the delivery of reducing equivalents for electricity-driven microbial $CO_2$ reduction." *Nature Catalysis.* **2019**, 2, 407-414.

## Introduction

Our results in **Chapter 2** demonstrated an enhanced utilization of the electrochemically generated $H_2$ with the addition of PFC nanoemulsions leading to improved *F.E.* at all applied current densities. We performed a mechanistic investigation into the enhancement, through experiments of flow cytometry and rotating disk electrode (RDE) to study how the reducing equivalent was transferred within the solution and to the microbes. Based on the flow cytometry experiments were able to confirm a non-specific binding of PFC nanoemulsions to the microbes. The RDE experiments demonstrated that the interaction of the PFC nanoemulsions with the microbes promotes the kinetics of $H_2$ transfer and subsequent oxidation by more than three-fold. A 30% increase of local $H_2$ concentration at the nanoemulsion's interface was also observed. We hypothesized that the combination of enhanced transfer kinetics and local $H_2$ concentration could be attributed to the non-specific binding of the PFC nanoemulsions. Additionally, we hypothesized that the enhanced *F. E.* and improved throughput observed in **Chapter 2** was caused by the enhanced utilization and transfer rates of the $H_2$. Introducing nanoscale gas carrier is a viable approach to alleviate the throughput bottlenecks in electricity-driven microbial $CO_2$ reduction into commodity chemicals.

## Results

### Mechanistic understanding of PFC nanoemulsions as a $H_2$ carrier.

The observed increase of $r_{CO2}$ reported in **Chapter 2** cannot be completely accounted for if only the average $H_2$ solubility in PFC is considered. Research on microbial gas fermentation predicts $r_{CO2} \propto (P^{0.5} \times C_{gas}^{0.5})$, in which $P$ is the gas permeability and $C_{gas}$ is average gas solubility in the solution.[1] In our case, $P$ is constant as the experimental setup remains the same. The addition of 2.5% PFC nanoemulsions increased the average $H_2$ solubility from 0.79 mM [2] to approximately 0.95 mM under 1 bar $H_2$ pressure (see Methods for details), which translates to a relative enhancement of about 1.1 times for $r_{CO2}$ based on the model. This is much smaller than the experimentally observed enhancement of 2.9 times between entry *5* and *6* (Fig. 2.2B and Supplementary Table 2.1) and indicates some other factors must be considered. We note that such mathematical relationship was derived based on mean-field assumptions, which neglects the impact of microscopic local $H_2$ concentration and transfer kinetics.[1] We postulate that this model is not sufficient when the size of the $H_2$ carrier approaches the nanoscale, as the microscopic local $H_2$ concentration and the local transfer kinetics become much more important than the ensemble averaged values. Such a hypothesis led us to further investigate the interaction between the microbes and nanoemulsions, as well as to obtain microscopic kinetic information of $H_2$ transfer at the nanoemulsions' surface.

PFC nanoemulsions exhibit non-specific binding with the microbes in the solution as determined by flow cytometry. Fluorescently tagged PFC nanoemulsions were prepared by adding fluorinated rhodamine during the synthesis (see Methods for details).[3] The fluorinated rhodamine, with $\lambda_{max,abs}$ = 550 nm and $\lambda_{max,em}$ = 571 nm, has shown high stability within the nanoemulsions and negligible leaching into the aqueous phase when emulsified.[3]

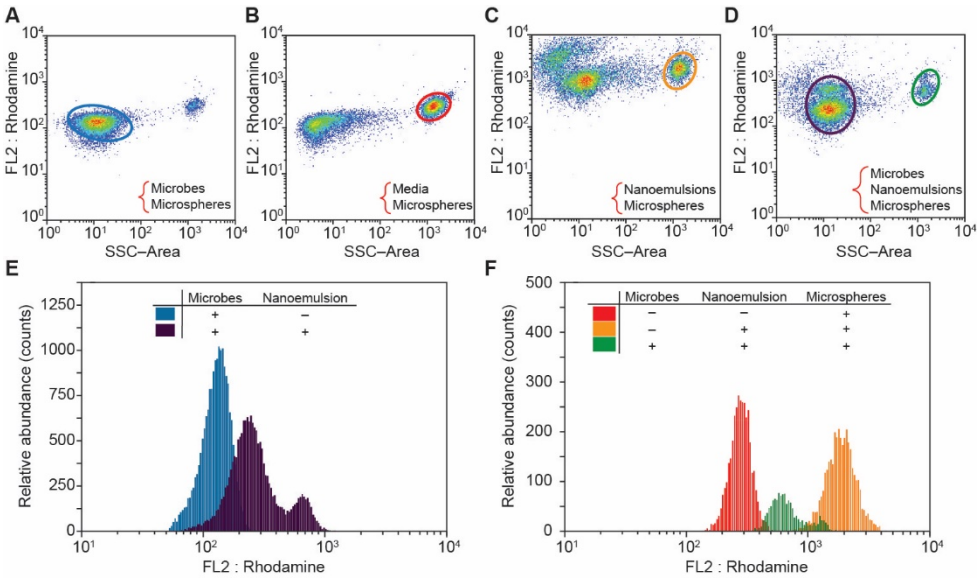


**Figure 3.1. Flow cytometry analysis indicates non-specific binding between nanoemulsion and bacteria. A** to **D**, Flow cytometry analysis of fluorescent intensity (F. I.) of rhodamine dye at 571 nm versus the area of side-scattering (SSC) for *S. ovata* culture (**A**), polystyrene microbeads (**B**), fluorescently tagged PFC nanoemulsions (**C**), and the combination of *S. ovata* and fluorescently tagged PFC nanoemulsions (**D**). Polystyrene microspheres were added to experiments **A**, **C**, and **D** as an internal reference. **E**, Histogram of the fluorescent intensities for *S. ovata* populations without (blue from **a**) and with (purple from **d**) the introduction of fluorescently tagged PFC nanoemulsions. **E**, Histogram of the fluorescent intensity for microspheres in its neat condition (red from **B**), in the presence of fluorescently tagged PFC nanoemulsions (yellow from **C**), and with both *S. ovata* and fluorescently tagged PFC nanoemulsion (green from **D**).

Flow cytometry was conducted with samples of different combinations of *S. ovata* culture, fluorescent PFC nanoemulsions, as well as polystyrene microspheres as an internal standard and control to study binding specificity (Figure 3.1A, 3.1B, 3.1C, and 3.1D). The integration area of side-scattering (SCC) signals, which are indicative of particle sizes, were monitored along with

the fluorescent intensity (F. I.) at 571 nm from the tagged PFC nanoemulsions (see Methods for details). Polystyrene microspheres alone (SSC area ~ $10^3$ a.u.) exhibited minimal emission at 571 nm (Fig. 3.1B). Fig. 3.1A showed that the *S. ovata* (SSC area ~ $10^1$ a.u.) combined with polystyrene microspheres displayed distinctive size features and small background emission, approximately 4.6% of the gated *S.ovata* was determined to be due to background signal (see Supplementary Information for details). The combination of nanoemulsions with polystyrene microspheres exhibits stronger emission at 571 nm for the microspheres (Fig. 3.1C), suggesting a binding affinity between nanoemulsions and microspheres. When all three components are added together (Fig. 3.1D), both *S. ovata* and microspheres showed stronger emission at 571 nm, indicative of non-specific binding from the nanoemulsions. The observations were summarized in the histograms of fluorescent intensity at 571 nm: 1) adding fluorescent nanoemulsions increased the fluorescent intensity of *S. ovata* (Fig. 3.1D); 2) the emission of microspheres increased with the addition of fluorescent nanoemulsions but to a lesser extent when *S. ovata* is also present due to competitive binding (Fig. 3.1E). Contrary to what the mean-field model assumes, PFC nanoemulsions as a proposed $H_2$ carrier exhibits non-specific binding with microorganisms and the local density of nanoemulsion around the microbes is much higher than the ensemble average.

The local kinetic rate of $H_2$ transfer from PFC nanoemulsions can be increased by more than three-fold as compared to the one in aqueous solution. Electrochemical $H_2$ oxidation reaction on a Platinum (Pt) rotating disk electrode (RDE) was applied as a surrogate for the kinetics of $H_2$ consumption on microbes (Fig. 3.2A). Such a practice avoids other interfering biochemical factors and allows us to quantitatively determine the kinetic rate constant and the local $H_2$ concentration.[4]

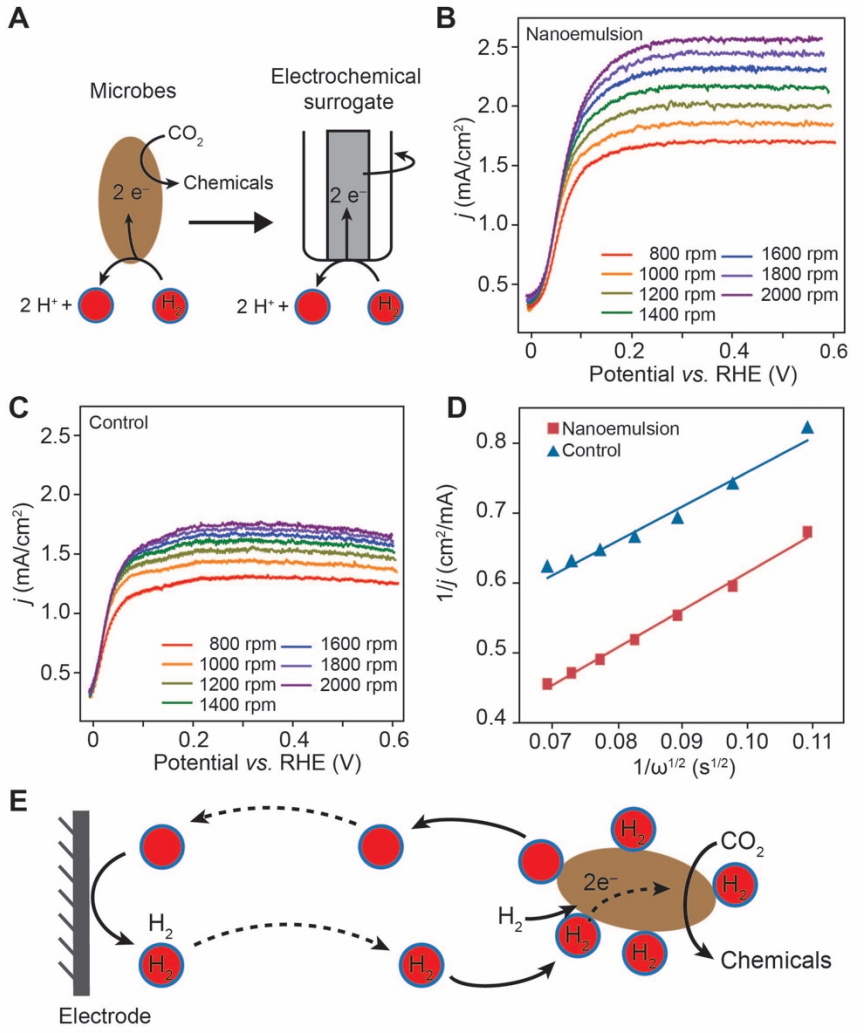


**Figure 3.2. Investigation of the local $H_2$ concentration and transfer kinetics. A**, Electrochemical $H_2$ oxidation with the use of Pt rotating disk electrode (RDE) are employed as a surrogate to probe the kinetics of $H_2$ oxidation in microbes in the presence of PFC nanoemulsions. **B** and **C**, *j*-V relationships with (**B**) and without (**C**) the addition of PFC nanoemulsion (0.5% v/v) in the media solution. The spin rates (ω) of the RDE were changed from 800 to 2000 rpm. The non-zero background was attributed to the residual current in the media solution. RHE, reversible hydrogen electrode. **D**, Koutechý-Levich plots to evaluate the kinetics of $H_2$ oxidation at 0.1 V vs. RHE. $j^{-1}$ ($cm^2$/mA) was plotted versus $\omega^{-1/2}$ ($s^{1/2}$) without (blue) and with (black) the addition of PFC nanoemulsions (0.5%). All RDE experiments were carried out under an atmosphere of 80/20

$H_2/CO_2$ mixture. **E**, Proposed mechanism of PFC nanoemulsion in electricity-driven $CO_2$ reduction with microorganisms.

We found that the surfactant added in the nanoemulsion deactivates the catalytic activity of Pt electrode and the RDE experiments were only capable to be performed in solution with 0.5% PFC nanoemulsion (Figure S2.1). Despite this deactivation, solutions with PFC nanoemulsions displayed much higher steady-state current density of $H_2$ oxidation in $H_2/CO_2$ (80/20) gas mixture (Fig. 3.2B), as compared to the one without nanoemulsions under the same experimental conditions (Fig. 3.2C). This qualitatively suggests that the $H_2$ transfer rate was higher when the nanoemulsions were introduced. Quantitative evaluation of $H_2$ oxidation kinetics was conducted based on the Koutechý-Levich equation that dictates a linear correlation between the inverse of current density ($1/j$) and the inverse of the square root of RDE spin rate ($1/\omega^{0.5}$),[4]

$$\frac{1}{j} = \frac{1}{j_k} + \frac{1}{0.62nFD^{2/3}\nu^{-1/6}C_0}\omega^{-1/2} \qquad (1)$$

Here $j_k$ is the kinetic current density that is intrinsic rate of $H_2$ transfer and oxidation at the interface, $n = 2$ for $H_2$ oxidation to water, $F$ the Faraday's constant, $D$ the diffusion coefficient of $H_2$, $\nu$ the kinematic viscosity of the media, and $C_o$ the local $H_2$ concentration. In Fig. 3.2D, comparison of the Koutechý-Levich plots showed that the y-intercept of solutions containing PFC nanoemulsions (black) is much smaller than the control (blue). The $j_k$ equals 12.9 mA/cm$^2$ when nanoemulsions are present, 3.5 times of the value from control experiment (3.7 mA/cm$^2$). These data suggest that the $H_2$ oxidation kinetics are much faster at the nanoemulsions' surface. We also extracted the local $H_2$ concentration from the RDE results. The diffusion coefficient of $H_2$ in PFC nanoemulsions was determined with Diffusion Ordered Spectroscopy (DOSY) $^1$H NMR experiments; the kinematic viscosities of liquids were determined by a glass kinematic viscometer (see Methods for details). The calculated local $H_2$ concentrations are 0.78 and 1.24 mM at 1 bar

$H_2$ pressure without and with the presence of PFC nanoemulsions, respectively. While the calculated local $H_2$ concentration without nanoemulsions is consistent with the ensemble average (0.79 mM), the calculated local $H_2$ concentration with nanoemulsions is 30% higher than the bulk value (0.95 mM). While the average increase in $H_2$ concentration in the bulk solution is low, there is a significant increase in the local $H_2$ concentration and in the kinetic transfer rate. We could design a nanoemulsion that might more suitably increase the bulk concentration of $H_2$. However, we believe that the increase in kinetic transfer rate is the most important factor to developing an improved system, and we believe in that regard our chosen nanoemulsion is suitable to improve the system. As compared to conventional emulsions,[1] the interfacial effect of faster $H_2$ transfer and higher local $H_2$ concentration is much more prominent in PFC nanoemulsions, thanks to its small size and large surface area.

**Conclusions**

Combining the information obtained from our experiments, we propose a mechanism describing the function of PFC nanoemulsions in electricity-driven microbial $CO_2$ fixation. On the surface of $CO_2$-fixing microbes, there is likely a large coverage of PFC nanoemulsions, due to their non-specific interaction and microscopic size (Fig. 3.2E). When electrochemical water-splitting reaction takes place on the Co-P alloy catalyst, the generated $H_2$ will be delivered either by the unattached nanoemulsion as a $H_2$ carrier or through the mass transport in the aqueous medium. The process of transferring $H_2$ as a reducing equivalent to microbes is significantly accelerated and the local environment is enriched with $H_2$ at the nanoemulsion's surface.

## Methods

### Materials and chemicals.

All chemicals were purchased from Sigma−Aldrich, Thermo Fisher Chemical, or VWR International, unless otherwise stated. Perfluorocarbons (PFCs) were purchased from SynQuest Laboratories. All deionized (DI) water was obtained from a Millipore Millipak® Express 40 system.

### Synthetic procedures of materials

*PFC Nanoemulsions.* Nanoemulsions were prepared via previously reported procedure.[5] 2.8 wt% of surfactant, Pluronic F68, was added to the relevant buffer and sonicated in a bath sonicator, Branson 3800 ultrasonic cleaner, to thoroughly dissolve the polymer. 450 μL of perfluorodecalin, PFD, and 450 μL of perfluorohexane, PFH, were combined in a 15-mL centrifuge tube. The total volume was diluted up to 10 mL with relevant surfactant-containing buffer. Baseline medium, detailed in section "Medium Recipes of Microbial Cultures", was used as the buffer for all experiments, except rotating disk electrode experiments where a phosphate buffer was used instead. The liquid was then sonicated at 35% amplitude for 5 minutes (3 watts, Qsonica). Size distributions of resulting nanoemulsions were analyzed following procedure outlined below in section "Dynamic Light Scattering".

*Fluorescently tagged PFC nanoemulsion.* Fluorous rhodamine was synthesized as previously reported.[6] Fluorous rhodamine was solubilized in 4 μL methoxyperfluorobutane, 8 μL of PFD, and 8 μL of PFH. And the mixture was added to 200 μL of phosphate-buffered saline (PBS) buffer and sonicated at 35% amplitude for 90 seconds. The synthesis of the fluorescently tagged PFC nanoemulsion could be scaled up to 1 mL when needed.

**Protocols of culturing microorganisms**

*Protocol of culturing anaerobic microorganisms.* The anaerobic bacterium *Sporomosa ovata* (ATCC 35899, DSM 2662) was purchased from American Type Culture Collection (ATCC).[3] Detailed recipes of the culture media mentioned in this section are provided in section "Medium Recipes of Microbial Cultures". An ampule of the bacterium was removed from the −80°C freezer. The ampule was broken open under $N_2$ gas and rehydrated with 0.5 mL of DSMZ 311 medium following previous methods for opening an ampule under anaerobic conditions.[7] The microbes were then added to a sealed anaerobic culture tube containing 20 mL of DSMZ 311 medium. The bacterial culture was then incubated at 34°C for three days until the culture reached the stationary phase of growth. At stationary phase, the microbes were transferred to two anaerobic bottles each containing 250 mL of DSMZ 311 medium. A large quantity of *S. ovata* cultures was obtained after a three-day incubation at 34°C. The microbes were transferred to anaerobic culture tubes containing 20% (v/v) dimethyl sulfoxide (DMSO) and 80% (v/v) DSMZ 311 medium. These vials were sealed under anaerobic conditions and stored in a −80°C freezer until experimental use.

When needed a frozen sample of *S. ovata* was removed from the −80°C freezer and thawed. Vials containing 10 mL of the baseline medium were sealed under $H_2/CO_2$ (80/20) gas mixture. Before adding microbes to the container, the sulfide-containing reducing agent was added in a ratio of 0.25 mL per 10 mL of solution to ensure an air-free environment. Microbial culture was subsequently added in a ratio of 0.5 mL per 10 mL of solution. The inoculated tube was then incubated for 3 days at 34°C.

**Electrochemical characterizations**

The electrochemical potentials reported in this manuscript were all referenced to the Reversible Hydrogen Electrode (RHE). We converted experimental data with a Ag/AgCl reference electrode (0.209 V *vs.* SHE, Standard Hydrogen Electrode) with the following formula: Voltage *vs*. RHE = Voltage *vs.* SHE + pH × 0.059 V. Here pH denotes the pH of the solution tested in experiments. All potentials reported here are after *i*R correction.

*Experiments with rotating disk electrode*. The setup of rotating disk electrode (RDE) consisted of a Gamry Interface 1000E potentiostat, a MSR rotator (Pine Research Instrumentation), and an electrochemical glass cell under a controlled gas environment. The electrochemical cell was a 150 mL, five-neck, flat bottom glass flask. The temperature of the setup was maintained at 34 °C by a circulating water bath. A platinum RDE disc electrode of 5.0 mm disk OD (AFE5T050PT, Pine Research Instrumentation), a Ag/AgCl (1M KCl) reference electrode, and a Pt counter electrode were used. Prior to experiments, the working electrode was polished with 0.05 μm diamond, sonicated with DI water, and air dried. The Pt counter electrode was cleaned with dilute $HNO_3$ then DI water. For every measurement, 120 mL fresh electrolyte was saturated with a stream of 13 sccm $N_2/CO_2$ (80/20) or $H_2/CO_2$ (80/20) for at least 10 min. Linear-sweep voltammograms were obtained at spin rates of 800, 1000, 1200, 1400, 1600, 1800, and 2000 rpm, respectively. The interval between each measurement was 1 min. The scanning rate was 50 mV/s.

*Determining the thickness of diffusion layer.* The thickness of diffusion layer was determined based on the following equation,[4]

$$L = nFA\frac{D[C]}{|i|} \quad (2)$$

Where $i$ is current, $n$ the number of electrons in the redox reaction, $F$ the Faraday's constant, $A$ the area of electrode, $D$ the diffusion coefficient of redox molecule, [$C$] is the concentration of redox species, and $L$ the thickness of the diffusion layer. In our study, we chose potassium ferrocyanide ($K_3Fe(CN)_6$) as a single-electron outer-sphere probe molecule. The same configuration as the experiments of bulk electrolysis was set up, except the counter electrode was a Pt wire and the electrolytes were air-saturated. Chronoamperometry was conducted in baseline medium with 3 mM of $K_3Fe(CN)_6$ at −0.6, −0.5, and −0.4 V *vs.* reference for 2 mins each. Similar experiments were conducted with bare baseline medium as a background sample. The resulting changes in electric current when $K_3Fe(CN)_6$ was added were used to calculate the thickness of the diffusion layer, which is about 190 µm. During such a calculation we accounted both sides of the electrode area and applied $6.6\times10^{-6}$ $cm^2/s$ as the value of diffusion coefficient for $K_3Fe(CN)_6$.[8]

**Characterizations with Flow Cytometry**

Experiments of flow cytometry were performed on a Biorad S3e cell sorter with a sample volume of 1.00 mL when two excitation lasers on the instrument (488 and 561 nm, 100mW for both) were turned on. The percentage of the trigger signal, threshold, that would be counted as a single and individual event was 1%. The 488 nm laser was used to collect the signals of forward scattering (FSC) and side scattering (SSC). The photomultiplier tube (PMT) settings for FSC and SSC were 350 and 250 V, respectively. The 561 nm excitation laser was applied to the FL2 detector, which detects 585/25 nm wavelengths. The FL2 detector had a PMT setting of 900 V. 20,000 events were collected for each sample during the measurement. The FL2 detector was used to collect the emission of rhodamine fluorophore at 571 nm under the excitation of 561 nm laser. As an internal standard, polystyrene microspheres from the Invitrogen™ LIVE/DEAD™ *Bac*Light™ bacterial

viability and counting kit for flow cytometry were used under a dilution ratio of 1:100 to achieve in a final concentration of 1 x $10^6$ beads per mL. All data was analyzed using a FlowJo software (version 10). The blank samples containing only the polystyrene microspheres (Fig. 3.1B) were used to distinguish the range of SSC-area for the population of microspheres. Subsequently, samples with *S. ovata* (Fig. 3.1A) were analyzed to determine the range of SSC-area for the microbial population. These gate settings were used to evaluate the populations for other samples (Fig. 3.1C and 3.1D).

Living cultures of *S. ovata* after a three-day incubation were prepared as outlined above for the experiments. Minimal medium, which described in the section "Medium Recipes of Microbial Cultures", was prepared anaerobically with the addition of reducing agent and was subsequently mixed with polystyrene micropsheres (1:100 dilution) along with various combinations of *S. ovata* culture and/or fluorescently tagged PFC nanoemulsion whose preparation was listed above. Our reported data is from results with a dilution ratio of 1:50 for microbial culture. We attempted dilution ratios of PFC nanoemulsion between 1:10 and 1:1000, and the reported data is from results with a dilution ratio of 1:10 in order to obtain a large enough population of signals from PFC nanoemulsion.

**List of samples tested**

| Figures | Nanoemulsion | Cultures of *S. ovata* | Microspheres |
|---|---|---|---|
| Fig. 3B | - | - | + |
| Fig. 3C | + | - | + |
| Fig. 3A | - | + | + |
| Fig. 3D | + | + | + |

The unidentified SSC low population marked as * in Fig. 3.1B is from the medium solution and mostly likely due to the residual particles that were not completely removed during the filtration process. Although these signals overlap with the ones of bacteria shown in Fig. 3.1A, these unidentified signals have minimal interference with other measurements. As stated in above, the concentration of microspheres as an internal standard are the same among all the samples (1:100 dilution) and a total of 20,000 events were collected for each sample during the measurements. In Fig. 3.1B, the microspheres accounts for 45.3% of all the events, and the rest is attributed to the residual particles. In contrast, in Fig. 3.1A, only 3.7% of the 20,000 events is from the microspheres and 92.4% of events is correlated with the addition of bacterial culture. This suggests that the unidentified events from the medium solution only contributes about 4.6% of the counts in Fig. 3.1A. Therefore, we concluded that a predominant majority of the SSC low population in Fig. 3.1A indeed represented the added bacteria, and our conclusion of a non-specific binding with the microbes remains valid.

**Analysis of Experiments with Rotating Disk Electrode**

The Koutechý-Levich plot is governed by the equation below,[4]

$$\frac{1}{j} = \frac{1}{j_k} + \frac{1}{0.62nFD^{2/3}\nu^{-1/6}C_o}\omega^{-1/2} \quad (3)$$

In this equation, $j$ is the current density, $j_k$ the kinetic current density, $n$ is the number of electrons involved in the electrochemical reaction, $F$ the Faraday's constant, $D$ the diffusion coefficient, ν is the kinematic viscosity, $C_o$ is the concentration of the species being reacted at the electrode, and ω is the spin rate. Specifically, in our case, $n = 2$ for electrochemical $H_2$ oxidation. The y-intercepts in the Koutechý-Levich plots lead us to conclude that the values of $j_k$ were 12.9 mA/cm$^2$ and 3.7 mA/cm$^2$ for solutions without and with PFC nanoemulsions, respectively. In order to obtain the

effective concentration of $H_2$ from the Koutechý-Levich equation, the kinematic viscosity ν and diffusion coefficient of $H_2$, *D,* needed to be determined.

*Measurement of kinematic viscosities.* The kinematic viscosity was experimentally determined with a Fisherbrand™ Glass Kinematic Viscometer following the procedures in ASTM D 446. Three measurements were performed for each sample and the average results were used in our analysis. For water, $\nu = 1.04 \times 10^{-6}$ $m^2/s$. For 0.5% PFC nanoemulsion, $\nu = 1.06 \times 10^{-6}$ $m^2/s$.

*Determination of Diffusion Coefficients.* The diffusion coefficients were determined using diffusion-ordered spectroscopy (DOSY) $^1H$ NMR Bruker AV300 at the Molecule Instrumentation Center in UCLA. 0.5% PFC nanoemulsion was prepared using $D_2O$ as the solvent so that there would be no interference from $H_2O$ signal. 1D spectra were taken prior to running DOSY to optimize spectral width and acquisition time. The DOSY spectra were obtained with a diffusion time (Δ) of 50 ms, a diffusion gradient length (δ) of 1.5 ms, a recycle delay between scans of 2 s, and the maximum gradient was 50 gauss·$cm^{-1}$. The spectra are reported in log of diffusion coefficient ($m^2 \cdot s^{-1}$) versus chemical shift (ppm). The diffusion coefficients were found to be 3.72 x $10^{-9}$ $m^2 \cdot s^{-1}$ without the emulsion and 3.02 x $10^{-9}$ $m^2 \cdot s^{-1}$ with the emulsion.

*Calculations of effective $H_2$ concentrations.* Using the values determined above and the slopes in the Koutechý-Levich plots from the RDE experiments, the effective concentrations of $H_2$ were calculated to be 0.75 mM for the nanoemulsion and 0.71 mM for the control under an environment of $H_2/CO_2$ (80/20) mixture at 1 bar. These values correspond to 0.89 and 0.94 mM for nanoemulsion and control under a $H_2$ pressure of 1 bar.

**References**

1. Ju, L. K., Lee, J. F. & Armiger, W. B. Enhancing oxygen transfer in bioreactors by perfluorocarbon emulsions. *Biotechnol Prog* **7**, 323−329 (1991).
2. Gevantman, L. H. in *CRC Handbook of Chemistry and Physics* (ed W. M. Haynes) Ch. 5, 147 (CRC Press, 2015).
3. Möller, B., Oßmer, R., Howard, B. H., Gottschalk, G., Hippe, H. Sporomusa, a new genus of gram-negative anaerobic bacteria including Sporomusa sphaeroides spec. nov. and Sporomusa ovata spec. nov. *Arch. Microbiol.* **139**, 388−396 (1984).
4. Bard, A. J., Faulkner, L. R. *Electrochemical Methods: Fundamentals and Applications*. 2 edn, (John Wiley & Sons, inc., 2001).
5. Sletten, E. M., Swager, T. M. Readily accessible multifunctional fluorous emulsions. *Chem Sci.* **7**, 5091−5097 (2016).
6. Sletten, E. M., Swager, T. M. Fluorofluorophores: fluorescent fluorous chemical tools spanning the visible spectrum. *J Am Chem Soc* **136**, 13574−13577 (2014).
7. Nichols, E. M. *et al.* Hybrid bioinorganic approach to solar-to-chemical conversion. *Proc Natl Acad Sci U S A* **112**, 11461−11466 (2015).
8. Konopka, S. J., McDuffie, B. Diffusion coefficients of ferri- and ferrocyanide ions in aqueous media, using twin-electrode thin-layer electrochemistry. *Anal Chem.* **42**, 1741−1746 (1970).

**Supplementary Information**

**Medium Recipes of Microbial Cultures**

*DSMZ 311 Medium*

| | |
|---|---|
| $NH_4Cl$ | 0.50 g |
| $MgSO_4$ • 7 H2O | 0.50 g |
| $CaCl_2$ • 2 $H_2O$ | 0.25 g |
| NaCl | 2.25 g |
| $FeSO_4$ • 7 $H_2O$ | 0.002g |
| Trace element solution SL-10 (see below) | 1.00 ml |
| Selenite-tungstate solution (see below) | 1.00 ml |
| Yeast extract | 2.00 g |
| Casitone | 2.00 g |
| Betaine • $H_2O$ | 6.70 g |
| Na-resazurin solution (0.1% w/v) | 0.50 ml |
| $K_2HPO_4$ | 0.35 g |
| $KH_2PO_4$ | 0.23 g |
| $NaHCO_3$ | 4.00 g |
| Vitamin solution (see below) | 10.00 ml |
| Distilled water | 1000.00 ml |

All ingredients (except phosphates, bicarbonate, vitamins, cysteine and sulfide) were dissolved first. And the medium was sparged with $N_2/CO_2$ (80/20) gas mixture while boiling to make the

solution anoxic. Once cool, and while still sparging with the same gas, phosphates, vitamins (sterilized by filtration) and carbonate were added. The medium was dispensed under the same gas into anaerobic culture tubes and then autoclaved. The pH of the complete medium was adjusted to pH 7.0, if necessary.

*Trace element solution (SL-10)*

| | |
|---|---|
| Nitrilotriacetic acid | 1.50 g |
| $MgSO_4 \cdot 7\ H_2O$ | 3.00 g |
| $MnSO_4 \cdot H_2O$ | 0.50 g |
| NaCl | 1.00 g |
| $FeSO_4 \cdot 7\ H_2O$ | 0.10 g |
| $CoSO_4 \cdot 7\ H_2O$ | 0.18 g |
| $CaCl_2 \cdot 2\ H_2O$ | 0.10 g |
| $ZnSO_4 \cdot 7\ H_2O$ | 0.18 g |
| $CuSO_4 \cdot 5\ H_2O$ | 0.01 g |
| $KAl(SO_4)_2 \cdot 12\ H_2O$ | 0.02 g |
| $H_3BO_3$ | 0.01 g |
| $Na_2MoO_4 \cdot 2\ H_2O$ | 0.01 g |
| $NiCl_2 \cdot 6\ H_2O$ | 0.03 g |
| $Na_2SeO_3 \cdot 5\ H_2O$ | 0.30 mg |
| Na2WO4 • 2 $H_2O$ | 0.40 mg |
| Distilled water | 1000.00 ml |

The nitrilotriacetic acid was first dissolved and the pH adjusted to 6.5 with KOH, then the minerals were added. The final pH was adjusted to pH 7.0 with KOH.

*Vitamin solution*

| | |
|---|---|
| Biotin | 2.00 mg |
| Folic acid | 2.00 mg |
| Pyridoxine-HCl | 10.00 mg |
| Thiamine-HCl • 2 H2O | 5.00 mg |
| Riboflavin | 5.00 mg |
| Nicotinic acid | 5.00 mg |
| D-Ca-pantothenate | 5.00 mg |
| Vitamin B12 | 0.10 mg |
| p-Aminobenzoic acid | 5.00 mg |
| Lipoic acid | 5.00 mg |
| Distilled water | 1000.00 ml |

*Selenite-tungstate solution*

| | |
|---|---|
| NaOH | 0.5 g |
| $Na_2SeO_3 \cdot 5\ H_2O$ | 3.0 mg |
| $Na_2WO_4 \cdot 2\ H_2O$ | 4.0 mg |
| Distilled water | 1000.0 ml |

*Reducing agent solution*

All the water used in this procedure was boiled and gassed under $N_2$ prior to the experiments. 12.5 g cysteine-HCl was dissolved in 500 mL water in a 2-L Erlenmeyer flask. The pH of the solution was adjusted to 9.5 with NaOH. 12.5 g of washed crystals of $Na_2S{\cdot}9H_2O$ was weighted in a plastic tray and then transferred into the flask containing cysteine-HCl. The volume of the solution was brought up to 1000 mL. The whole solution was brought to boil and cool again under gassing with $N_2$. 20 mL of the prepared solution was dispensed into one 25-mL vial which was pre-flushed with $N_2$. The vials were sealed and then autoclaved for 15 min at 121 ºC.

*Baseline Medium*

| | |
|---|---|
| $K_2HPO_4$ | 0.348 g |
| $KH_2PO_4$ | 0.227 g |
| $Na_2HPO_4 \bullet 7H_2O$ | 2.145 g |
| $NaH_2PO_4 \bullet H_2O$ | 0.938 g |
| $NH_4Cl$ | 0.500 g |
| $MgSO_4 \bullet 7H_2O$ | 0.500 g |
| $CaCl_2 \bullet 2H_2O$ | 0.250 g |
| NaCl | 0.918 g |
| $FeSO_4 \bullet 7H_2O$ | 0.002 g |
| $NaHSeO_3$ | 10-7 mol/L |
| $NaHCO_3$ | 4.000 g |
| SL-10 solution | 1 mL |
| Vitamin solution | 10 mL |
| Yeast extract | 2.000 g |

Compared to the DSMZ-recommended growth medium, the concentration of phosphate buffer was increased by 5 times from 3.7 mM to 18.5 mM without changing the overall $K^+$ and $Na^+$ concentration. All ingredients (except phosphates, bicarbonate, vitamins, cysteine and sulfide) were dissolved first. And the medium was sparged with $N_2/CO_2$ (80/20) gas mixture while boiling to make the solution anoxic. Once cool, and while still sparging with the same gas, phosphates, vitamins (sterilized by filtration) and carbonate were added. The medium was dispensed under the same gas into anaerobic culture tubes and then autoclaved. The pH of the complete medium was adjusted to pH 7.0, if necessary. High-salinity medium was prepared based on the recipe above, while the concentration of the phosphate buffer was increased three-fold from 18.5 mM to 55.5 mM. Minimal medium, which was used in the experiments of flow cytometry, was prepared following the same procedure as the baseline media, however it only included $NH_4Cl$, NaCl, $K_2HPO_4$, $KH_2PO_4$, and $NaHCO_3$.

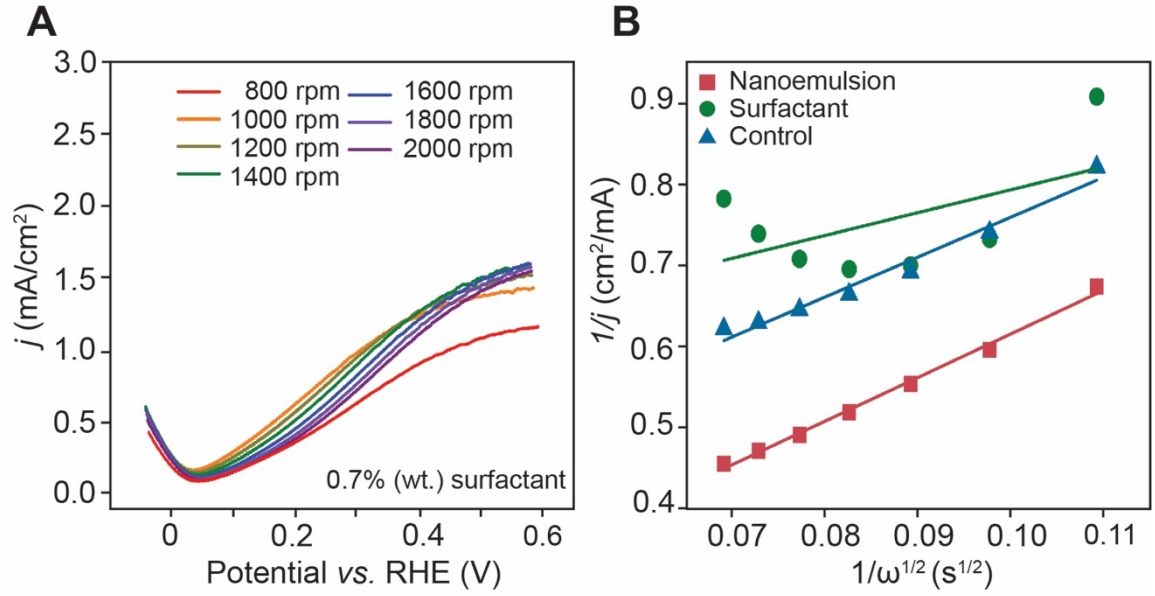


**Supplementary Fig. 3.1. a,** Linear-sweep voltammograms of Pt RDE electrode under an environment of $H_2/CO_2$ (80/20) gas mixture (50 mV/s) with 0.7 wt% surfactant, which corresponds to 2.5% PFC nanoemulsion. The introduction of surfactants deactivates the hydrogen oxidation activity on Pt electrode. **b**, Koutechý-Levich plots of Pt RDE electrode at 0.1 V *vs.* RHE in the control medium (blue), with 0.5% PFC nanoemulsion (red), and with 0.14 wt% surfactant that was added when preparing 0.5% PFC nanoemulsion (green).

# CHAPTER 4. PERFLUOROCARBON NANOEMULSION ASSISTED HYBRID BIO-INORGANIC NITROGEN FIXATION.

This chapter is a version of Lu, S.; Rodrigues, R. M.; Huang, S.; Estabrook, D. A.; Chapman, J. O.; Guan, X.; Sletten, E. M.; and Liu, C. "Perfluorocarbon Nanoemulsions Create a Beneficial $O_2$ Microenvironment in $N_2$-fixing Biological | Inorganic Hybrid." *Chem Catalysis. In press.*


## Abstract

Powered by renewable electricity, a biological | inorganic hybrid employs water-splitting electrocatalysis and generates $H_2$ as reducing equivalents for microbial catalysis. The approach integrates the beauty of biocatalysis with the energy efficiency of inorganic materials for sustainable chemical production. Yet a successful integration requires delicate control of the hybrid's extracellular chemical environment. Such an argument is evident in the exemplary case of $O_2$ because biocatalysis has a stringent requirement of $O_2$ but the electrocatalysis may inadvertently perturb the oxidative pressure of biological moieties. Here we report that the addition of perfluorocarbon (PFC) nanoemulsions promote a biocompatible $O_2$ microenvironment in a $O_2$-sensitive $N_2$-fixing biological | inorganic hybrid.


## Introduction

Natural biological systems possess time-tested catalytic capability of chemical synthesis. Therefore, one approach to tackle the challenge of distributed chemical production with renewable energy is to interface microbial catalysts with inorganic electrochemical materials powered by solar panels, namely the biological | inorganic hybrid, which combines the energy efficiency of synthetic materials with the selectivity and specificity of biochemical synthesis[1-3]. Significant

development has been observed in this fledgling direction for solar-driven reduction of $CO_2$ and $N_2$ with high efficiency and reaction throughput[4-10].Water-splitting inorganic electrocatalysts generate $H_2$ as the reducing equivalents for microbial catalysts, which enables a selective production of multi-carbon commodity chemicals[4,8,10-16] pharmaceutical precursors[10,11] and nitrogen fertilizers from $N_2$ even at low partial pressures[5,6,9,17-20] Fundamentally, the key towards a successful hybrid system is the compatibility between the abiotic and biological components. For example, the design and application of an inorganic water-splitting electrocatalytic system that yields minimal reactive oxygen species achieves high biocompatibility with bacteria of $CO_2$/$N_2$ fixation, leading to energy efficiency of solar-driven $CO_2$ fixation up to 10%[8,9]. Addressing biocompatibility with ingenious materials design offers a general route viable for effective production of chemicals with a biological | inorganic hybrid.

Reconciling the $O_2$ demand of biochemical synthesis with water-splitting electrocatalysis in a biological | inorganic hybrid is essential for efficient production of a wide range of chemicals. $O_2$ serves as the terminal electron acceptor in many biochemical pathways and is ubiquitous in extracellular medium[21]. Nonetheless, many of the upstream catalysts in biochemical pathways are sensitive if not incompatible with even trace amounts of $O_2$. Take biological $N_2$ fixation as one example. $N_2$-fixing nitrogenase enzymes reduce $N_2$ with the supply of reducing equivalents and adenosine triphosphate (ATP), and are sensitive to $O_2$ due to its low-valence Fe- and FeMo-based sulfur clusters[22-24]. Meanwhile, many $N_2$-fixing diazotrophs demand $O_2$ as the terminal electron acceptor for the production of ATP and reducing equivalents, the ubiquitous energy source for all biochemical reactions and microbial survival. Therefore, there is a stringent requirement of microbial $O_2$-intake flux, represented as an extracellular $O_2$ concentration of roughly 1~5%, for

typical $N_2$-fixing microbes that utilize $O_2$ as the terminal electron acceptors in the electron transport chain[9,25-27].

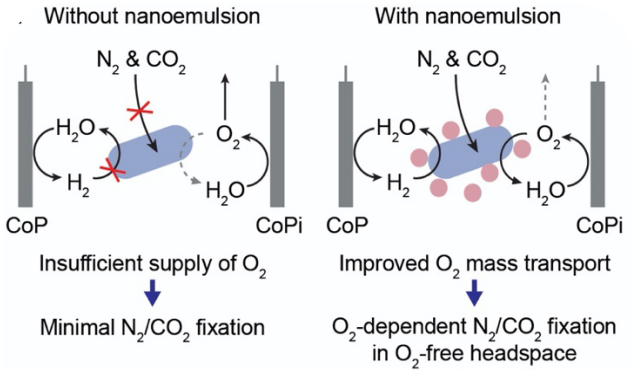


**Figure 4.1. Microbial microenvironment created by perfluorocarbon (PFC) nanoemulsion.** Schematic of the bacterial microenvironment created by PFC nanoemulsions and its benefits for $O_2$ mass transport. CoP, cobalt-phosphorous alloy for hydrogen evolution reaction; CoPi, cobalt phosphate for water oxidation reaction.

In the biological | inorganic hybrid, the water-splitting electrocatalysis and its generation of $O_2$ introduce perturbations to the extracellular environment that may adversely impact the delicate $O_2$ balance for $N_2$-fixing microbes. Previously reported biological | inorganic hybrids with $N_2/CO_2$-fixing bacterium *Xanthobacter autotrophicus*[26,27] addresses such an $O_2$ requirement by feeding a constant gas stream of $O_2/CO_2/N_2$ gas with 2% $O_2$ and forcing a biocompatible microaerobic atmosphere[9]. Such an enforced microaerobic environment is not ideal for practical application nor energy efficient at the system level due to the energy cost of gas mixing for a precise $O_2$ partial pressure. $O_2$-reactive redox mediators such as viologen[28-30] or $O_2$-reducing wire array electrodes[19] were employed previously to create microenvironments of reduced $O_2$ concentrations commensurate with the enzymatic or microbial $O_2$ demands. Yet those designs based on redox reactions with $O_2$ consume electricity and pose additional overhead towards the hybrids' efficiency. Alternatively, we aim to design a strategy that does not consume electrons

while still creates a desirable extracellular $O_2$ microenvironment. We hypothesize that the oxidative generation of $O_2$ from water-splitting electrocatalysis, previously untapped and perceived as an unwanted perturbation to biological $O_2$ compatibility, should be sufficient to support the $O_2$ demand of the $N_2$-fixing *X. autotrophicus* in an $O_2$-free external environment, if the electrochemically generated $O_2$ can be efficiently transported for a desirable bacterial extracellular microenvironment (Figure 4.1). Such consideration leads to the search of a design from a materials perspective that creates a controllable biological gas microenvironment.

**Results**

The persistency of the bacterial microenvironment created by biocompatible PFC nanoemulsions and the associated enhancement of $O_2$ availability presents PFC nanoemulsions as a suitable candidate to tackle the issue of $O_2$ biocompatibility without consuming additional electrons as the cases reported previously[10,19]. In a single-chamber hybrid system without an external $O_2$ supply, the introduction of PFC nanoemulsions presumably enable the $O_2$ generated from electrochemical water oxidation alone to be sufficient to satisfy the $O_2$-dependent $N_2/CO_2$ fixation in *X. autotrophicus*, by facilitating the mass transport and availability of $O_2$ in the bacterial microenvironment (Figure 4.1). We strive to test this working hypothesis and one preparatory step in our investigation is to ensure that the introduction of PFC nanoemulsions does not adversely affect the electrochemical water-splitting process in the hybrid. Biocompatible cobalt phosphate ($CoP_i$) loaded on carbon cloth and cobalt-phosphorous alloy (CoP) loaded on stainless steel mesh, whose water-splitting mechanisms have been studied before,[31,32] were prepared following previous literature for electrochemical generation of $O_2$ and $H_2$, respectively (See experimental procedures)[8,9,12]. PFC nanoemulsions of 0%, 1.25%, 2.5% and 3.75% (v/v) were added into

minimal medium without any nitrogen and organic carbon along with *X. autotrophicus* inoculations (See Methods) (Figure 4.2A).

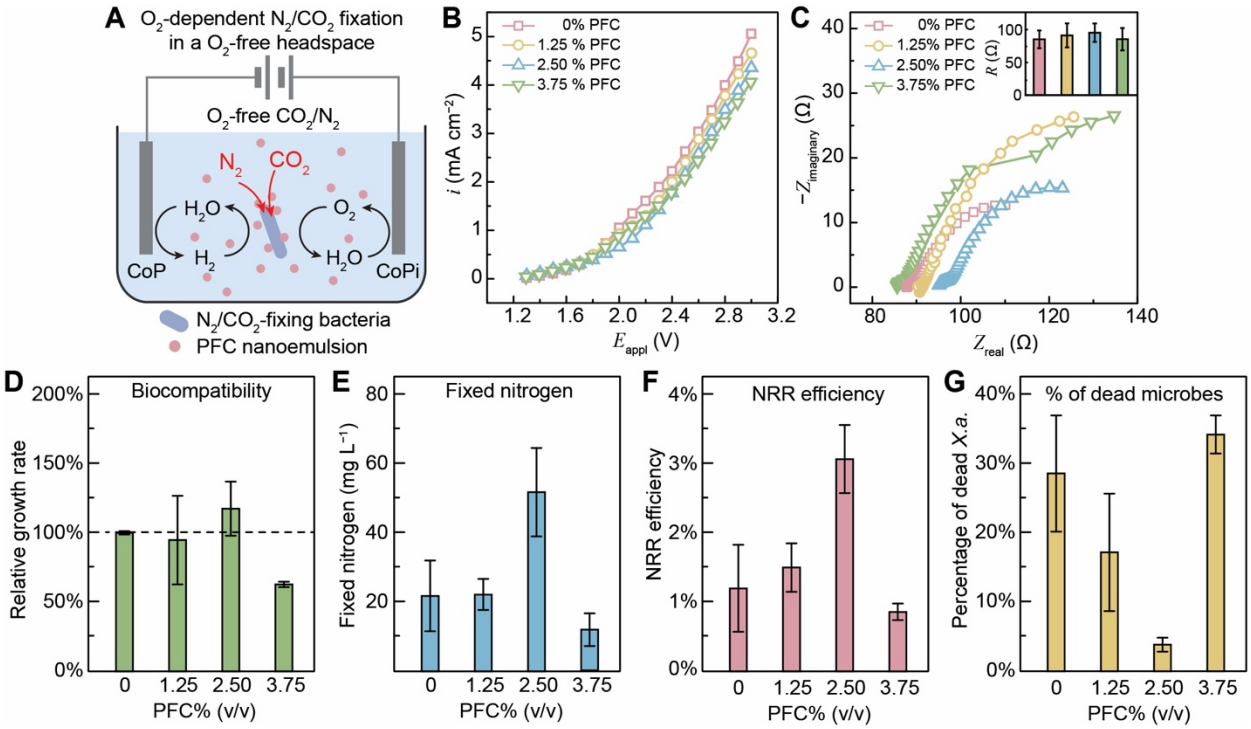


**Figure 4.2. $O_2$-dependent microbial $N_2/CO_2$ fixation in a $O_2$-free headspace driven by electricity. A**, Reactor schematic of the biological | inorganic hybrid in a $O_2$-free headspace for $N_2/CO_2$ fixation. **B** & **C**, The relationships between current density ($i$) and applied potential ($E_{appl}$) (**B**), and representative Nyquist plots from electrochemical impedance spectroscopy (**C**), between CoP and CoPi electrodes for reactors of varying concentrations of PFC nanoemulsions. Inset in **C**, series resistance ($R$) of the reactor determined from the Nyquist plots ($n$ = 8). **D**, The relative growth rate of *X. autotrophicus* in mineral medium during a 5-day gas fermentation under varying concentrations of PFC nanoemulsions. $n$ = 4. **E** to **G**, the amount of fixed nitrogen (**E**), the corresponding overall electron efficiency of nitrogen reduction reaction (NRR) (**F**), and the percentage of dead *X. autotrophicus* (*X. a.*) (**G**), after a 5-day reaction under varying concentrations

of PFC nanoemulsions. 1-bar $O_2$-free atmosphere of 20% $CO_2$ and 80% $N_2$; $E_{appl}$ = 3.0 V; 30 ºC; $n$ = 4.

Multi-step choronoamperometry yields near-identical *i-V* curves among all four conditions (Figure 4.2B). It shows that the constitution of PFC nanoemulsions used in this work does not have a significant influence on the catalytic activity of the electrodes over the range of applied potentials. It also hints that the accelerated mass transport enabled by nanoemulsion for gas-consuming reaction does not alter the kinetics of gas-generating water-splitting reaction. Electrochemical impedance spectroscopy was also conducted in the hybrid system and the Nyquist plots at all four conditions are similar to each other as displayed in Figure 4C. The derived values of series resistance *R* form such measurements, indicative of solution's electrical conductivity, remain unchanged (inset in Figure 4.2C). Those electrochemical measurements reveal that PFC nanoemulsions, within the percentage range used in this work, do not have significant impacts on the electrochemical water splitting reaction in our hybrid system. We further tested whether the introduction of PFC nanoemulsions affects the growth of *X. autotrophicus*. *X. autotrophicus* were cultured in minimal medium with 0 %, 1.25 %, 2.5 % and 3.75 % (v/v) PFC nanoemulsions under a 1-bar gas mixture of 2% $O_2$, 60% $N_2$, 20% $H_2$ and 18% $CO_2$ (See Methods). Similar growth rates of *X. autotrophicus*, determined from the changes of total nitrogen values in a 5-day period, were observed among 0 %, 1.25% and 2.5% PFC, while a slightly lower growth rate was observed for microbes in 3.75% PFC nanoemulsions (Figure 4.2D). The absence of any significant growth enhancement under a $O_2$-containing gas environment, different from the observed enhancement for *S. ovata* in $H_2$,[12] indirectly suggests that the similarly enhanced mass transport of $H_2$ should not contribute significantly in our current system. The similar growth rates of *X. autotrophicus* in

the presence of PFC nanoemulsions suggest the biocompatibility of PFC nanoemulsions up to 3.75% (v/v).

Experimental results support our working hypothesis that the nanoemulsion-induced microenvironment leads to full utilization of electrochemically generated $O_2$, enhanced cell viability, and a boosted efficiency for electricity-driven microbial $N_2/CO_2$ fixation. In a single-chamber, two-electrode reactor at 30 ºC, a $O_2$-free gas environment was maintained with 20% $CO_2$ and 80% $N_2$ as the sole carbon and nitrogen source for *X. autotrophicus*. Chronoamperometry at $E_{appl}$ = 3.0 V was conducted for 5 days and the resultant yields of $CO_2$ and $N_2$ fixation were quantified based on appropriate calibrations (Figure S4.1) following previously published procedure (See Methods)[12,19,33,34]. Among the experiments with different PFC nanoemulsion contents (0, 1.25, 2.50, and 3.75 %, v/v), a maximal yield of $N_2$ fixation was observed with a concentration of 2.50% PFC nanoemulsion (Figure 4.2E). The amount of fixed total nitrogen tops at 52±13 mg/L, *i.e.* ~ 3 mM (n = 4). The resultant overall electron efficiency that calculates the percentage of electric charge towards $N_2$ fixation, in addition to the roughly 21 % overall electron efficiency of $CO_2$ fixation (See Methods)[21], reaches 3.07±0.49 % (n = 4) and is about 250 % higher than the control case when no PFC nanoemulsions were introduced (0 % v/v) (Figure 4.2F). In those experiments, along with free nanoemulsions there are bacterial-bound PFC nanoemulsions of a fully surrounded microenvironment due to the high binding constant $K_{sp}$ (*vide supra*). Since previous literature[25-27] and our own experience of culturing *X. autotrophicus* suggest minimal microbial growth when $O_2$ is depleted, our observed $N_2$ fixation of the hybrid system in an $O_2$-free headspace is in accordance with the hypothesis that the created microenvironment enables an $O_2$-dependent biocatalytic $N_2/CO_2$ fixation in an $O_2$-free gas headspace, by fully utilizing the electrochemically generated $O_2$ from water oxidation via the enhanced $O_2$ transport kinetic.

Experimental evidence that further supports our argument can be obtained from the percentage of bacterial cells remaining viable during the electricity-driven process of $N_2/CO_2$ fixation. Aliquots of bacterial cultures were sampled at the day 4 of electrolysis and the viabilities of those bacteria were determined by flow cytometry with a bacterial Live/Dead staining kit (See Methods, Figure S4.2). About 30 % of *X. autotrophicus* were dead without the addition of nanoemulsion (0% PFC in Figure 4.2G), while only 3% of dead bacteria were detected with 2.75% nanoemulsion (2.75% PFC in Figure 4.2G). The latter value in a presumably unfit $O_2$-free headspace is comparable with the < 5% observed in healthy cultures grown under a previously reported microaerobic atmosphere of 2% $O_2$[9]. While the percentage of dead cells did not fully capture the fitness and metabolic status of the microbes due to the presence of stationary cells, the increased cell viability (Figure 4.2G) and $N_2$ fixation efficiency (Figure 4.2F) corroborate that the increased $O_2$ mass transport induced by nanoemulsion addition enhanced ATP generation, the production of reducing equivalents, and subsequently $N_2$ fixation with concurrent cell growth. Our results shows that the creation of nanoemulsion-based microenvironment and the subsequently enhanced $O_2$ transport from electrochemical water oxidation preserves the viability of $O_2$-demanding *X. autotrophicus* without external gas supply of $O_2$.

An excessive amount of PFC nanoemulsion may be detrimental towards the biological | inorganic hybrid despite the created microenvironment. Cell viability assay indicates that excessively high concentration of PFC nanoemulsion (3.75% PFC in Figure 4.2G) leads to about 35% of dead bacteria in the culture, which is much higher than the 3% of dead microbes observed with 2.75% loading of PFC nanoemulsions. This finding agrees with the biocompatibility test results, where *X. autotrophicus* cultured in 3.75% PFC are showing slower growth than those under conditions with lower PFC percentage (Figure 4.2D). Such a decrease of cell viability is in

accordance with the observed decrease for fixed nitrogen amount and the overall electron efficiency of $N_2$ fixation (Figure 4.2E and 4.2F). One interpretation to such results is that excessively high PFC concentration will lead to a high concentration of intracellular $O_2$, which benefits cellular ATP and energy production but impedes the activity of bacterial $N_2$ fixation. Therefore, while a suitable dose of PFC nanoemulsion creates a beneficial microenvironment for bacterial survival, other detrimental factors will overwrite such a benefit under excessively high PFC loading amount. Advanced design of the PFC nanoemulsions with more biocompatible surfactants or PFC composition[35,36] will help to mitigate the toxicity issue at high nanoemulsion concentrations. As the liquid culture of *X. autotrophicus* themselves were considered as an "organic" version of biofertilizers for crop growth,[9] our knowledge obtained here will guide future general designs for biological | inorganic hybrid with the production of organic fertilizers.

**Conclusions**

In addition to ensuring biocompatibility, biological | inorganic hybrid offers a great opportunity of expanding the operation conditions for biocatalysis with the advanced designs in materials. In this work, we tackled on one ubiquitous issue: the mismatch of the $O_2$ demand between the native requirement in biocatalysis and the constrains in practical application. We demonstrate the feasibility of $O_2$-depenent microbial $N_2/CO_2$ fixation in a $O_2$-free headspace, by employing PFC nanoemulsions to maximize the use of electrochemically generated $O_2$, a typically deemed "waste" in electricity-driven $N_2/CO_2$ fixation. Given the various application situations and the multitude of intertwining among anaerobic and aerobic pathways in biochemistry[37], our design is applicable to other biochemical systems whenever the $O_2$ incompatibility arises in a biological | inorganic hybrid, thanks to PFC's biocompatibility and the strong, non-specific binding of nanoemulsions.

## Methods

### Biocompatibility test of *X. autotrophicus* with nanoemulsions

For each set of tests, four 20-mL glass screw top vials were autoclaved with a small stir bar. Microbial culture, PFC nanoemulsions, and minimal medium were combined to achieve a starting volume of 8 mL total. The volume of culture used was adjusted from $OD_{600}$ after resuspension in the minimal medium to give a final $OD_{600}$ of 0.2 in the experiment. PFC nanoemulsion was added to achieve final 1.25, 2.5 and 3.75 % PFC nanoemulsion in the 8 mL, respectively. The total volume was then adjusted to 8 mL with the minimal medium. All samples were cultured autotrophically at 30 °C in the all-inorganic minimal medium with an anaerobic jar (Vacu-Quick Jar System, Almore) under a 1-bar gas mixture of 2% $O_2$, 60% $N_2$, 20% $H_2$ and 18% $CO_2$. One set of viability tests, which consisted of 4 20-mL vials, one for each percent PFC nanoemulsion (0, 1.25, 2.5 and 3.75 %) were placed in an aforementioned air-tight jar and incubated under $N_2$ fixation condition for 5 days. 1 mL of sample was taken from each vial and frozen right before the incubation starts and right after the incubation ends. The total nitrogen contents of the samples were analyzed as described in "quantification of total nitrogen**"**. The increase of total nitrogen content after 5 days' incubation compared to the total nitrogen content before incubation was considered as the relative growth of microbes.

### Electrochemical characterizations and the setup of biological | inorganic hybrid

The experiments of biological | inorganic hybrids were conducted in a 250-mL GL45 glass bottles using modified bottle caps with four 1/4-28 ports (Western Analytics). A two-electrode setup was established in which the working electrode is a CC electrode loaded with CoPi catalyst and the reference/counter end is a SS mesh loaded with Co-P alloy catalyst. The total liquid volume was

100 mL, and the electrolyte is a mixture of microbes, minimal medium, and PFC nanoemulsion, with a starting $OD_{600}$ of 0.2 for microbes and the appropriate PFC percentage for the given experiment. A maximum of 8 electrochemical experiments were run in parallel using a Gamry Interface 1000E potentiostat coupled with a Gamry ECMB multiplexer. Steady-state *i-V* correlations were established with multi-step chronoamperometry. The applied potential ($_{l}E_{appl}$) ranges from 1.3 to 3.0 V with at an interval of 0.05 V. At each voltage step, the corresponding $E_{appl}$ was maintained for 2 min. Electrochemical impedance spectroscopy (EIS) were measured at open circuit potential with an AC amplitude of 50 mV. Measurements were performed at frequencies between 100 kHz and 10 Hz with 10 data points per decade. Nyquist plots were plotted and used to extract the approximated series resistances ($R$) of reactors at day 0 of experiments under different conditions. The hybrid operates at a constant $E_{appl}$ for 5 days under a $O_2$-free headspace gas environment that only contains $N_2$ and $CO_2$ (80/20) for microbial fixation of $N_2$ and $CO_2$. Liquid cultures that include both microbial suspension and soluble chemicals were sampled and frozen right before and after the bulk electrolysis for further analysis. Samples for cell viability determination under different concentrations of PFC nanoemulsion were collected on the 4$^{th}$ day of the experiment.

**Performance of biological | inorganic hybrid**

The total nitrogen and carbon in both the biomass and liquid solution was analyzed using commercial assay kit from Hach Company. Total nitrogen was performed using the Hach Company total nitrogen reagent kit, Test ‘N Tube (Product #2714100), following the provided procedural instructions (DOC316.53.01085) by observing the absorbance of 410 nm at the end of protocol. As used previously for electricity-driven microbial $N_2$ fixation,[9] this measurement

protocol allows the quantification of nitrogen content from all nitrogen-containing compounds notwithstanding $N_2$, which are either dissolved in the liquid solution or accumulated in the biomass. The total nitrogen content was then quantified using calibration curves correlating the absorbance at 410 nm and total nitrogen concentration, constructed using the kit on different standard nitrogen sample solutions (ammonium *p*-toluenesulfonate, Hach). For each of the different percentage of PFC nanoemulsion (0%, 1.25%, 2.5% and 3.75% in minimal medium) a calibration curve was made using the corresponding PFC nanoemulsion as solvent to prepare standard solutions (Figure S4). The absorbance was measured using Agilent Cary 60 UV-Vis spectrophotometer.

The overall electron efficiency (*E. E.*) of $N_2$ reduction reaction in each experiment was determined using the following formula[9,19]:

$$E.E. = \frac{\left[\left(\Delta N_{\mathrm{TNT}}(\mathrm{mg}\ )\right)}{1000 \times 14\ \mathrm{g\ mol^{-1}}] \times V_{\mathrm{solution}}(\mathrm{L}) \times 3 \times F(\mathrm{C\ mol^{-1}})}{Overall\ charge\ (\mathrm{C})} \times 100\% \qquad (1)$$

Here $\Delta N_{\mathrm{TNT}}$ (mg $L^{-1}$) is the change of nitrogen content from day 0 to day 5 in the experiment; $V_{\mathrm{solution}}$ the total volume of solution; $F$ the Faraday constant, and *Overall charge* is the total electric charges passed through the cathodic chamber. The number 3 is the number of electrons required to reduce one nitrogen atom in $N_2$ reduction reaction. We note that our calculation did not consider the possible loss of electrochemically generated $H_2$ along with other possible side reactions. Therefore, the calculated values are a lower-bound estimate for the $N_2$ fixation capablity in our system.

The overall electron efficiency (*E. E.*) of $CO_2$ reduction reaction in each experiment was estimated based on previous C/N ration of *X. autotrophicus* (1.5 mg N $cell^{-1}$ vs. 6.4 mg C $cell^{-1}$,

*i.e.* C/N ~ 4.27)[21], assuming all fixed carbon and nitrogen forms biomass based on the following formula[9,19]:

$$E.E. = \frac{\left[\frac{(\Delta N_{\mathrm{TNT}}(\mathrm{mg}\ ) \times 4.3)}{1000 \times 12\ \mathrm{g\ mol^{-1}}}\right] \times V_{\mathrm{solution}}(\mathrm{L}) \times 4 \times F(\mathrm{C\ mol^{-1}})}{Overall\ charge\ (\mathrm{C})} \times 100\% \qquad (2)$$

Here $\Delta N_{\mathrm{TNT}}$ (mg $L^{-1}$) is the change of nitrogen content from day 0 to day 5 of the experiment; $V_{\mathrm{solution}}$ the total volume of solution; $F$ the Faraday constant, and *Overall charge* is the total electric charges passed through the cathodic chamber. The number 4 is the number of electrons required to reduce one carbon atom in $CO_2$ reduction reaction.

**Experiments of flow cytometry related to microbes and PFC nanoemulsions**

Experiments of flow cytometry (BD LSR II cytometer) were conducted at the Janis V. Giorgi Flow Cytometry Core, UCLA. The flow cytometer was operated under a slow flow rate setting. Forward Scattering (FSC) was used as the threshold for events. For each sample and control, 10,000 events were collected and recorded. The recorded events were plotted as 2-D scatter plots of FSC and Side Scattering (SSC) for the gating of microbes, particles, and nanoemulsions. Data were analyzed using FlowJo ver. 10 and the gating represents >95% of the clustered events.

The following procedures were applied to quantify viability of *X. autotrophicus* in different concentrations of PFC nanoemulsions. Samples of *X. autotrophicus* were harvested via centrifugation (6000 rpm, 5 min), and re-suspended in 1 mL of 0.85% NaCl. The samples were then added with 1.5 μL of SYTO™ 9 dye solution and 1.5 μL of propidium iodide solution from the LIVE/DEAD™ BacLight™ Bacterial Viability and Counting Kit, following the instructions from the manufacturer. After a 15-min incubation in dark, the samples were tested by a flow cytometer after a dilution of about 20~50 times. Two pre-defined fluorescence measurement

channels, one for AlexaFluor-488 and the other for PE (Phycoerythrin), were used to measure the fluorescence intensity of SYTO $^{TM}$ 9 and propidium iodide, respectively. The gating of live and dead cells (>95% events) were determined from sample actively grown under $N_2/CO_2$-fixing condition in a anaerobic jar (live reference) and the one treated with pure ethanol for 1 hr before staining (dead reference). Results of dead and live reference samples were shown in Figure S5.

**References**


1. Chen, H. *et al.* Fundamentals, Applications, and Future Directions of Bioelectrocatalysis. *Chem. Rev.* **120**, 12903-12993, doi:10.1021/acs.chemrev.0c00472 (2020).
2. Sakimoto, K. K. *et al.* Physical Biology of the Materials-Microorganism Interface. *J Am Chem Soc* **140**, 1978-1985, doi:10.1021/jacs.7b11135 (2018).
3. Nangle, S. N., Sakimoto, K. K., Silver, P. A. & Nocera, D. G. Biological-inorganic hybrid systems as a generalized platform for chemical production. *Curr Opin Chem Biol* **41**, 107-113, doi:10.1016/j.cbpa.2017.10.023 (2017).
4. Nevin, K. P., Woodard, T. L., Franks, A. E., Summers, Z. M. & Lovley, D. R. Microbial electrosynthesis: feeding microbes electricity to convert carbon dioxide and water to multicarbon extracellular organic compounds. *mBio* **1**, doi:10.1128/mBio.00103-10 (2010).
5. Brown, K. A. *et al.* Light-driven dinitrogen reduction catalyzed by a CdS:nitrogenase MoFe protein biohybrid. *Science* **352**, 448, doi:10.1126/science.aaf2091 (2016).
6. Hickey, D. P. *et al.* Pyrene hydrogel for promoting direct bioelectrochemistry: ATP-independent electroenzymatic reduction of N2. *Chem Sci* **9**, 5172-5177, doi:10.1039/c8sc01638k (2018).

7. Sakimoto, K. K., Wong, A. B. & Yang, P. D. Self-photosensitization of nonphotosynthetic bacteria for solar-to-chemical production. *Science* **351**, 74-77, doi:10.1126/science.aad3317 (2016).
8. Liu, C., Colon, B. C., Ziesack, M., Silver, P. A. & Nocera, D. G. Water splitting-biosynthetic system with CO2 reduction efficiencies exceeding photosynthesis. *Science* **352**, 1210-1213, doi:10.1126/science.aaf5039 (2016).
9. Liu, C., Sakimoto, K. K., Colon, B. C., Silver, P. A. & Nocera, D. G. Ambient nitrogen reduction cycle using a hybrid inorganic-biological system. *Proc. Natl. Acad. Sci. U. S. A.* **114**, 6450-6455, doi:10.1073/pnas.1706371114 (2017).
10. Liu, C. *et al.* Nanowire-bacteria hybrids for unassisted solar carbon dioxide fixation to value-added chemicals. *Nano Lett* **15**, 3634-3639, doi:10.1021/acs.nanolett.5b01254 (2015).
11. Guo, J. *et al.* Light-driven fine chemical production in yeast biohybrids. *Science* **362**, 813-816, doi:10.1126/science.aat9777 (2018).
12. Rodrigues, R. M. *et al.* Perfluorocarbon nanoemulsion promotes the delivery of reducing equivalents for electricity-driven microbial CO2 reduction. *Nat Catal* **2**, 407-414, doi:10.1038/s41929-019-0264-0 (2019).
13. Su, Y. *et al.* Close-Packed Nanowire-Bacteria Hybrids for Efficient Solar-Driven $CO_2$ Fixation. *Joule*, doi:10.1016/j.joule.2020.03.001.
14. Jourdin, L. *et al.* High Acetic Acid Production Rate Obtained by Microbial Electrosynthesis from Carbon Dioxide. *Environ Sci Technol* **49**, 13566-13574, doi:10.1021/acs.est.5b03821 (2015).
15. Zhang, H. *et al.* Bacteria photosensitized by intracellular gold nanoclusters for solar fuel production. *Nat Nanotechnol* **13**, 900-+, doi:10.1038/s41565-018-0267-z (2018).

16. Nichols, E. M. *et al.* Hybrid bioinorganic approach to solar-to-chemical conversion. *Proc Natl Acad Sci U S A* **112**, 11461-11466, doi:10.1073/pnas.1508075112 (2015).
17. Rago, L. *et al.* Bioelectrochemical Nitrogen fixation (e-BNF): Electro-stimulation of enriched biofilm communities drives autotrophic nitrogen and carbon fixation. *Bioelectrochemistry* **125**, 105-115, doi:https://doi.org/10.1016/j.bioelechem.2018.10.002 (2019).
18. Soundararajan, M. *et al.* Phototrophic N2 and CO2 Fixation Using a Rhodopseudomonas palustris-H2 Mediated Electrochemical System With Infrared Photons. *Front. Microbiol.* **10**, doi:10.3389/fmicb.2019.01817 (2019).
19. Lu, S., Guan, X. & Liu, C. Electricity-powered artificial root nodule. *Nat Commun* **11**, 1505, doi:10.1038/s41467-020-15314-9 (2020).
20. Milton, R. D. *et al.* Nitrogenase bioelectrocatalysis: heterogeneous ammonia and hydrogen production by MoFe protein. *Energy Environ. Sci.* **9**, 2550-2554, doi:10.1039/c6ee01432a (2016).
21. Schmidt-Rohr, K. Oxygen Is the High-Energy Molecule Powering Complex Multicellular Life: Fundamental Corrections to Traditional Bioenergetics. *ACS Omega* **5**, 2221-2233, doi:10.1021/acsomega.9b03352 (2020).
22. Goldberg, I., Nadler, V. & Hochman, A. Mechanism of Nitrogenase Switch-Off by Oxygen. *J. Bacteriol.* **169**, 874-879, doi:DOI 10.1128/jb.169.2.874-879.1987 (1987).
23. Hartmann, A. & Burris, R. H. Regulation of Nitrogenase Activity by Oxygen in Azospirillum-Brasilense and Azospirillum-Lipoferum. *J. Bacteriol.* **169**, 944-948, doi:DOI 10.1128/jb.169.3.944-948.1987 (1987).
24. Wong, P. P. & Burris, R. H. Nature of Oxygen Inhibition of Nitrogenase from Azotobacter-Vinelandii. *Proc. Natl. Acad. Sci. U. S. A.* **69**, 672-&, doi:DOI 10.1073/pnas.69.3.672 (1972).

25. Malik, K. A. & Schlegel, H. G. Enrichment and isolation of new nitrogen-fixing hydrogen bacteria. *FEMS Microbiol. Lett.* **8**, 101-104, doi:http://dx.doi.org/ (1980).

26. Malik, K. A. & Schlegel, H. G. Chemolithoautotrophic Growth of Bacteria Able to Grow under N-2-Fixing Conditions. *FEMS Microbiol. Lett.* **11**, 63-67 (1981).

27. Wiegel, J. in *The Prokaryotes: Volume 5: Proteobacteria: Alpha and Beta Subclasses* (eds Martin Dworkin *et al.*) 290-314 (Springer New York, 2006).

28. Oughli, A. A. *et al.* A Redox Hydrogel Protects the O2-Sensitive [FeFe]-Hydrogenase from Chlamydomonas reinhardtii from Oxidative Damage. *Angew. Chem., Int. Ed.* **54**, 12329-12333, doi:10.1002/anie.201502776 (2015).

29. Plumere, N. *et al.* A redox hydrogel protects hydrogenase from high-potential deactivation and oxygen damage. *Nat Chem* **6**, 822-827, doi:10.1038/Nchem.2022 (2014).

30. Cai, R. & Minteer, S. D. Nitrogenase Bioelectrocatalysis: From Understanding Electron-Transfer Mechanisms to Energy Applications. *Acs Energy Lett* **3**, 2736-2742, doi:10.1021/acsenergylett.8b01637 (2018).

31. Surendranath, Y., Kanan, M. W. & Nocera, D. G. Mechanistic Studies of the Oxygen Evolution Reaction by a Cobalt-Phosphate Catalyst at Neutral pH. *J. Am. Chem. Soc.* **132**, 16501-16509, doi:10.1021/ja106102b (2010).

32. Popczun, E. J., Read, C. G., Roske, C. W., Lewis, N. S. & Schaak, R. E. Highly Active Electrocatalysis of the Hydrogen Evolution Reaction by Cobalt Phosphide Nanoparticles. *Angew. Chem., Int. Ed.* **53**, 5427-5430, doi:10.1002/anie.201402646 (2014).

33. Dubber, D. & Gray, N. F. Replacement of chemical oxygen demand (COD) with total organic carbon (TOC) for monitoring wastewater treatment performance to minimize disposal of toxic

analytical waste. *J Environ Sci Heal A* **45**, 1595-1600, doi:10.1080/10934529.2010.506116 (2010).

34. Fraser, L. H., Carty, S. M. & Steer, D. A test of four plant species to reduce total nitrogen and total phosphorus from soil leachate in subsurface wetland microcosms. *Bioresource Technology* **94**, 185-192, doi:https://doi.org/10.1016/j.biortech.2003.11.023 (2004).
35. Sletten, E. M. & Swager, T. M. Readily accessible multifunctional fluorous emulsions. *Chemical Science* **7**, 5091-5097, doi:10.1039/C6SC00341A (2016).
36. Estabrook, D. A., Ennis, A. F., Day, R. A. & Sletten, E. M. Controlling nanoemulsion surface chemistry with poly(2-oxazoline) amphiphiles. *Chem Sci* **10**, 3994-4003, doi:10.1039/c8sc05735d (2019).
37. Salimijazi, F. *et al.* Constraints on the Efficiency of Engineered Electromicrobial Production. *Joule*, doi:10.1016/j.joule.2020.08.010 (2020).
38. Möller, B., Oßmer, R., Howard, B. H., Gottschalk, G. & Hippe, H. Sporomusa, a new genus of gram-negative anaerobic bacteria including Sporomusa sphaeroides spec. nov. and Sporomusa ovata spec. nov. *Arch Microbiol* **139**, 388-396, doi:10.1007/BF00408385 (1984).

**Supplementary Information**

**Medium Recipes of Microbial Cultures**

*Minimal medium*

| | |
|---|---|
| $K_2HPO_4$ | 1 g |
| $KH_2PO_4$ | 0.5 g |
| $NaHCO_3$ | 2 g |
| $MgSO_4 \cdot 7\ H_2O$ | 0.1g |
| $CaSO_4 \cdot 2\ H_2O$ | 0.04 g |
| $FeSO_4 \cdot 7\ H_2O$ | 0.001g |
| Trace mineral mix (see below) | 1.00 ml |
| Deionized water | 1000.00 ml |

All ingredients were combined and sonicated for about 10 minutes to dissolve. The medium was autoclaved at 120 °C with water for 30 min. Once cool the medium was filtered via vacuum filtration through a 0.22 μm filter. The pH of the complete medium was adjusted to pH 7.0, if necessary.

*Trace mineral mix*

| | |
|---|---|
| $H_3BO_3$ | 2.8 g |
| $MgSO_4 \cdot 4\ H_2O$ | 2.1 g |
| $Na_2MoO_4 \cdot 2\ H_2O$ | 0.75 g |
| $ZnSO_4 \cdot 7\ H_2O$ | 0.24 g |
| $Cu(SO_3)_2 \cdot 3\ H_2O$ | 0.04 g |
| $NiSO_4 \cdot 6\ H_2O$ | 0.13 g |

| | |
|---|---|
| Deionized water | 1000.00 ml |

All components were mixed and stirred for 1 hr to dissolve. The solution was vacuum filtered through a 0.22 μm filter to sterilize.

*Succinate nutrient broth*

| | |
|---|---|
| Nutrient broth | 5 g |
| Yeast extract | 4 g |
| NaCl | 3 g |
| Sodium succinate | 5 g |
| Deionized water | 1000.00 ml |

All ingredients were combined and sonicated for about 10 minutes to dissolve. The solution was autoclaved at 120 °C with water for 30 min.

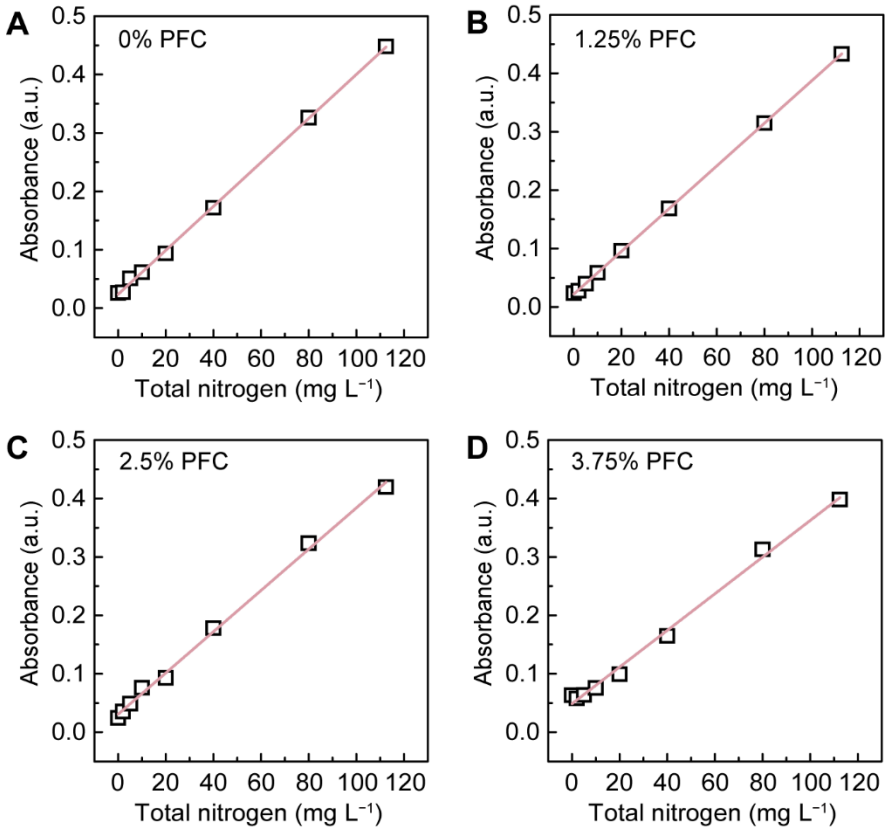


**Figure S4.1. Calibration curves of total nitrogen contents in different solution media**

Calibration curves of total nitrogen contents based on the optical absorbance at 410 nm, when Hach Company total nitrogen reagent kit, Test 'N Tube (Product #2714100) was employed. **A** to **D**, 0%, 1.25%, 2.5%, and 3.75% PFC nanoemulsion in minimal medium, respectively. A specific calibration curve at each PFC concentration is required because we experimentally found that the presence of PFC affect the assay sensitivity of total nitrogen contents.

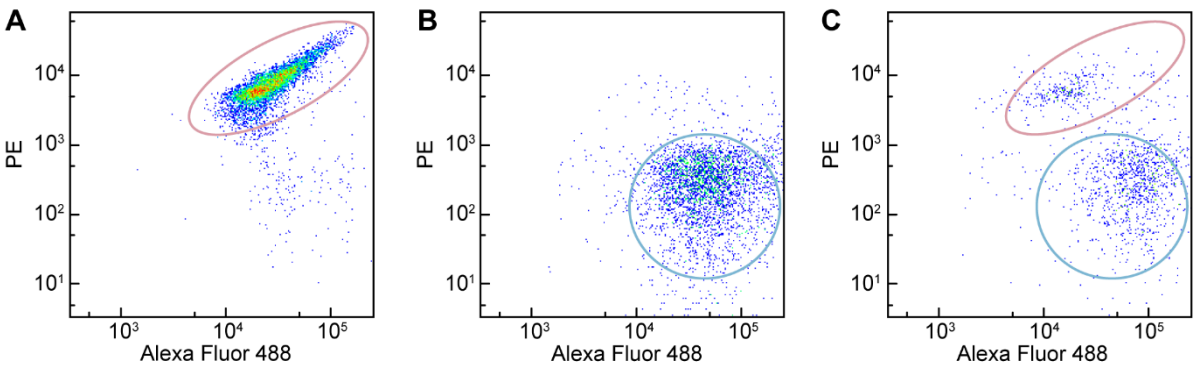


**Figure S4.2. Representative Live/Dead microbial stain flow cytometry data**

(**A, B** and **C**) Two-parameter density plot based on fluorescence intensity of Alexa Fluor 488 channel and phycoerythrin (PE) for a 100% dead microbes (**A**), 100% live microbes (**B**) and a representative sample that contains a mixture of live and dead microbes (**C**). Red circle is the gate for dead microbes and blue circle is the gate of live microbes.

# CHAPTER 5. CHARACTERIZING ALTERED MICROBIAL OXYGEN GAS ENVIRONMENT WITH PERFLUOROCARBON NANOEMULSIONS

This chapter is a version of Lu, S.; Rodrigues, R. M.; Huang, S.; Estabrook, D. A.; Chapman, J. O.; Guan, X.; Sletten, E. M.; and Liu, C. "Perfluorocarbon Nanoemulsions Create a Beneficial $O_2$ Microenvironment in $N_2$-fixing Biological | Inorganic Hybrid." *Chem Catalysis. In press.*


## Abstract

In this mechanistic study, we found that PFC nanoemulsion can be adsorbed to the surface of microbes and increase both the speed of $O_2$ reduction and the local solubility of $O_2$. Rotation disk electrode measurements have shown a 20-fold increase of $O_2$ reduction speed with the presence of PFC nanoemulsion. The adsorption of PFC nanoemulsions on microbial surface were visually observed via microscopy. Flow cytometry was used to quantify the adsorption of PFC nanoemulsions on microbes. The process follows the Langmuir adsorption model. The adoption will lead to a higher local concentration of PFC nanoemulsion, leading to a significant increase of $O_2$ solubility around the microbe. The adsorption of PFC nanoemulsion on various particles/microbes was also quantified to show that such interaction could be influenced by the properties of the particle/microbe.


## Introduction

Nature's biological system has gone through billions of years to evolve and develop efficient ways to harness available resources and produce energy or useful chemicals. Such ways have encouraged numerous scientists to design biomimetic systems, aiming to harness some of nature's most efficient methods for a wide variety of applications. Biocatalysis has taken a prominent role

in industrial processes to produce various chemicals in a more environmentally friendly manner than traditional organometallic catalytic processes.[1-3] Recently, attention has been given to interfacing biological catalysts with inorganic electrocatalytic systems for a variety of applications, including nitrogen[4-9] and carbon dioxide fixation[10-18]. This hybrid approach combines the environmentally benign benefits of biocatalysis with the enhanced throughput and efficiency of electrocatalysis. However, interfacing biologic and inorganic components has presented challenges such as the biocompatibility of electrode materials. Additionally, the mass transport, especially that of the gaseous components (*i.e.* $O_2$, $N_2$, etc.) in the aqueous solutions required by the biotic components may also be a limiting of the hybrid system. While significant research has been done to develop efficient and biologically compatible electrode materials[19-24], little focus has been on fundamentally understanding the role that the gas transport plays in these hybrid systems.

In this work, the gas environment in the hybrid system discussed in **Chapter 4** was studied. Experiments of confocal microscopy allowed us to visualize the adsorption of PFC nanoemulsion onto the microbe for the first time. Such adsorption was also quantitatively studied, and it was found that the adsorption process follows the Langmuir gas adsorption model. We were able to quantify the equilibrium constant and maximum number of PFC nanoemulsions adsorbed onto the surface of the *X. autotrophicus* strain used in this hybrid system, the *Sporomusa ovata* microbe strain used in the previous $CO_2$ hybrid system, and polystyrene (PS) spheres of different surface modifications. The results show that the shape and surface chemistry can influence the adsorption of PFC nanoemulsions onto microparticles such as microbes.

**Results**

Fluorescent colocalization experiments using confocal microscopy suggest that PFC nanoemulsions bind strongly to $CO_2/N_2$-fixing *X. autotrophicus* and creates a unique bacterial microenvironment. *X. autotrophicus* (American Type Culture Collection, ATCC 35674) was autotrophically cultured in a minimal medium without any nitrogen and organic carbon under a 1-bar gas environment of 2% $O_2$, 60% $N_2$, 20% $H_2$, and 18% $CO_2$ (See Supplementary Information)[7,25,26]. PFC nanoemulsions of perfluorodecalin and perfluorohexane were prepared by ultrasonication in the same minimal medium with Pluronic F68 as surfactant (See Methods)[27]. Experiments of dynamic light scatting determined an averaged diameter of about 240 nm for the prepared PFC nanoemulsions (Figure S5.1), consistent with the diameter of a stable emulsion formulated in our previous report[28]. In order to tag the microbes and nanoemulsions with different fluorescent emitters, *X. autotrophicus* was incubated with SYTO™ 9, a green fluorescent nucleic acid stain, while red-emitting fluorous rhodamine reported previously[29] was incorporated into nanoemulsion during the ultrasonication stage of nanoemulsion preparation (See Methods).

When mixtures of fluorescently tagged *X. autotrophicus* ($OD_{600}$ = 0.1) and PFC nanoemulsions (2.5% volume percentage, v/v) were deposited on a coverslip (Figure 5.1A), *in vitro* confocal microscopy images in Figure 5.1B, 5.1C and Figure S5.2 suggest strong colocalization of the green emission from microbes (490~520 nm, named "STYO™ 9" in the figure) and the red emission from nanoemulsions (590~650 nm, named "Rhodamine" in the figure). Control experiment of *X. autotrophicus* in the absence of nanoemulsions displays minimal red emission, excluding any significant contribution of red microbial autofluorescence in the results. A closer examination of the overlay from both emissions (Figure 5.1B and 5.1C) display a corona of red emissions surrounding the green ones. This indicates that the PFC nanoemulsions

surround and bind strongly to *X. autotrophicus*, creating an extracellular microenvironment that could dictate bacterial metabolism.

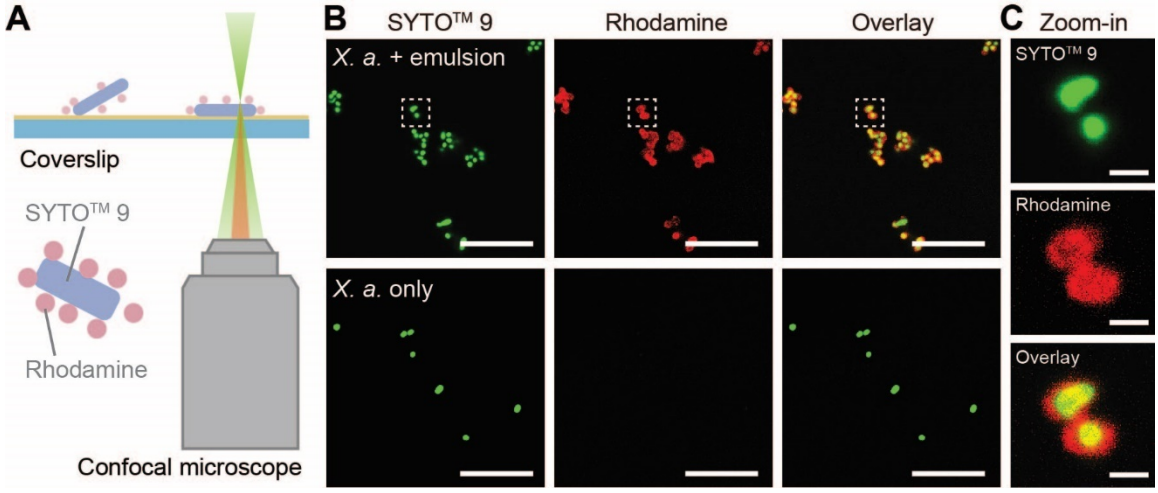


**Figure 5.1. Microbe and nanoemulsion colocalization. A**, Schematic of colocalization experiment with fluorescent confocal microscopy. **B**, Fluorescent images of bacteria *Xanthabacter autotrophicus* (*X. a.*) stained with SYTO™ 9 (pseudo-colored green), PFC nanoemulsions tagged with fluorous rhodamine (pseudo-colored red), and the overlay images of both fluorescent emissions. PFC nanoemulsion loading, 2.5 volume percentage (v/v). **C**, Zoom-in images in the highlighted area in **B**. Scale bars = 10 and 1 μm in **B** and **C**, respectively.

The binding between bacteria and PFC nanoemulsions can be quantitatively described by a Langmuir-type adsorption model with high binding affinity and low binding specificity towards microbial surface properties (Figure 5.2A). Non-labelled *X. autotrophicus* cultures were mixed with fluorescently tagged PFC nanoemulsions (10 % v/v) at different dilution ratios. The resultant mixture, whose concentrations $C_{PFC} = C_{PFC,0}$ / dilution ratio ($C_{PFC,0}$ = 10 % v/v), were studied by flow cytometry.

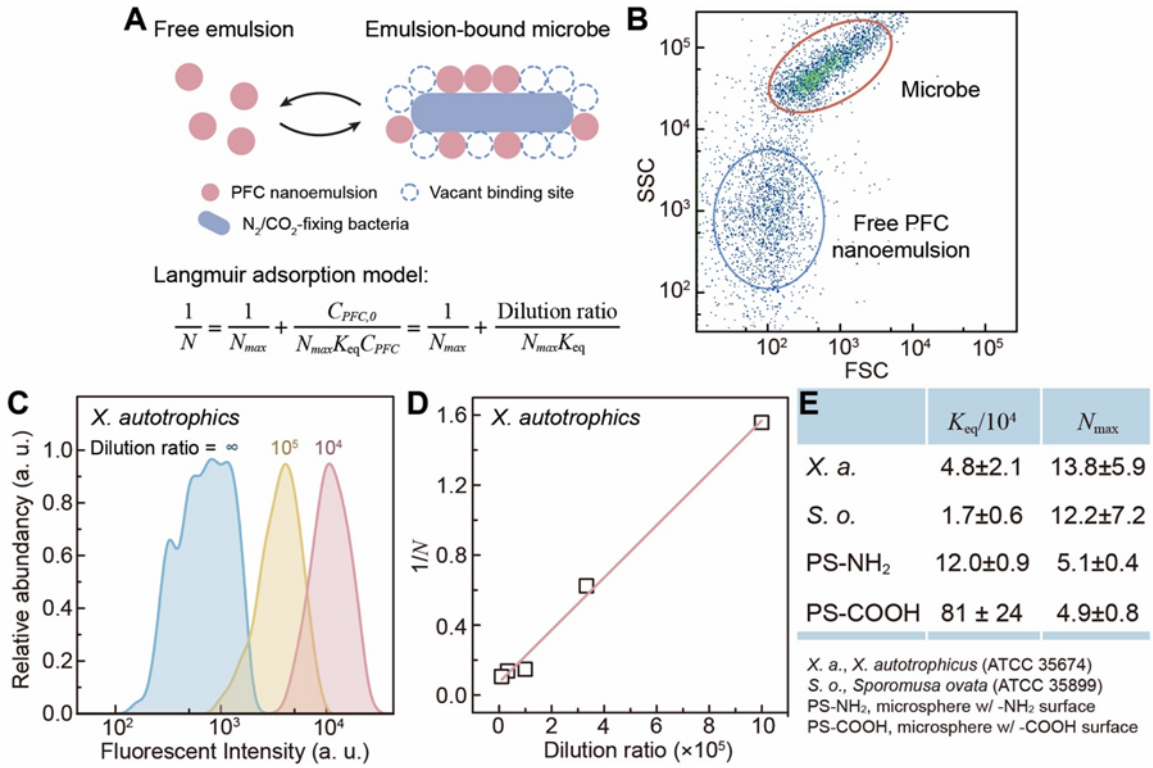


| | $K_{eq}/10^4$ | $N_{max}$ |
|---|---|---|
| *X. a.* | 4.8±2.1 | 13.8±5.9 |
| *S. o.* | 1.7±0.6 | 12.2±7.2 |
| PS-$NH_2$ | 12.0±0.9 | 5.1±0.4 |
| PS-COOH | 81 ± 24 | 4.9±0.8 |

**Figure 5.2. Quantification of microenvironment formation with flow cytometry. A**, The binding between the bacteria and PFC nanoemulsions follows the Langmuir adsorption model. $N$ and $N_{max}$, the experimentally determined average and theoretical maximal number of nanoemulsions per microbe; $K_{eq}$, the dimensionless binding constant; $C_{PFC,0}$ & $C_{PFC}$, the concentrations of PFC nanoemulsion before and after dilution under a certain "dilution ratio", respectively. **B**, Representative two-parameter density plot in flow cytometry based on forward scattering (FSC) and side scattering (SSC) which gates the populations of *X. autotrophicus* potentially with nanoemulsion adsorption (red circle) and free PFC nanoemulsion (blue circle). **C**, Histograms of fluorescent intensities for *X. autotrophicus* (red circle in **B**) in PFC-free microbial suspension (blue, dilution ratio = ∞), emulsion-microbe mixture with a dilution ratio = $10^5$ (yellow) and $10^4$ (red). **D**, Plot of $1/N$ vs. dilution ratio for *X. autotrophicus*. **E**, Experimentally determined $K_{eq}$ and $N_{max}$ values for *X. autotrophicus* (*X. a.*), *Sporomusa ovata* (*S. o.*), and 2-μm polystyrene

microspheres with $-NH_2$ and $-COOH$ surface functionalization groups ("PS-$NH_2$" and "PS-COOH, respectively). n = 3.

Here the employment of flow cytometry allows us to quantitatively distinguish the free and microbe-bound nanoemulsions (Figure 5.2B and 5.2C) and determine the average number of PFC nanoemulsions per microbe ($N$) as a function of nanoemulsion dilution ratios. We observed a linear relationship between $1/N$ and the dilution ratio, we subsequently concluded that $1/N$ is linearly dependent on $1/C_{PFC}$ (Figure 5.2D). This observation suggests that a Langmuir monolayer adsorption model, illustrated in Figure 5.2A, is sufficient to describe the binding between microbes and nanoemulsions:[30]

$$\frac{1}{N} = \frac{1}{N_{max}} + \frac{1}{N_{max}K_{eq}(C_{PFC}/C_{PFC,0})} = \frac{1}{N_{max}} + \frac{dilution\ ratio}{N_{max}K_{eq}} \quad (1)$$

Here $N_{max}$ denotes the maximum number of adsorbed nanoemulsions for one bacterial cell, $K_{eq}$ the dimensionless equilibrium constant of the binding event, and $C_{PFC,0}$ = 10 % (v/v) as the PFC concentration in the starting nanoemulsion. Linear regression was conducted to extract the values of $K_{eq}$ and $N_{max}$ for *X. autotrophicus*: $N_{max}$ = 13.8±5.9 and $K_{eq}$ = 4.8±2.1×$10^4$ (Figure 5.2D; n = 3, same below unless noted specifically). Because the PFC nanoemulsions are about 240 nm in diameter (Figure S1) and *X. autotrophicus* exhibits a typical ellipsoidal morphology of about 1 μm in size (Figure 5.1C, 5.1D and Figure S5.2)[25,31], the measured $N_{max}$ value suggests a near-complete surrounding of nanoemulsion on the bacterial surface at maximum binding, *i.e.* a compartmentalized microenvironment created by the nanoemulsion for the $N_2$/$CO_2$-fixing bacterium. The large value of measured $K_{eq}$ between PFC nanoemulsion and *X. autotrophicus* ensures the stability and prevalence of the created microenvironment under typical working conditions for the biological | inorganic hybrid (*vide infra*). We also determined the values of $K_{eq}$ and $N_{max}$ for 2-μm polystyrene microspheres of positive or negative charges ($-NH_2$ or $-COOH$

functionalized, respectively), as well as acetogenic *Sporomusa ovata* that were previously employed with PFC nanoemulsions for boosted throughput in electricity-driven $CO_2$ fixation (Figure S5.3)[28]. The values of $K_{eq}$ and $N_{max}$ persist at about $10^4$~$10^5$ and $10^0$~$10^1$ (Figure 5.2E), respectively. In comparison with microbes, the mildly higher value of $K_{eq}$ for polystyrene microspheres hints that the binding strength could be enhanced with enriched surface charges, yet other factors are also at play given the slightly lower values of $N_{max}$ despite microspheres' slightly larger size. Nonetheless, the microbial binding of PFC nanoemulsion seems strong, nonspecific, and can serve as a general venue of creating a customized microenvironment for microbial catalysts.

The observed bacterial microenvironment created by PFC nanoemulsions led us to probe the possible modulation of local $O_2$ supply due to PFC's high gas solubilities[32-34]. As the binding of PFC nanoemulsion appears nonspecific and persistently strong (*vide supra*), we posit that a platinum-based metallic electrode could serve as a surrogate of the bacterial surface for $O_2$-respiring *X. autotrophicus*, thus the electrochemical activity of the 4-electron $O_2$ reduction on Pt electrode[35,36] in the presence of nanoemulsions will yield information of the created microenvironment, similar to our previous study that employed PFC nanoemulsions for electricity-driven microbial $CO_2$ reduction[28]. A Pt-based rotating disk electrode[37] (RDE) was deployed to create a well-defined $O_2$ mass transport for quantitative study (Figure 5.3A). A pH = 7.0 phosphate buffer solution was applied in lieu of the microbial minimal medium solution to avoid the interference from trace metals and other competing biochemical reactions. In this phosphate buffer, a PFC nanoemulsion concentration of 0.75% (v/v) was used for the RDE experiments, as the emulsion's surfactant interferes with the catalytic activity of the Pt electrode at higher concentrations[28].

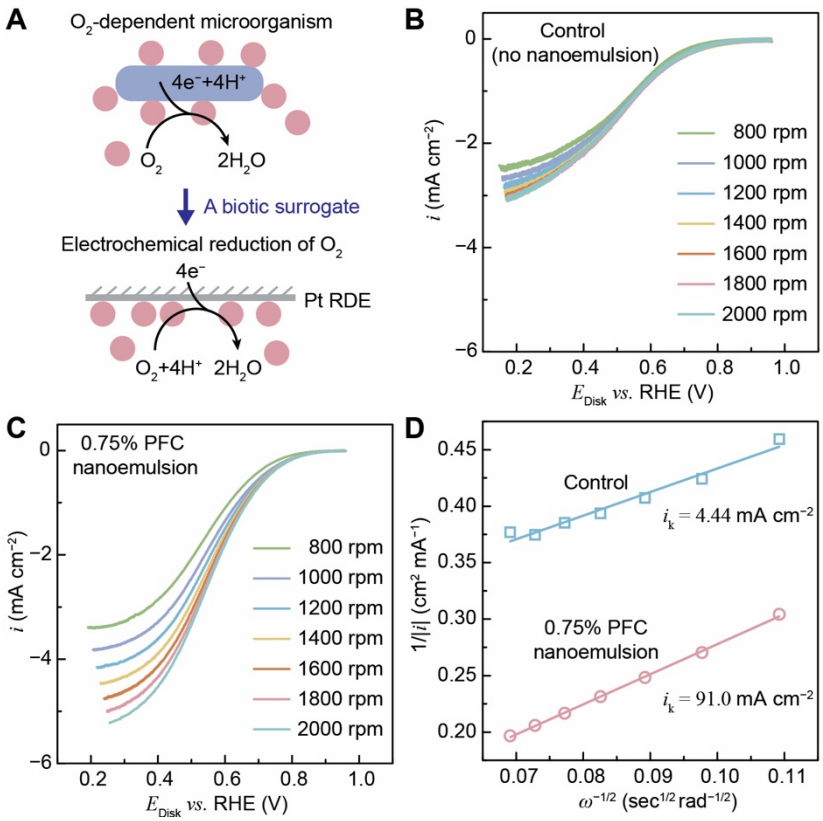


**Figure 5.3. Electrochemical probing of $O_2$ kinetics in a nanoemulsion-based microenvironment. A**, Electrochemical reduction of $O_2$ at a Pt rotating disk electrode (RDE) as a surrogate detects the kinetics of $O_2$ mass transport at the microbial microenvironment created by PFC nanoemulsions. **B** & **C**, linear scan voltammograms depicting the current density (*i*) *vs.* electrode potential ($E_{Disk}$) on a Pt RDE of different spinning rates for oxygen reduction reaction in the absence (**B**) and presence (**C**) of 0.75% (v/v) PFC nanoemulsion. 1-bar $O_2$; 0.1 M sodium phosphate buffer (pH 7.0); 50 mv/dec; *iR* corrected; RHE, reversible hydrogen electrode. **D**, the Koutecký-Levich plot of $|i_{Disk}|^{-1}$ *vs.* $\omega^{-1/2}$ at 0.3 V *vs.* RDE that extracts the kinetic of $O_2$ delivery expressed as $i_k$. ω, angular rotating frequency of RDE.

Linear scan voltammograms at different rotation rates at 1-bar $O_2$ condition were obtained with the absence and presence of PFC nanoemulsions in the microbial minimal medium (Figure 5.3B and 5.3C, respectively), under a three-electrode electrochemical setup (See Methods). A

larger magnitude of reduction current densities ($|i|$) were observed with the 888nanoemulsion's presence, suggesting a facilitated mass transport induced by nanoemulsions. Quantitatively, RDE's well-defined profile of mass transport introduces the Koutecký-Levich equation[37]:

$$\frac{1}{|i|} = \frac{1}{i_k} + \frac{1}{0.62nFD^{2/3}\nu^{-1/6}C_0}\omega^{-1/2} \quad (2)$$

Here $i_k$ denotes the intrinsic current density of $O_2$ reduction on Pt surface, $n = 4$ for the presumed 4-electron reduction of $O_2$ on Pt[36], $F$ the Faradaic constant, $D$ the diffusion coefficient of $O_2$ in water, $\nu$ the kinematic viscosity of liquid, $C_0$ the $O_2$ solubility at 1-bar $O_2$ condition, and ω the RDE's angular rotation rate. Figure 5.3D plots $1/|i|$ versus $\omega^{-1/2}$ at 0.3 V *vs*. Reversible Hydrogen Electrode (RHE) based on the data in Figure 5.3B and 5.3C. The similar slope between the two curves in Figure 5.3D suggest that the local $O_2$ solubility near the Pt electrode is not significantly perturbed with the presence of PFC nanoemulsion. Indeed, at 0.3 V *vs.* RHE, $C_0$ = 1.05 and 0.82 mM with and without nanoemulsion, respectively, when treating the values of $D$ and $\nu$ in the phosphate buffer the same as the ones in pure water ($D = 2.5\times10^{-9}$ $m^2 \bullet sec^{-1}$, $\nu = 0.801\times10^{-6}$ $m^2 \bullet sec^{-1}$)[38]. Despite the similar values of $C_0$, at 0.3 V *vs.* RHE $i_k$ = 91.0 and 4.44 mA/cm$^2$ in the presence and absence of PFC nanoemulsions, respectively. The 20-times difference in the value of $i_k$ indicates that the observed bacterial microenvironment with PFC nanoemulsions facilitates the $O_2$ transport in the extracellular space proximate to the microbes without perturbing the local $O_2$ solubility. Since it is the $O_2$ transport into the microbes that dictates the intracellular $O_2$ concentration, the $O_2$ transport also dictates the delicate balance between biological $N_2$ fixation and $O_2$-dependent respiration,[39,26,31] the enhanced $O_2$ transport kinetic introduced by PFC nanoemulsion under steady state can be considered as the reason for the observed increased $O_2$ availability for microbial metabolism in the $O_2$-limited gas environment in which the only $O_2$ supply comes from electrochemical water oxidation.

## Conclusions

The characterizations presented here offer a microscopic and quantitative picture of the created extracellular microenvironment, which will be beneficial for future development and optimization in other applicable scenarios. We were able to visualize the binding of the nanoemulsion on the microbe surface and quantify this binding affinity by assuming a Langmuir adsorption model. Our research discovered an enhanced kinetic $O_2$ transport with the addition of the PFC nanoemulsions. The techniques developed in this work lead the way for characterizing the microbe and nanoemulsion interaction, and the customization of the gas environment at the microbe interface. The strategy of creating a microbial microenvironment with nanomaterials despite an unwelcoming macroscopic environment offers a viable solution to resolve incompatibility and create synergy at the materials-biology interface.

## Methods

### Materials and chemicals

All chemicals were purchased from Thermo Fisher, Sigma−Aldrich, or VWR International, unless otherwise stated. Perfluorocarbons (PFCs) were purchased from SynQuest Laboratories. All deionized (DI) water was obtained from a Millipore Millipak® Express 40 system. Electrochemical supplies noted here were purchased from CH Instruments, inc.. The LIVE/DEAD™ BacLight™ Bacterial Viability and Counting Kit and the included SYTO™ 9 dye were purchased from ThermoFisher (L34856). 2-μm polystyrene microspheres with surface-functionalized with $-NH_2$ and −COOH moieties were purchased from Sigma−Aldrich (L0280 and L4530, respectively).

**Preparation and characterization of PFC nanoemulsions**

Nanoemulsions were prepared via previously reported procedure[27]. Surfactant solution was prepared by combining 2.8 wt.% of surfactant, Pluronic F68, with the relevant buffer and sonicating in a bath sonicator, Branson 3800 ultrasonic cleaner, to thoroughly dissolve the polymer. Perfluorodecalin, PFD, and perfluorohexane, PFH, were combined (450μL each) in a 15-mL centrifuge tube. The relevant surfactant-containing buffer was then added to achieve a total final volume of 10 mL. All-inorganic microbial minimal medium, detailed in Supplemental Information section 1.1, was used as the buffer for all experiments, except rotating disk electrode experiments where a phosphate buffer (pH 7.0, 0.1 M sodium phosphate), was used instead. The PFCs and surfactant-containing buffer were then sonicated at 35% amplitude for 5 mins using a Qsonica point sonicator. Fluorescently tagged PFC nanoemulsion was prepared for microscopic and flow cytometry experiments. Fluorous rhodamine was synthesized as previously reported. Fluorous rhodamine was stabilized in 4 μL methoxyperfluorobutane, and 8 μL of both PFH and PFD (a total of 16 μL). This mixture was then combined with 200 μL of minimal medium, and point-sonicated at 35% amplitude for 90 sec. Procedures were scaled up when larger volumes were needed. Dynamic light scattering (DLS) experiments were conducted with a Malvern Zetasizer Nano ZSP instrument. 20 μL PFC nanomulsions were diluted in 2 mL DI water in a plastic cuvette. A total of 3 measurements, each consisting of 10 scans, were run to determine the average size of the nanoemulsions (~240 nm, see Figure S5.1).

**Protocols of microbial culturing**

The freeze-dried samples of aerobic bacterium *Xanthobacter autotrophicus* (ATCC 35674) and anaerobic bacterium *Sporomosa ovata* (ATCC 35899) were purchased from American Type

Culture Collection (ATCC)[40]. Detailed recipes of culture media listed below are provided in Supplemental Information section 1[25,28]. Yellow colonies of *X. autotrophicus* were selected from succinate agar plates (succinate nutrient broth solidified with 1.5% agar), incubated at 30 °C in succinate nutrient broth, and stored at −80 °C in a mixture of glycerol and succinate nutrient broth (20/80, v/v). Cultures of *S. ovata* were obtained at 34°C under strict anaerobic condition with DSMZ 311 medium under $H_2/CO_2$ (80/20) atmosphere, and stored at −80 °C in a mixture of dimethyl sulfoxide and DSMZ 311 medium (20/80, v/v).

*X. autotrophicus* reported in this work were first grown at 30 °C in succinate nutrient broth for 1 day, collected by centrifugation (6000 rpm, 5 min; Sorvall ST8, Fisher Scientific) after adjusting the culture pH to about 12 with NaOH, and cultured autotrophically at 30 °C in the all-inorganic minimal medium with an anaerobic jar (Vacu-Quick Jar System, Almore) under a 1-bar gas mixture of 2% $O_2$, 60% $N_2$, 20% $H_2$ and 18% $CO_2$ (200 rpm stirring)[7,25,26]. The microbial culture started at $OD_{600}$ ~ 0.2 (optical density at 600 nm) and reached $OD_{600}$ ~ 1 within 5 days under a condition of $N_2$ and $CO_2$ fixation. The bacteria were harvested via centrifugation (6000 rpm, 5 min) before experiments. *S. ovata* were strictly anaerobically cultured at 34°C in DSMZ 311 medium under $H_2/CO_2$ (80/20) atmosphere for a 3-days autotrophic growth before use.

**Colocalization experiment with fluorescent confocal microscopy**

Cultures of *X. autotrophicus* ($OD_{600}$ = 1.0) were harvested and re-suspended with 0.85% NaCl solution with $OD_{600}$ adjusted to 0.1. Each 1 mL of the resulted bacterial suspension was incubated in hard at room temperature for 15 mins with 1.5 μL of microbial-binding SYTO™ 9 dye solution from the LIVE/DEAD™ BacLight™ Bacterial Viability and Counting Kit. The fluorescently tagged *X. autotrophicus* was separated via centrifugation (6000 rpm, 5 min) and re-suspended in

1 mL minimal medium containing 2.5% fluorescently tagged PFC nanoemulsion (*vide supra*) [29]. Suspension of *X. autotrophicus* without the addition of nanoemulsion was prepared in parallel as the control sample. The prepared samples incubated in dark for 1 hr for completion of nanoemulsion binding and loaded to a 35-mm glass bottom dish (μ-dish, ibidi), whose bottom glass was coated with a layer of poly-l-lysine (treated with 0.01% poly-l-lysine solution overnight and dried). The mixture was allowed to sit in the dish for 0.5 hr before all liquid was slowly removed by pipetting. The glass-surface of the dish was gently washed 5 times with filtered microbial minimal medium. Last, 1 mL of minimal medium was added to the dish to keep the sample hydrated before imaging.

Experiments of confocal microcopy (Leica Confocal SP8 MP) was conducted at Advanced Light Microscopy and Spectroscopy Laboratory at California Nanoscience Institute, UCLA. The data was acquired using Leica Application Suite X (LASX) on *x-y* mode at a scanning resolution of 14.6 nm per pixel, taking *x-y* cross-sectional images with a 100× oil objective lens (Leica 100× HC PL APO OIL CS2 NA/1.4). Fluorescence from SYTO$^{TM}$ 9 in the microbes was monitored at 490nm~520nm by a 470-nm laser excitation; the fluorescence from fluorous rhodamine in PFC nanoemulsions was monitored at 580nm~650nm by a 550-nm laser excitation. The intensities of fluorescence emissions were collected by photon multiplier tube (PMT) detectors. We note that the contribution of out-of-focus signals for SYTO, much brighter than rhodamine in those experiments, is larger than the one from rhodamine dye in the nanoemulsion. Subsequently, the imaged PFC nanoemulsion is more concentrated within the microscopy's focal plane as compared to the imaged bacteria. The fluorescence images of microbes and PFC nanoemulsions were taken separately and merged as shown in Figure 5.1C, 5.1D and S5.2.

**Experiments of flow cytometry related to microbes and PFC nanoemulsions**

Experiments of flow cytometry (BD LSR II cytometer) were conducted at the Janis V. Giorgi Flow Cytometry Core, UCLA. The flow cytometer was operated under a slow flow rate setting. Forward Scattering (FSC) was used as the threshold for events. For each sample and control, 10,000 events were collected and recorded. The recorded events were plotted as 2-D scatter plots of FSC and Side Scattering (SSC) for the gating of microbes, particles, and nanoemulsions. Data were analyzed using FlowJo ver. 10 and the gating represents >95% of the clustered events.

The following procedures were applied to quantify the binding between microbes and nanoemulsion. Cultures of *X. autotrophicus* and *S. ovata* ($OD_{600}$ ~ 1.0) were harvested and re-suspended in 200-nm filtered minimal medium ($OD_{600}$ = 0.002). Solution of Fluorescently tagged PFC nanoemulsions (10 %, v/v)[27] was serial diluted by dilution ratios ranging between $10^3$ and $10^6$. The diluted solution was mixed with equal volume of microbes to reach a final microbial $OD_{600}$ = 0.001, incubated for 30 mins in dark for the completion of nanoemulsion binding, and tested directly by a flow cytometer without further dilution. Control samples were prepared and tested similarly by mixing solutions of diluted nanoemulsions and filtered minimal medium. A pre-defined fluorescence measurement channel for PE (phycoerythrin) was used to measure the fluorescence intensity of fluorinated rhodamine. When 2-μm polystyrene microspheres surface-functionalized with $-NH_2$ and $-COOH$ moieties were tested, filtered microsphere solutions whose particle density was about $2\times10^6$ $mL^{-1}$ were used in lieu of the microbial suspension of $OD_{600}$ = 0.002. The average number of PFC nanoemulsions bound to a bacterial cell or microsphere ($N$) for a specific PFC concentration was determined based on the mean fluorescent intensity with the following equation:

$$N = \frac{I_{mix} - I_{bg}}{I_{PFC}} \quad (3)$$

Here $I_{mix}$ and $I_{PFC}$ are the mean emission intensities of fluorous rhodamine for microbe-nanoemulsion complex and individual PFC nanoemulsion, respectively, at a specific PFC concentration. $I_{bg}$ is mean background emission intensity for the microbe-nanoemulsion complex.

**Electrochemical characterizations**

The experiments of rotating disk electrode (RDE) consisted of a Gamry Interface 1000E potentiostat, an MSR rotator (Pine Research Instrumentation), and an electrochemical glass cell under a controlled gas environment. The electrochemical cell was a 150 mL, five-neck, flat bottom glass flask. The temperature of the setup was maintained at 30 °C by a circulating water bath. A platinum RDE disc electrode of 5.0 mm disk dimeter (AFE5T050PT, Pine Research Instrumentation) was used as working electrode, a Ag/AgCl (1M KCl) as reference electrode and a Pt wire as counter electrode. Prior to experiments, the working electrode was polished, sonicated in DI water, and air dried. The Pt counter electrode was cleaned with dilute $HNO_3$ then DI water. For every measurement, 120 mL fresh electrolyte was saturated with a stream of 13 sccm $N_2$ or $O_2$ for at least 20 min. Linear scanning voltammograms were obtained at a controlled spin rates. The interval between each measurement was 1 min. The scanning rate was 50 mV $s^{-1}$ and the *iR*-corrected results were displayed in Figure 5.3B and 5.3C.

**References**


1. Schmid, A. *et al.* Industrial biocatalysis today and tomorrow. *Nature* **409**, 258-268, doi:10.1038/35051736 (2001).
2. Schoemaker, H. E., Mink, D. & Wubbolts, M. G. Dispelling the Myths--Biocatalysis in Industrial Synthesis. *Science* **299**, 1694, doi:10.1126/science.1079237 (2003).

3. Bornscheuer, U. T. *et al.* Engineering the third wave of biocatalysis. *Nature* **485**, 185-194, doi:10.1038/nature11117 (2012).
4. Dong, G., Ho, W. & Wang, C. Selective photocatalytic N2 fixation dependent on g-C3N4 induced by nitrogen vacancies. *Journal of Materials Chemistry A* **3**, 23435-23441, doi:10.1039/c5ta06540b (2015).
5. Milton, R. D. *et al.* Nitrogenase bioelectrocatalysis: heterogeneous ammonia and hydrogen production by MoFe protein. *Energy & Environmental Science* **9**, 2550-2554, doi:10.1039/c6ee01432a (2016).
6. Brown, K. A. *et al.* Light-driven dinitrogen reduction catalyzed by a CdS:nitrogenase MoFe protein biohybrid. *Science* **352**, 448, doi:10.1126/science.aaf2091 (2016).
7. Liu, C., Sakimoto, K. K., Colón, B. C., Silver, P. A. & Nocera, D. G. Ambient nitrogen reduction cycle using a hybrid inorganic–biological system. *Proceedings of the National Academy of Sciences* **114**, 6450-6455 (2017).
8. Milton, R. D. & Minteer, S. D. Enzymatic Bioelectrosynthetic Ammonia Production: Recent Electrochemistry of Nitrogenase, Nitrate Reductase, and Nitrite Reductase. *ChemPlusChem* **82**, 513-521, doi:10.1002/cplu.201600442 (2017).
9. Hickey, D. P. *et al.* Pyrene hydrogel for promoting direct bioelectrochemistry: ATP-independent electroenzymatic reduction of N2. *Chem Sci* **9**, 5172-5177, doi:10.1039/c8sc01638k (2018).
10. Nevin, K. P., Woodard, T. L., Franks, A. E., Summers, Z. M. & Lovley, D. R. Microbial electrosynthesis: feeding microbes electricity to convert carbon dioxide and water to multicarbon extracellular organic compounds. *MBio* **1**, doi:10.1128/mBio.00103-10 (2010).

11. Licht, S. Efficient solar-driven synthesis, carbon capture, and desalinization, STEP: solar thermal electrochemical production of fuels, metals, bleach. *Adv Mater* **23**, 5592-5612, doi:10.1002/adma.201103198 (2011).
12. Nevin, K. P. *et al.* Electrosynthesis of organic compounds from carbon dioxide is catalyzed by a diversity of acetogenic microorganisms. *Appl Environ Microbiol* **77**, 2882-2886, doi:10.1128/AEM.02642-10 (2011).
13. Li, H. *et al.* Integrated electromicrobial conversion of CO2 to higher alcohols. *Science* **335**, 1596, doi:10.1126/science.1217643 (2012).
14. Liu, C. *et al.* Nanowire-bacteria hybrids for unassisted solar carbon dioxide fixation to value-added chemicals. *Nano Lett* **15**, 3634-3639, doi:10.1021/acs.nanolett.5b01254 (2015).
15. Nichols, E. M. *et al.* Hybrid bioinorganic approach to solar-to-chemical conversion. *Proc Natl Acad Sci U S A* **112**, 11461-11466, doi:10.1073/pnas.1508075112 (2015).
16. Ganigue, R., Puig, S., Batlle-Vilanova, P., Balaguer, M. D. & Colprim, J. Microbial electrosynthesis of butyrate from carbon dioxide. *Chem Commun (Camb)* **51**, 3235-3238, doi:10.1039/c4cc10121a (2015).
17. Jourdin, L. *et al.* High Acetic Acid Production Rate Obtained by Microbial Electrosynthesis from Carbon Dioxide. *Environ Sci Technol* **49**, 13566-13574, doi:10.1021/acs.est.5b03821 (2015).
18. Nangle, S. N., Sakimoto, K. K., Silver, P. A. & Nocera, D. G. Biological-inorganic hybrid systems as a generalized platform for chemical production. *Curr Opin Chem Biol* **41**, 107-113, doi:10.1016/j.cbpa.2017.10.023 (2017).

19. Rosenbaum, M., Aulenta, F., Villano, M. & Angenent, L. T. Cathodes as electron donors for microbial metabolism: which extracellular electron transfer mechanisms are involved? *Bioresour Technol* **102**, 324-333, doi:10.1016/j.biortech.2010.07.008 (2011).
20. Nie, H. *et al.* Improved cathode for high efficient microbial-catalyzed reduction in microbial electrosynthesis cells. *Phys Chem Chem Phys* **15**, 14290-14294, doi:10.1039/c3cp52697f (2013).
21. Bajracharya, S. *et al.* Carbon dioxide reduction by mixed and pure cultures in microbial electrosynthesis using an assembly of graphite felt and stainless steel as a cathode. *Bioresour Technol* **195**, 14-24, doi:10.1016/j.biortech.2015.05.081 (2015).
22. Milton, R. D., Wang, T., Knoche, K. L. & Minteer, S. D. Tailoring Biointerfaces for Electrocatalysis. *Langmuir* **32**, 2291-2301, doi:10.1021/acs.langmuir.5b04742 (2016).
23. Jourdin, L., Freguia, S., Flexer, V. & Keller, J. Bringing High-Rate, CO2-Based Microbial Electrosynthesis Closer to Practical Implementation through Improved Electrode Design and Operating Conditions. *Environ Sci Technol* **50**, 1982-1989, doi:10.1021/acs.est.5b04431 (2016).
24. Liu, C., Colón, B. C., Ziesack, M., Silver, P. A. & Nocera, D. G. Water splitting–biosynthetic system with $CO_2$ reduction efficiencies exceeding photosynthesis. *Science* **352**, 1210 (2016).
25. Lu, S., Guan, X. & Liu, C. Electricity-powered artificial root nodule. *Nat Commun* **11**, 1505, doi:10.1038/s41467-020-15314-9 (2020).
26. Malik, K. A. & Schlegel, H. G. Chemolithoautotrophic Growth of Bacteria Able to Grow under N-2-Fixing Conditions. *FEMS Microbiol. Lett.* **11**, 63-67 (1981).
27. Sletten, E. M. & Swager, T. M. Readily accessible multifunctional fluorous emulsions. *Chemical Science* **7**, 5091-5097, doi:10.1039/C6SC00341A (2016).

28. Rodrigues, R. M. *et al.* Perfluorocarbon nanoemulsion promotes the delivery of reducing equivalents for electricity-driven microbial CO2 reduction. *Nat Catal* **2**, 407-414, doi:10.1038/s41929-019-0264-0 (2019).

29. Sletten, E. M. & Swager, T. M. Fluorofluorophores: fluorescent fluorous chemical tools spanning the visible spectrum. *J Am Chem Soc* **136**, 13574-13577, doi:10.1021/ja507848f (2014).

30. Langmuir, I. THE ADSORPTION OF GASES ON PLANE SURFACES OF GLASS, MICA AND PLATINUM. *J. Am. Chem. Soc.* **40**, 1361-1403, doi:10.1021/ja02242a004 (1918).

31. Wiegel, J. in *The Prokaryotes: Volume 5: Proteobacteria: Alpha and Beta Subclasses* (eds Martin Dworkin *et al.*) 290-314 (Springer New York, 2006).

32. Ju, L. K., Lee, J. F. & Armiger, W. B. Enhancing oxygen transfer in bioreactors by perfluorocarbon emulsions. *Biotechnol. Prog.* **7**, 323-329, doi:10.1021/bp00010a006 (1991).

33. Spahn, D. Blood substitutes Artificial oxygen carriers: perfluorocarbon emulsions. *Critical Care* **3**, R93, doi:10.1186/cc364 (1999).

34. Castro, C. I. & Briceno, J. C. Perfluorocarbon-based oxygen carriers: review of products and trials. *Artif Organs* **34**, 622-634, doi:10.1111/j.1525-1594.2009.00944.x (2010).

35. Tian, X. L. *et al.* Unsupported Platinum-Based Electrocatalysts for Oxygen Reduction Reaction. *Acs Energy Lett* **2**, 2035-2043, doi:10.1021/acsenergylett.7b00593 (2017).

36. Li, M. F. *et al.* Ultrafine jagged platinum nanowires enable ultrahigh mass activity for the oxygen reduction reaction. *Science* **354**, 1414-1419, doi:10.1126/science.aaf9050 (2016).

37. Bard, A. J. & Faulkner, L. R. *Electrochemical methods : fundamentals and applications 2nd Edition*. (Wiley, 2000).

38. Xing, W. *et al.* in *Rotating Electrode Methods and Oxygen Reduction Electrocatalysts* (eds Wei Xing, Geping Yin, & Jiujun Zhang) 1-31 (Elsevier, 2014).

39. Malik, K. A. & Schlegel, H. G. Enrichment and isolation of new nitrogen-fixing hydrogen bacteria. *FEMS Microbiol. Lett.* **8**, 101-104, doi:http://dx.doi.org/ (1980).

40. Möller, B., Oßmer, R., Howard, B. H., Gottschalk, G. & Hippe, H. Sporomusa, a new genus of gram-negative anaerobic bacteria including Sporomusa sphaeroides spec. nov. and Sporomusa ovata spec. nov. *Arch Microbiol* **139**, 388-396, doi:10.1007/BF00408385 (1984).

**Supplementary Information**

**Medium Recipes of Microbial Cultures**

*Minimal medium*

| | |
|---|---|
| $K_2HPO_4$ | 1 g |
| $KH_2PO_4$ | 0.5 g |
| $NaHCO_3$ | 2 g |
| $MgSO_4 \cdot 7\ H_2O$ | 0.1g |
| $CaSO_4 \cdot 2\ H_2O$ | 0.04 g |
| $FeSO_4 \cdot 7\ H_2O$ | 0.001g |
| Trace mineral mix (see below) | 1.00 ml |
| Deionized water | 1000.00 ml |

All ingredients were combined and sonicated for about 10 minutes to dissolve. The medium was autoclaved at 120 °C with water for 30 min. Once cool the medium was filtered via vacuum filtration through a 0.22 μm filter. The pH of the complete medium was adjusted to pH 7.0, if necessary.

*Trace mineral mix*

| | |
|---|---|
| $H_3BO_3$ | 2.8 g |
| $MgSO_4 \cdot 4\ H_2O$ | 2.1 g |
| $Na_2MoO_4 \cdot 2\ H_2O$ | 0.75 g |
| $ZnSO_4 \cdot 7\ H_2O$ | 0.24 g |
| $Cu(SO_3)_2 \cdot 3\ H_2O$ | 0.04 g |
| $NiSO_4 \cdot 6\ H_2O$ | 0.13 g |

| | |
|---|---|
| Deionized water | 1000.00 ml |

All components were mixed and stirred for 1 hr to dissolve. The solution was vacuum filtered through a 0.22 μm filter to sterilize.

*Succinate nutrient broth*

| | |
|---|---|
| Nutrient broth | 5 g |
| Yeast extract | 4 g |
| NaCl | 3 g |
| Sodium succinate | 5 g |
| Deionized water | 1000.00 ml |

All ingredients were combined and sonicated for about 10 minutes to dissolve. The solution was autoclaved at 120 °C with water for 30 min.

*DSMZ 311 Medium*

| | |
|---|---|
| $NH_4Cl$ | 0.50 g |
| $MgSO_4$ • 7 H2O | 0.50 g |
| $CaCl_2$ • 2 $H_2O$ | 0.25 g |
| NaCl | 2.25 g |
| $FeSO_4$ • 7 $H_2O$ | 0.002g |
| Trace element solution SL-10 (see below) | 1.00 ml |
| Selenite-tungstate solution (see below) | 1.00 ml |
| Yeast extract | 2.00 g |
| Casitone | 2.00 g |

| | |
|---|---|
| Betaine • $H_2O$ | 6.70 g |
| Na-resazurin solution (0.1% w/v) | 0.50 ml |
| $K_2HPO_4$ | 0.35 g |
| $KH_2PO_4$ | 0.23 g |
| $NaHCO_3$ | 4.00 g |
| Vitamin solution (see below) | 10.00 ml |
| Distilled water | 1000.00 ml |

All ingredients (except phosphates, bicarbonate, vitamins, cysteine and sulfide) were dissolved first. The medium was sparged with a $N_2$: $CO_2$ gas mixture in a ratio of 80: 20 while boiling to make the solution air free. Once cool, and while continuously sparging with the same gas, phosphates, vitamins (sterilized by filtration) and carbonate were added. The medium was transfered under the same gas into anaerobic culture tubes and then autoclaved. The pH of the complete medium was adjusted to pH 7.0, if necessary.

*Trace element solution (SL-10)*

| | |
|---|---|
| Nitrilotriacetic acid | 1.50 g |
| $MgSO_4$ • 7 $H_2O$ | 3.00 g |
| $MnSO_4$ • $H_2O$ | 0.50 g |
| NaCl | 1.00 g |
| $FeSO_4$ • 7 $H_2O$ | 0.10 g |
| $CoSO_4$ • 7 $H_2O$ | 0.18 g |
| $CaCl_2$ • 2 $H_2O$ | 0.10 g |
| $ZnSO_4$ • 7 $H_2O$ | 0.18 g |

| | |
|---|---|
| $CuSO_4 \cdot 5\ H_2O$ | 0.01 g |
| $KAl(SO_4)_2 \cdot 12\ H_2O$ | 0.02 g |
| $H_3BO_3$ | 0.01 g |
| $Na_2MoO_4 \cdot 2\ H_2O$ | 0.01 g |
| $NiCl_2 \cdot 6\ H_2O$ | 0.03 g |
| $Na_2SeO_3 \cdot 5\ H_2O$ | 0.30 mg |
| Na2WO4 • 2 $H_2O$ | 0.40 mg |
| Distilled water | 1000.00 ml |

The nitrilotriacetic acid was first dissolved and the pH adjusted to 6.5 with KOH before the minerals were added. The final pH was then adjusted to pH 7.0 with KOH.

*Vitamin solution*

| | |
|---|---|
| Biotin | 2.00 mg |
| Folic acid | 2.00 mg |
| Pyridoxine-HCl | 10.00 mg |
| Thiamine-HCl • 2 H2O | 5.00 mg |
| Riboflavin | 5.00 mg |
| Nicotinic acid | 5.00 mg |
| D-Ca-pantothenate | 5.00 mg |
| Vitamin B12 | 0.10 mg |
| p-Aminobenzoic acid | 5.00 mg |
| Lipoic acid | 5.00 mg |
| Distilled water | 1000.00 ml |

All ingredients were dissolved and the resulting solution was filter-sterilized.

*Selenite-tungstate solution*

| | |
|---|---|
| NaOH | 0.5 g |
| $Na_2SeO_3 \cdot 5\ H_2O$ | 3.0 mg |
| $Na_2WO_4 \cdot 2\ H_2O$ | 4.0 mg |
| Distilled water | 1000.0 ml |

*Reducing agent solution*

All the water used in this procedure was boiled and gassed under $N_2$ prior to the experiments. In a 2-L Erlenmeyer flask, 12.5 g cysteine-HCl was dissolved in 500 mL water. The pH of the solution was adjusted to 9.5 with NaOH. In a plastic tray, 12.5 g of washed crystals of $Na_2S \cdot 9H_2O$ was weighed and then transferred into the flask containing cysteine-HCl. The volume of the solution was brought up to 1000 mL. While under $N_2$ gas, the whole solution was brought to boil and then allowed to cool. 20 mL of the prepared solution was transfered into one 25-mL vial which was pre-flushed with $N_2$. The vials were sealed and then autoclaved for 15 min at 121 $^oC$.

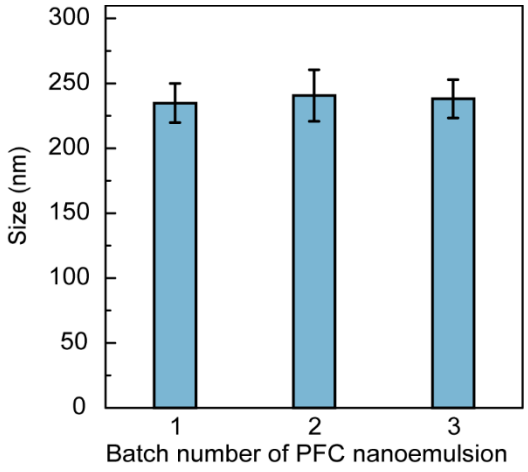


**Figure S5.1. The size of PFC nanoemulsions measured by dynamic light scattering.**

The size of perfluorocarbon (PFC) nanoemulsion measured using a Malvern Zetasizer Nano ZSP instrument. 20 μL PFC nanomulsions were diluted in 2 mL DI water in a plastic cuvette. A total of 3 samples (n = 3), each consisting of 10 measurement scans, were conducted.

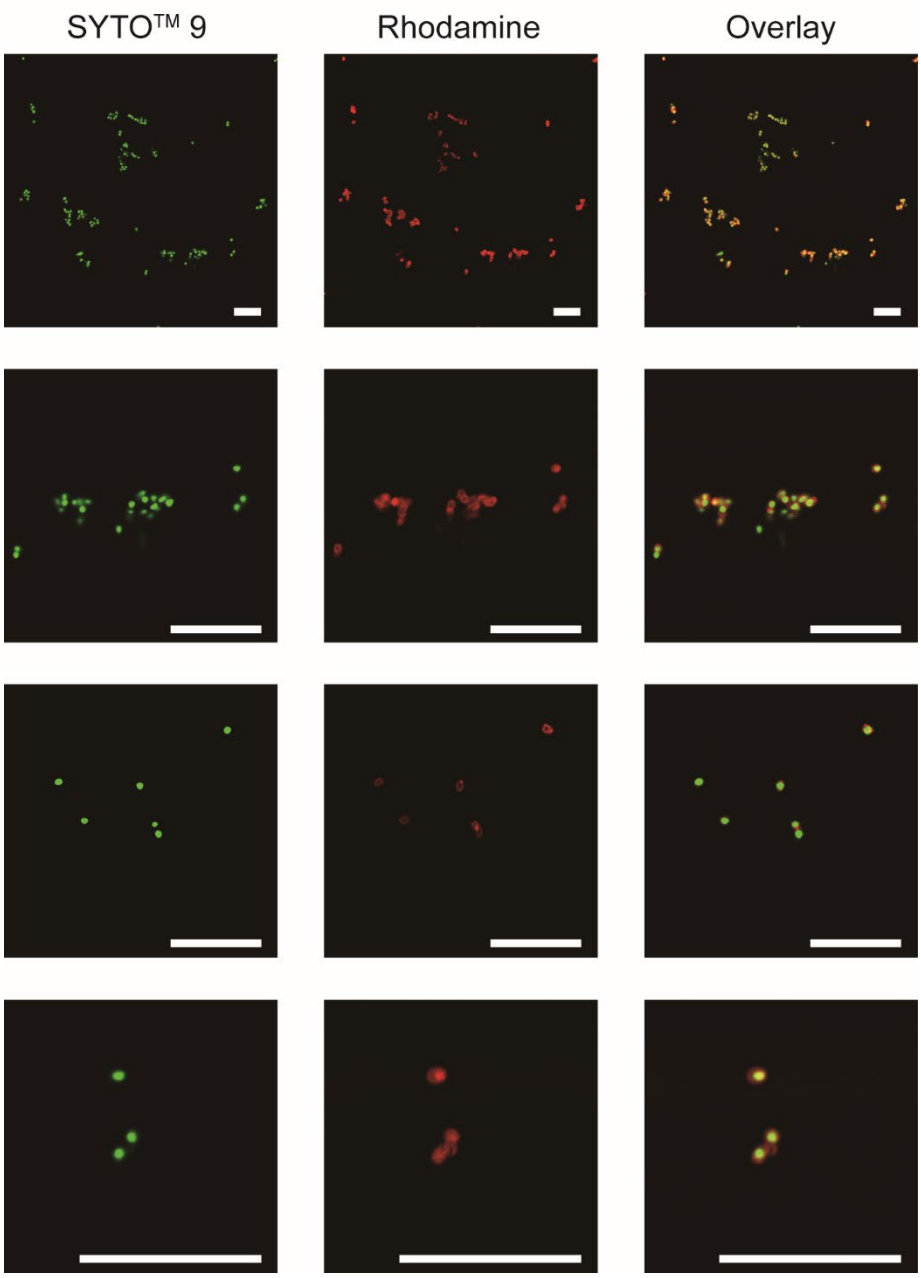


**Figure S5.2. Additional images for the colocalization of *X. autotrophicus* stained by SYTO™ 9 and PFC nanoemulsion tagged by fluorinated rhodamine.**

Fluorescence images showing SYTO™ 9 (pseudo-colored in green), rhodamine (pseudo-colored in red) and the overlay image of both in a mixture of SYTO™ 9-stained *X. autotrophicus* and rhodamine-stained PFC nanoemulsion (2.5%, v/v) at different magnification. Scale bars = 10 μm.

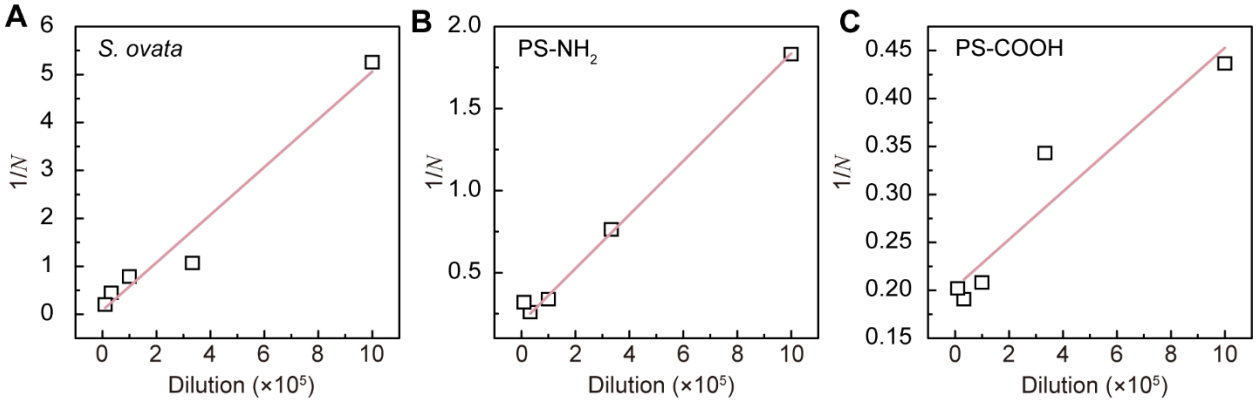


**Figure S5.3. Plots of the reciprocals of the average number of adsorbed PFC nanoemulsion per microbe/particle (1/*N*) against the final dilution ratios of PFC nanoemulsion**.

Plots of the reciprocals of the average number of adsorbed PFC nanoemulsion per microbe/particle (1/*N*) against the final dilution ratio of PFC nanoemulsion in the mixture consisting PFC nanoemulsions with *Sporomusa ovata* (**A**), 2-μm polystyrene microspheres with $-NH_2$ and −COOH surface functionalization groups (**B** and **C**, respectively),. Linear regression was applied according to Langmuir adsorption model. The calculated maximum possible number of adsorbed PFC nanoemulsion per microbe ($N_{max}$) and the equilibrium constant ($K_{eq}$) were displayed in Fig. 4E.

## CHAPTER 6. CONCLUDING REMARKS

As shown in this dissertation, the goal of my research has been to combine PFC nanoemulsions with hybrid biological inorganic systems to enhance the efficiency of the systems and customize the gas environment. This research started with simply enhancing the solubility of the reducing equivalent, $H_2$ gas, in the hybrid $CO_2$ fixation system for increased throughput. After observing the success of the PFC nanoemulsion to increase the acetate production by the *S. ovata*, I explored the mechanism of enhancement of the PFC nanoemulsions. I found that there was non-specific binding and that the kinetic $H_2$ transfer reaction to the microbe was enhanced. This discovery led me to apply the PFC nanoemulsions to the hybrid $N_2$ reduction system with the intention that it will have similar enhancement and control of the gas environment. I found that the PFC nanoemulsions enhanced the $N_2$ fixation and allowed for control of the $O_2$ environment within the system. In the mechanistic study, I discovered that we could alter the binding affinity and the maximum number of nanoemulsions that could bind to a particle by adjusting the size or surface functionalization of the PFC nanoemulsion. This research is only the beginning of using the PFC nanoemulsions to design and control the gas environment in aqueous reactions.

I believe that there are several future directions that this research should go in after my completion of my thesis. The first direction that I would take this research in is to work on optimizing the binding affinity of the nanoemulsions with specific particles. Understanding the relationship between the surface functionalization of the target particle and the chosen PFC nanoemulsion would allow for future development of ideal gas environments for specific reactions. To accomplish this, I would focus on using different surfactants or surface modifications on the PFC nanoemulsion to alter the surface charge. Once precise control of surface charge of the nanoemulsion is achieved I would use the flow cytometry techniques discussed in my thesis to

determine the binding affinity and maximum number of nanoemulsions that could bind to target particles of different sizes and surface functionalities. After determining the correlation between surface charge and binding, I would perform experiments of RDE to ascertain if there is a relationship between the binding affinity of the nanoemulsions and the transfer kinetics. Currently, we have not explored if a larger or smaller binding affinity is more favorable to enhance gas transfer kinetics. Understanding the correlation between binding affinity, maximum number of nanoemulsions, and gas transfer kinetics would allow for a more complete control of the gas environment using the nanoemulsion. This could enhance other microbial reactions, with and without electrochemical assistance, as well as other aqueous reactions where a precise control of the gas environment is vital.